ELUCIDATING THE ROLE OF THE EXTRACELLULAR MATRIX IN SKELETOGENIC CONDENSATION GROWTH

By

Danielle Gaitor

Submitted in partial fulfilment of the requirements
for the degree of Master of Science

at

Dalhousie University
Halifax, Nova Scotia
August 2020

To mom, all that I am is because of you.

TABLE OF CONTENTS

LIST OF TABLES

LIST OF FIGURES

ABSTRACT

Skeletogenic condensations are critical to bone development. The scleral ossicles of chickens, *Gallus gallus*, are a convenient model to study intramembranous ossification. In this study on chicken scleral ossicle primordia, histological analyses of developing condensations revealed that condensation depth changes over developmental time. The variation of condensation depth within a given eye suggested that the scleral ossicle ring is orientated at a tilt within the eye. Immunohistochemical analysis of tenascin-C demonstrated its dynamic spatial expression over developmental time, pointing towards its potential role in condensation development, and possibly in condensation boundary formation. Although further investigation is needed to confirm the presence of MMP1 and MMP2 in chick scleral mesenchyme, preliminary data in this study have set the stage for further studies on a potential role of matrix remodeling by MMPs in condensation development. These data therefore aid in bridging the gap in knowledge of condensation development and intramembranous ossification.

LIST OF ABBREVIATIONS AND SYMBOLS USED

º- Degree

1º- Primary

2º- Secondary

µm- Micrometer

mm- Millimeter

µL- Microliter

mL- Milliliter

∑- Sum

AP – Alkaline phosphatase

APTES- (3-Aminopropyl) triethoxysilane

BMP – Bone morphogenetic protein

CE – Conjunctival epithelium

CI – Control injection

CNI – Control no injection

CONT- Control

CP- Ciliary Process

ECM – Extracellular matrix

D – Dorsal

DAB – Diaminobenzidine

dH_20- Distilled water

df – Degrees of freedom

dpf- Days post fertilization

EtOH- Ethanol

FGF- Fibroblast growth factor

HBQ – Hall's and Brunt's Quadruple Stain

HCI – Hydrocortisone Injection

HH – Hamburger and Hamilton

Hh- Hedgehog

HOXA- Homeobox A

IHC – Immunohistochemistry

MMP – Matrix Metalloproteinases

MSX- Msh Homeobox

N – Nasal

N-CAM – Neural cell adhesion molecule

NR – Neural retina

PBS – Phosphate buffered saline

PFA – Paraformaldehyde

PRX- Class III peroxidase

RIPA- Radioimmunoprecipitation assay

RPE – Retinal pigmented epithelium

SC – Scleral cartilage

SO- Scleral ossicle

T – Temporal

TIMP – Tissue Inhibitors of Metalloproteinases

V – Ventral

ACKNOWLEDGEMENTS

I would like to thank Tamara- Franz-Odendaal, PhD, for giving me the opportunity to expand my skillset as a researcher. Thank you for going above and beyond to assist me in securing the funding to be able to embark on this journey. Your consistent guidance and support have been of the uttermost importance in completing this research project. To my committee members, Frank Smith, PhD, Boris Kablar, MD, PhD and Kazue Semba, PhD, thank you for your invaluable input, encouragement and constructive criticism. To the members of the Franz-Odendaal lab, you have all played an integral role in my success. Thank you to Dr. Franz-Odendaal, Beverly Hymes, and Nicholas Zinck for all of your help with learning various methods and techniques needed to complete my project. A special thank you to Nick Zinck for assisting with the dissections for protein extractions, and to Joseph Al Haddad (former co-op student) for carrying out the preliminary injections for the MMP inhibitor.

Thank you to Shirine Jeradi, PhD (especially), Jennifer Giffin, PhD, Paige Drake, and Shea McInnis for your invaluable input that aided in the completion of this thesis. Thank you to Paige Drake (and family) and Melanie Massey (former lab member) for your friendship and emotional support.

Thank you to my parents, Juliette Roberts and Ken Gaitor, other family members, and friends, who have consistently supported me throughout all of my endeavors. You have been my constant motivation through it all.

Thank you to Dalhousie University and Mount Saint Vincent University for providing me with the facilities to fulfill my degree requirements. A special thank you to the department of

Medical Neuroscience at Dalhousie, especially, Pauline Fraser, Dr. Semba and Dr. Baldridge for your help during challenging times. You are so appreciated!

Thank you to the Nova Scotia Graduate Scholarship Fund, the Nova Scotian Government, the Natural Sciences and Engineering Research Council of Canada, the Medical Neuroscience Department and the Faculty of Graduate Studies at Dalhousie University, and Dr. Franz-Odendaal, for providing the funding necessary for me to complete my research project.

Thank You to God, my constant center of faith, for "I can do all things through Christ who strengthens me." Philippians 4:13

1.0. INTRODUCTION

1.4. Bone Development

Bone development involves four key stages. First, mesenchymal cells migrate to the future site of the bone. Then, those mesenchymal cells interact with surrounding epithelia to initiate the following steps. Mesenchymal cells aggregate together to form a skeletogenic condensation which is the precursor to the bone or cartilage. The skeletogenic condensation grows until it reaches its critical size in order for overt differentiation to occur (Hall and Miyake 2000). The term skeletogenic condensation describes the aggregation of cells before the process of cell differentiation. Interestingly, the development of a skeletogenic condensation is arguably the most critical stage of skeletogenesis. There are two main modes of ossification. Endochondrally ossifying bones form a cartilage template that is later replaced by bone, while intramembranously ossifying bones form directly from the condensation. Examples of endochondrally ossifying bones include the long bones of the appendicular skeleton like the femur and tibia (Docherty 2007). Conversely, the skull roof bones and the lateral halves of the clavicles ossify intramembranously (Hall 1988; reviewed by Karsenty and Wagner 2002). While a lot is known about the molecular regulation of condensations involved in endochondral ossification, much is left to be discovered about intramembranous ossification. This gap in knowledge between these two modes of ossification is due to the fact that most of the skeleton forms via endochondral ossification and those bones are perhaps more accessible, while only some craniofacial (cranial neural crest derived) and few trunk bones (mesoderm derived) form via intramembranous ossification (Hall 1988; reviewed by Karsenty and Wagner 2002).

1.2. Condensation Growth and Development

As previously stated, condensation formation is the third phase of bone development (Hall and Miyake 2000). Within the phase of condensation formation, there are four key stages that have previously been identified in mouse. These stages and the factors that facilitate them, are concisely summarized in Figure 1 (Giffin et. al. 2019). Signaling between the mesenchyme and the epithelia occurs first. The condensation is initiated via signaling molecules that enable cell to cell adhesion to form an aggregate of mesenchymal cells. A condensation boundary is established around the aggregate that allows the condensation to grow and reach its critical size either through the migration of additional cells into the condensation, or proliferation of existing cells within the condensation (Hall and Miyake 2000; reviewed in Giffin et. al. 2019).

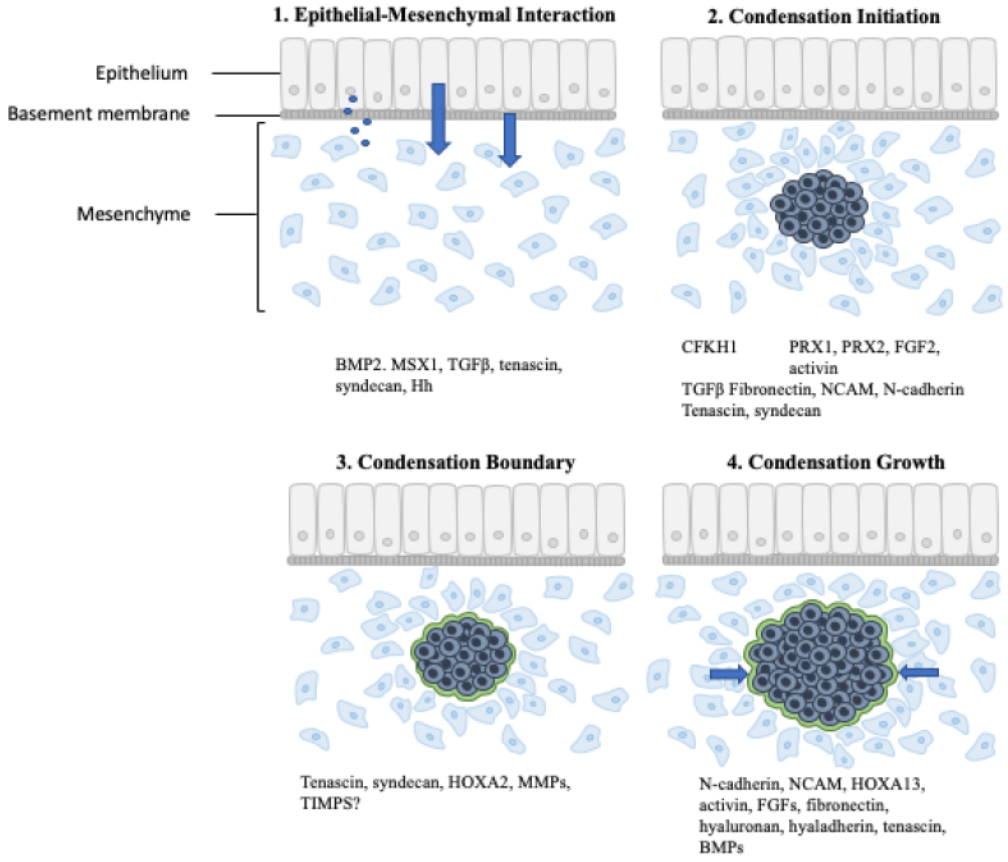

Figure 1. *Condensation Formation. (1) Epithelial-Mesenchymal interaction. Arrows in 1, signaling. (2) Condensation Initiation. (3) Condensation Boundary. (4) Condensation Growth (Cell proliferation or migration of additional mesenchymal cells into the condensation and continued cell adhesion). Arrows in 4, lateral ends. Grey- epithelial cells; Dark blue- condensed cells; Green- the condensation boundary; Light blue- mesenchymal cells. Modified from Giffin, Gaitor (thesis author) & Franz-Odendaal 2019.*

1.3. Overall Significance of Research Project

With the increasing incidences of congenital craniofacial defects around the world every year, the need for pediatric craniofacial surgery continues to increase correspondingly. Dr. Peter Cooney, Chief Dental Officer, Health Canada, reports that there are currently 672 active patients being treated for craniofacial anomalies in Halifax (Batsos 2010). While children born with craniofacial facial defects can seek surgical treatment, the cost and associated risk of surgery, are matters of great concern worldwide. Many individuals in lesser developed countries go without treatment due to the lack of access to proper healthcare or the high cost of surgery. Consequently, the appearance, speech, hearing, reproductive success and psychosocial competencies of untreated individuals are affected (Markus 2012). Genetic or cellular defects that occur during bone/cartilage development can result in craniofacial anomalies like craniosynostosis.

Craniosynostosis is the premature fusion of the cranial sutures between the calvariae (Lajeunie et. al 1995). There are various phenotypes of this pathology that are dependent on how many sutures fuse, and which ones fuse. Both environmental and genetic factors can initiate craniofacial defects at the cellular and molecular level to lead to craniosynostosis. Complications associated with craniosynostosis can specifically affect the neurological, sensory, and respiratory functions of the individual (Johnson and Wilkie 2011). The first identifiable phenotype or presentation of such pathology is an unusually shaped head. However, many other malformations can manifest, such as cleft palate and syndactyly. Corrective surgeries are usually performed between the tender ages of six months to two years (Johnson and Wilkie 2011), a frightening reality for the patients and their loved ones alike. Importantly, both the calvariae and the avian scleral ossicles, studied here, are intramembranously ossifying, neural crest derived flat bones

(reviewed in Franz-Odendaal 2011). Thus, using scleral ossicles to understand condensation formation, a critical step in skeletal development, may provide insight into the developmental mechanisms that lead to craniofacial defects and may be useful in the prognoses and prevention of these disorders.

1.4. Scleral Ossicles

The scleral ossicle system in the chicken, *Gallus gallus,* was used in this study as a model system to investigate the formation of skeletogenic condensations, which are the templates for bone development. Scleral ossicles are a ring of eye bones found in the vertebrate classes such as birds, some fish and many reptiles (reviewed in Franz-Odendaal 2020). Scleral ossicle number can differ among species. Some birds like the domestic quail, *Coturnix coturnix*, can have up to 18 scleral ossicles per eye, while teleost fish only have one or two ossicles per eye (Canavese et. al. 1987; reviewed in Franz-Odendaal and Vickaryous 2006). Intriguingly, scleral ossicles form via a modified endochondral ossification process in fish, but via intramembranous ossification in Reptilia (including birds) (Franz-Odendaal and Hall. 2006; Franz-Odendaal et. al. 2007). Scleral ossicles are speculated to function in either structural support, or visual accommodation (Lima et. al. 2009; reviewed in Franz-Odendaal 2020). In birds (and other Reptilia), a series of transient conjunctival papillae induce scleral ossicle formation and consequently, there is a direct correlation between the number of papillae and the number of ossicles that form (Pinto and Hall. 1991; Franz-Odendaal. 2008). Conjunctival papillae are specialized epithelial structures that induce the formation of scleral condensations (reviewed in Giffin et. al. 2019). In chicken, conjunctival papillae are relatively easy to identify, access and manipulate. Conjunctival papillae follow a unique but predictable pattern of development (Franz-Odendaal 2008; reviewed in

Franz-Odendaal and Vickaryous. 2006; reviewed in Drake et. al. 2020;). The scleral condensations do not split or fuse and therefore one can follow their pattern of development easily (Franz-Odendaal 2011).

The embryonic stages that will be investigated in this study are Hamburger-Hamilton stages 34-37, as outlined in the Hamburger-Hamilton chicken embryo staging table (Hamburger and Hamilton 1951, republished in 1992). At HH34 (eight days post incubation), 13 or 14 conjunctival papillae can be observed (Figure 2). These papillae gradually shrink and degenerate as skeletogenic condensations form and develop. Andrews and Franz-Odendaal (2018) demonstrated that small scleral condensations can be seen at HH34 with alkaline phosphatase staining which stains active osteoblasts. However, scleral condensations can also be clearly seen with the naked eye (without staining) at HH37, 11 days after incubation of a fertilized egg.

The Franz-Odendaal lab has substantial expertise studying, manipulating and analyzing the development of scleral ossicles in the chicken model system. For example, the Franz-Odendaal lab has previously determined that scleral condensations increase in size via cell migration and that these cells join the condensation at the lateral ends of the condensation as opposed to the middle of the condensation (Jabalee and Franz-Odendaal 2013).

1.5. Phases of Scleral Ossicle Development

Conjunctival papillae have recently been identified to have an overlooked placode stage to their development, likened to those seen in the development of teeth, feathers, scales, hair and mammary glands (reviewed in Drake and Franz-Odendaal 2020). Placodes are specialized epithelial thickenings that function as essential signaling centers to induce placode derivatives (such as feather placodes, teeth placodes, etc.) (reviewed in Drake and Franz-Odendaal 2018).

The scleral mesenchyme sends an inductive signal to the epithelium to induce the epithelium to thicken to become placodes; these placodes then develop into the transient conjunctival papillae. The latter marks the first induction phase of the process of scleral ossicle development (Widelitz 2008; Cobourne and Sharpe 2010; Huang et al. 2012). The initial papilla forms directly above the ciliary artery marking the temporal papillae group. Following this, the nasal group develops. Next, the dorsal group develops and lastly, the ventral group develops, ultimately forming a complete ring of 13-14 papillae (Franz-Odendaal 2008; Drake et al. 2020). These groups are outlined in Figure 2 .

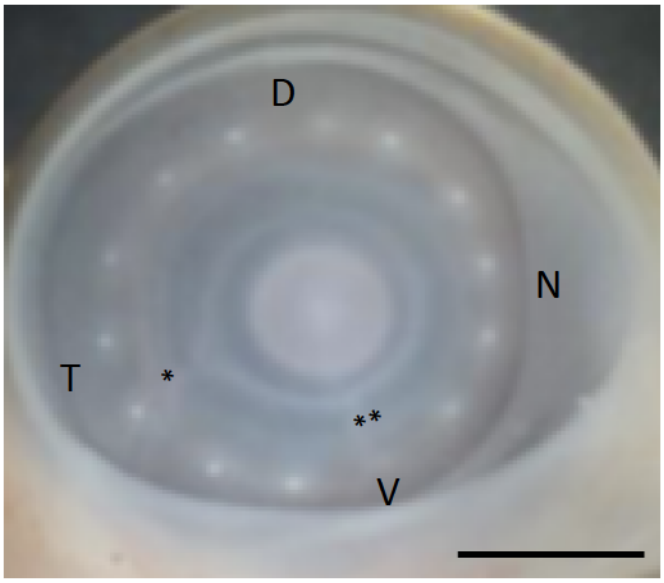

Figure 2*. A whole-mount image of the chicken eye at HH34 showing the four papillae groups. The temporal (T,) group forms first as the initial papilla forms directly above the ciliary artery. The other papillae groups form in the following order: nasal (N), dorsal (D), ventral (V), until a complete ring of 13-14 papillae is formed. Nasal group is adjacent to the beak. *, ciliary artery. **, choroid fissure. Photo from the Franz-Odendaal Lab. Scale bar, 2mm.*

Epithelial and mesenchymal interactions persist to produce an inductive cue to signal papillae degeneration and the development of the scleral condensations. This marks the second inductive phase of scleral ossicle development. Both phases are outlined in Figure 3 (Hall 1981; Franz-Odendaal 2008; Duench and Franz-Odendaal 2012; Jourdeuil 2015).

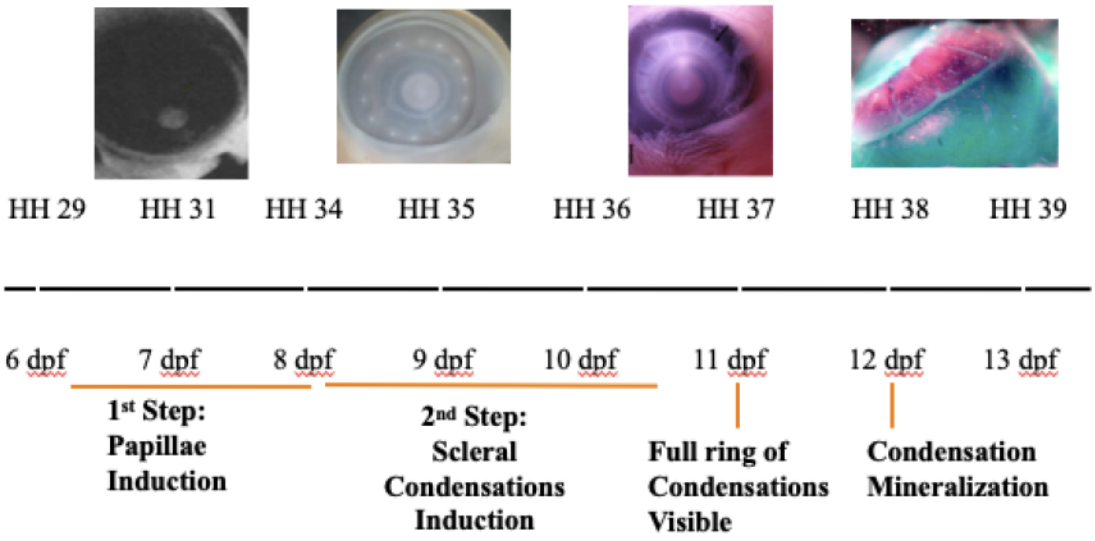

Figure 3. *A schematic depicting the developmental timeline of scleral ossicles from HH29 to HH39. There are two inductive phases involved in scleral ossicle formation: papillae induction and scleral ossicle condensation induction. Following induction of the placodes, the first papillae is seen under the microscope at HH30. Papillae continue to form until 13-14 papillae form a complete ring at HH34. At stage HH36, papillae degeneration is observed as scleral condensations become more visible. At HH37, a full ring of scleral condensations are present. These scleral condensations begin to mineralize at HH38. Dpf, days post fertilization. Image from T. A. Franz-Odendaal.*

To broadly contextualize each stage of interest (HH34-HH38) according to the development of the entire embryo and not only the sclera, HH stages are described below, highlighting the corresponding development of the nictitating membrane and the eyelids to that of conjunctival papillae and scleral condensations. At HH34, thirteen to fourteen conjunctival papillae are present and the papillae ring is completely formed. The nictitating membrane extends halfway between the eyelid and the conjunctival papillae. At HH35, the complete ring of conjunctival papillae remains, but the nictating membrane extends to right above the conjunctival papillae. The eyelids extend towards the beak and begin to cover the eyeball. At HH36, conjunctival papillae begin to degenerate and scleral condensations continue to grow. The nictitating membrane covers the dorsal conjunctival papillae and approaches the cornea. The lower eyelid is at the level of the cornea. At HH37, a full ring of thirteen-fourteen scleral condensations can be seen with the naked eye following the removal of the eyelids and the nictitating membrane. The nictitating membrane is at the anterior of the cornea. The lower eyelids covers approximately half of the cornea. At HH38, scleral condensations are mineralized and are now referred to as scleral ossicles. The lower eyelid covers three fourths of the cornea and the space between the upper and lower eyelids is quite decreased (Summarized from Hamburger and Hamilton 1951, republished in 1992). See Hamburger and Hamilton (1951, republished in1992) for complete staging details and images of embryos at each stage.

1.6. Extracellular Matrix, Matrix Metalloproteinases & Extracellular Matrix Molecules

The multifunctional extracellular matrix (ECM) regulates the dynamic behavior of cells and is itself, very dynamic. Fibrous proteins and proteoglycans constitute the ECM (Hynes. 2009). The ECM provides biochemical and structural support to surrounding cells, and facilitates

cell to cell communication and cell adhesion. Additionally, the ECM provides a microenvironment for cell migration, proliferation, differentiation, and apoptosis (Smith et. al. 1999; Leśniak-Walentyn 2016). The ECM is under a homeostatic state of remodeling in response to physiological changes of surrounding cells. Enzymes such as matrix metalloproteinases (MMPs) are key players in matrix remodeling, as they primarily degrade the ECM. MMPs are inhibited by tissue inhibitors of MMPs (TIMPs) to maintain homeostatic balance. MMPs were initially characterized for their function in matrix degradation, however, emerging research has shown that MMPs may influence a wider array of physiological processes (reviewed in Lint and Libert 2007, reviewed in McCawley and Matrisian 2001). MMPs are either membrane bound or are soluble and dispersed throughout the ECM. They are typically expressed in their inactive form and require activation by other MMPs or by proteolytic cleavage, to adopt their active conformation (Sternlicht and Web 2001). MMPs are metal ion dependent (Zinc (II)- and Calcium (II)-), hence the inclusion of 'metallo' in their name (Yang et. al. 2015). The number of MMPs varies across vertebrates. Twenty-seven MMPs have been identified in zebrafish (Wyatt wt. al. 2009), 23 in mice (Jackson et. al. 2010), 24 in humans (Nagase et. al. 2006), 26 in frogs (Fu et. al. 2009), and only six thus far in chicken (Yang et. al. 2008; Patterson et. al. 2013).

Tenascin-C, a matrix glycoprotein has emerged as a potential regulator of skeletogenic condensations boundaries (reviewed in Hall and Miyake 2000). In the homozygous scaleless mutant (sc/sc) where the development of several cutaneous structures as well as scleral ossicles, is defective, there is a mutation in fibroblast growth factor 20 (fgf20) and a defect in tenascin (Shames et al. 1991, 1994; Wells et al. 2012). The cell surface receptor of tenascin-C, syndecan-3, was also identified in developing condensations of other systems such as embryonic chick limb cartilages which are surrounded by a strongly positive syndecan-3 cell layer (reviewed in

Hall and Miyake 2000). Moreover, tenascin-C was observed at the lateral ends of HH37 scleral condensations (Hammer and Franz-Odendaal 2017). Fyfe et al. (1988) speculated that the role of tenascin in scleral condensation formation could be to promote migration to aid in the accumulation of sufficient cells for osteogenesis However, the mechanism by which this may occur, remains elusive even today.

Very little is known of the intricacies of the ECM of the chicken sclera, again revealing the importance of this study to investigate the role of the ECM in scleral condensation growth and development. A potential role for the ECM in condensation growth was recently highlighted by Hammer and Franz-Odendaal (2017), where hydrocortisone was used as a matrix manipulator. Furthermore, Drake and Franz-Odendaal (2018) reviewed the MMPs involved in matrix remodeling and highlighted their role in development. Tenascin-C is a substrate of both MMP1 and MMP2, which again points to a potential role for MMPs in scleral condensation development. Prior to this study, only tenascin-C was confirmed to be present in scleral mesenchyme. Thus, investigating the interactions between condensations and the surrounding ECM can provide significant insight into the complexities of intramembranous ossification in the scleral ossicle model system. The ECM molecules that are of interest to this study will be discussed in further detail in Objective 2.

1.7. Extracellular Matrix Manipulation

1.7.1. Hydrocortisone

Hydrocortisone is one of the matrix inhibitors used in this research project. Hydrocortisone is the medical application of the steroid hormone cortisol that is typically prescribed to treat inflammatory pathologies, and it works by slowing down the immune system (reviewed in Schäcke et al. 2002; Weidenfeller et al. 2005; Vegiopoulos and Herzig. 2007). Cortisol, a glucocorticoid, is secreted by the principal adrenal cortex and is widely known for facilitating the physiological 'fight or flight' response (reviewed in Anderson et al. 1991; reviewed in Schäcke et al. 2002; Weidenfeller et al. 2005; Vegiopoulos and Herzig. 2007). However, it's function is even more diverse. Cortisol facilitates glucose and energy metabolism by regulating the transcription of the enzymes needed for these metabolic processes (reviewed in Meyer et al. 1997; Schäcke et al. 2002). Interestingly, cortisol treatments can lead to bone necrosis and osteoporosis over time, as bone ECM composition is disrupted (presumedly by increasing transcription of enzymes that lead to necrosis and osteoporosis) following the administration of this glucocorticoid (reviewed in Meyer et al. 1997; Schäcke et al. 2002). This suggests a role of glucocorticoids in bone metabolism.

The effects of hydrocortisone have been previously studied in the chicken. Hydrocortisone injections into the chorioallantois of developing chicken embryos were seen to reduce feather development as well as proliferation in skin tissues (Stuart et al. 1972; Démarchez et al. 1984; El-Shabaka 1986; Desbiens et al. 1992; and Turque et al. 1993). Interestingly, a study revealed that hydrocortisone injections administered to both wild type chicken embryos and the *scaleless mutant* embryos, caused a reduction in feather and conjunctival papillae development in both phenotypes (Stuart et al. 1972; Démarchez et al. 1984; El-Shabaka 1986;

Desbiens et al. 1992; and Turque et al. 1993). The effects of hydrocortisone on conjunctival papillae, and consequently scleral ossicles, was also previously studied, and it was revealed that both the development of conjunctival papillae and scleral ossicles could be prevented with the use of hydrocortisone (Johnson 1973). More recently, Hammer and Franz-Odendaal (2017) showed that disruption of the ECM using hydrocortisone, disrupted chicken conjunctival papillae development and consequently, scleral condensation growth. Interestingly however, their study showed that the effects of hydrocortisone on conjunctival papillae was less severe than the effects observed on scleral condensations, despite the 1:1 ratio at which they develop. Ultimately, they determined that hydrocortisone disrupted scleral vasculature and scleral ECM, thus contributing to the more severe effects seen during scleral condensation development. That is, the hydrocortisone effect on condensations was likely indirect, given that their application of hydrocortisone was at earlier stages of development (two days before condensations are induced). They proposed that the ECM disruption observed following hydrocortisone treatment might be due to altered MMP expression and activity (Hammer and Franz-Odendaal 2017).

1.7.2. CP-471474

The global MMP inhibitor, CP-471474, or 2-(4-(4-fluorophenoxy) phenylsulfonamido)-N-hydroxy-2-methylpropanamide, is a sulfonamide hydroxamate as its chemical name reveals. CP-471474 has been studied in mice to deduce its efficacy in the therapeutic treatment of various pathologies such as cancer, rheumatoid arthritis, osteoarthritis and cardiovascular disease (Patterson 2006.). CP-471474 in such applications, works by inhibiting ECM degradation by MMPs, to slow down the progression of the aforementioned diseases. Based on data from the mouse model, the inhibitory activity of CP-471474 (measured as fifty percent inhibitory

concentration (IC_{50} ng/mL)) for various MMPs are as follows:- MMP1: 190; MMP2: 0.4; MMP3: 5.9; MMP8: 3.3; MMP9: 4.0; MMP12: 0.5; MMP 13: 0.1 Rohde et. al. 1999). IC_{50} is commonly used in pharmacology to quantitatively measure the effectiveness of a substance in inhibiting a biological process in vitro by 50% (Aykul and Martinez-Hackert 2016). Although, this matrix inhibitor was used in this research project, little to no previous data is available for the use of CP-471474 in the chicken model organism. Much is still to be discovered about the effects (if any) of this compound on the inhibition of MMPs during scleral ossicle growth and development.

2.0. OBJECTIVES AND HYPOTHESIS

2.1. Hypothesis

Hammer and Franz-Odendaal (2017) showed a role for the ECM in papillae and condensation development, and Jabalee et al. (2013) showed that condensation growth is achieved by the recruitment of mesenchymal cells into growing condensations at their lateral ends. Based on these findings, I hypothesize that the remodeling of the extracellular matrix by metalloproteinases (MMPs) may aid in enabling migratory mesenchymal cells to join the growing skeletogenic condensations at their lateral ends, as they (MMPs) could degrade a physical barrier (i.e. matrix fibers) that surrounds condensations.

2.2. Main Objective

The main objective of this thesis research project is therefore to investigate the role of ECM molecules and their matrix metallaproteinases in condensation growth and development, using the scleral ossicle primordia in chicken embryos as a model system.

2.3. Specific Objectives

The specific objectives of this research are as follows:

1. To investigate the histology of the developing skeletogenic condensations from HH34-38;
2. To deduce the ECM molecules and MMPs that may be involved in regulating condensation formation;

3. To determine the spatial and temporal expression profile of the Tenascin-C over the developmental stages of HH34-HH37;

4. To determine whether altering the ECM influences ossicle number and morphology.

3.0. MATERIALS AND METHODS

The following sections describe the materials and methods that were used in this thesis to examine scleral condensation growth and development in chicken scleral ossicle primordia.

For a histological analysis, serial sections of the sclera were analyzed to assess scleral condensation depth (HH36, HH37 and HH38) and area (HH36 and HH37) over the developmental stages where condensations are visible. Immunohistochemistry was conducted over four developmental stages (HH34-HH37) to examine the spatial and temporal expression profile of tenascin-C.

For inhibition studies, embryos were injected with two different matrix inhibitors-hydrocortisone and CP-471474, to assess the effect of the inhibitors on the development of scleral condensations. Alkaline Phosphatase staining was used to visualize the effects of the matrix inhibitors on scleral condensation development. Following matrix inhibitor injections, a western blot protocol was developed for two new MMP antibodies not previously identified as cross-reacting with chicken tissue. Ultimately, the western blot method would have been used to assess the expression pattern of MMPs following ECM manipulation/disruption. However, due to the COVID-19 pandemic, this experiment was not completed. Protocols for all experiments are listed in detail in the Appendices B-J.

3.1. Embryo Incubations

Chicken eggs were purchased from the Nova Scotia Agricultural College, and temporarily stored at 4°C. Fertilized eggs were then incubated in a Brinsea Ova-Easy Advance

Incubator at 37°C with 40% humidity. Eggs were incubated until desired stages were achieved (HH34- HH38).

3.2. Staging and Fixation

This project explored developmental stages, HH34-HH38. Embryos were removed from their shells and immediately decapitated and placed into a petri dish with chick saline (see Appendix A.1 for chick saline recipe). Distinct anatomical features of the embryo were observed using a Nikon SMZ 1000 dissecting microscope and cross referenced with the features in the Hamburger and Hamilton staging table (Hamburger and Hamilton (1951) to determine the embryonic stage. Embryos were then fixed overnight in 4% paraformaldehyde (Appendix A.2) in 1X phosphate buffered saline (PBS) (pH 7.4) (Appendix A.3) at 4°C. Embryos were then washed in 1XPBS (2 x 15 minutes) and stored in new 1X PBS at 4°C to avoid tissue degradation. Additionally, some embryos were fixed overnight in 10% neutral buffered formaldehyde (NBF) (Fisher Scientific 72210), processed, then stored in 70% EtOH at room temperature, depending on the protocol to follow.

3.3. Fine Tissue Dissections for Histology and Immunohistochemistry

Eyes of HH34-37 embryos were dissected out of the embryo heads. Two to three embryos were staged out of a batch of eggs to verify the age of the developing embryos according to the Hamburger and Hamilton (1951, republished in 1992) and were representative of the entire batch of eggs. Each eye was dissected in half and the vitreous humor and lens were removed. The anterior half of each eye (with respect to the cornea) was then isolated. A cut was made through the choroid fissure and the papilla closest to it. From this region, four papillae

were counted anticlockwise and another cut was made between the fourth and fifth papillae as shown in Figure 4. This group of papillae is largely comprised of the temporal group of papillae and will be referred to as such throughout this thesis. The other parts of the eye were stored in separate tubes in 1X PBS at 4°C in the event that they would be needed for additional experimentation (Figure 4).

For the HH38 histological data that compares the depth of temporal/dorsal condensations to the opposite nasal condensations, dissections differ, as outlined in Figure 5. Again, the whole eye was dissected in half, isolating the anterior half of the eye, and the vitreous humor and lens were removed. First, the anterior half of the eye was cut in half vertically. Then, two to four temporal/dorsal condensations and surrounding tissues were dissected as indicated by the red dashed box in Figure 5, and stored 1X PBS at 4°C. Next, two to four opposite nasal condensations were dissected as indicated by the black dashed box in Figure 5, and similarly stored, separately from the temporal/dorsal condensations. These dissected tissues were embedded separately in order to be able to compare condensation depth in these two regions (temporal vs nasal).

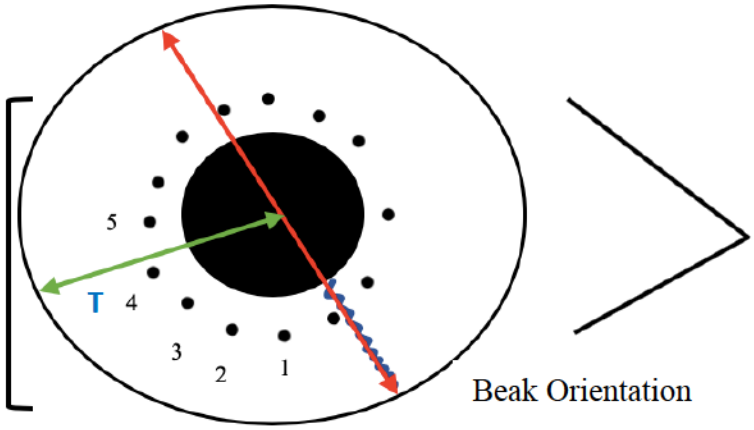

Figure 4. *A schematic showing the dissections used for tissue embedding and sectioning for Objective 1a and Objective 3. Dots represent either conjunctival papillae (HH34 and HH35) or scleral condensations (HH36 and HH37), depending on the developmental stage. The five papillae/condensations in the area of interest are numbered. The red arrow represents the first cut of the anterior half of the eye along the choroid fissure (blue squiggle line). The green arrow represents the second cut to retrieve the region of interest, which contains mostly papillae of the first forming papillae group, the temporal group. T, temporal.*

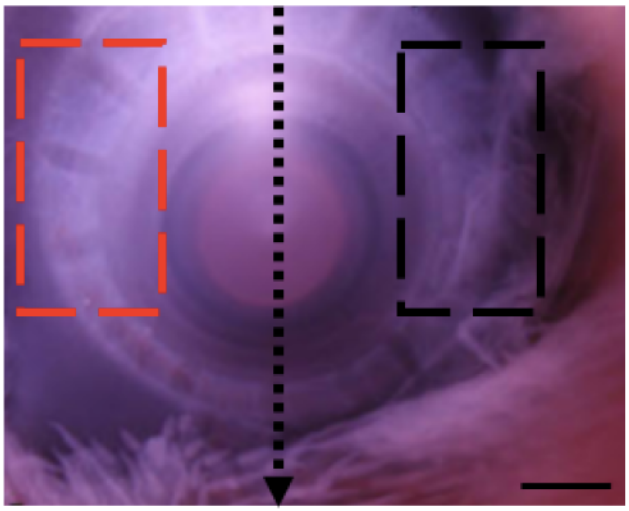

***Figure 5**. Wholemount image of the anterior of the chicken eye at HH37 demonstrating the dissections performed on HH38 eyes. The anterior half of the eye was cut in half as indicated by the black dashed arrow. Two to four ossicles of the temporal/dorsal groups and surrounding tissues were dissected out as indicated by the red dashed box and stored. Two to four opposite ossicles of the nasal group were dissected out as indicated by the black dashed box. Scale bar- 1mm. Photo from the Franz-Odendaal Lab.*

3.4. Paraffin Wax Embedding

Dissected eye samples (as previously described) were washed in 1X PBS 2x15 minutes and then dehydrated to 100% ethanol (EtOH) using an EtOH-distilled water series of 25%, 50%, 70%, 90%, 100%. In glass vials, samples were incubated in Citrisolv (Fisher Scientific: 22-143975) for one hour at room temperature. Citrisolv is a clearing agent that dissolves paraffin wax without hardening or shrinking tissues. After one hour, the Citrisolv was removed and replaced with fresh Citrisolv solution. Samples were then incubated in Citrisolv for another hour at room temperature. Using heated forceps, samples were placed into a heated metal mold

containing molten paraffin wax (Paraplast Xtra tissue embedding medium, Fisherbrand: 23-021-401). Metal molds were transferred to a Napco: Model 5831 vacuum oven where samples incubated at 15mmHg pressure and 58°C for two hours. After two hours, the molten wax was changed, and samples incubated in the vacuum oven overnight. The following day, new molten wax was added, and samples were placed back in the vacuum oven for two more hours. Wax was changed once again for fresh molten wax, then samples were embedded in the wax by immediately freezing on a square ice pack. Samples were oriented upright using forceps so that the edge of the cornea touched the bottom of the metal mold (as shown in Figure 6). Previously labeled plastic embedding holders were pressed down into place on top of the metal mold and filled with wax. Wax was left to harden for a few minutes at room temperature. Then, sample wax blocks were stored at -20°C to harden further for sectioning. This embedding procedure is provided in Appendix B.

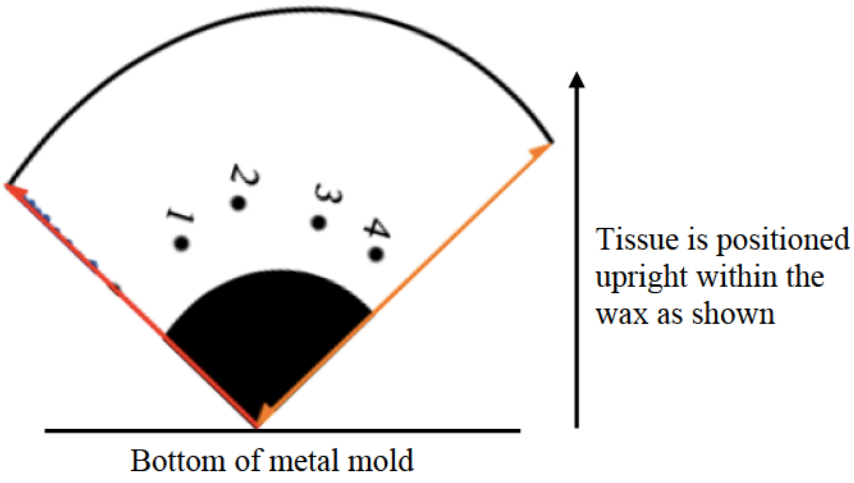

Figure 6. *A schematic showing the orientation of the eye tissue as it is embedded into the wax. This embedding orientation was consistent for all tissue embedding such that the cornea was at the bottom of the metal mold and therefore the cornea is sectioned first.*

3.5. Sectioning

Sample blocks were retrieved from the -20°C freezer and the plastic holders and excess wax surrounding the plastic holders was carefully removed using a razor blade. Sample blocks were then trimmed using a razor blade to form a tetrahedron around the sample to indicate orientation. A Leitz 1512 microtome was used to section samples at 6µm. Sample blocks were oriented vertically into the microtome so that samples could be sectioned longitudinally, starting at the edge of the cornea. Droplets of water were added to slides using a small paint brush to aid in positioning the section properly on the slide. Sections were picked up and placed on (3-Aminopropyl) triethoxysilane (APTES) (see Appendix C) coated slides with a small wet paint brush. Five to ten consecutive sections were collected per slide. Slides were then placed on metal trays and left in an incubator at 37°C overnight to dry. This procedure is outlined in Appendix D.

3.6. Hall's and Brunt's Quadruple Staining

Hall's and Brunt's Quadruple (HBQ) Stain was developed to distinguish cartilage from bone even at their earliest stages of differentiation (Hall 1986). This stain has five elements that stain four different tissue types. Alcian Blue stains cartilage bright blue. Mayer's Haematoxylin stains nuclei black. Direct Red stains calcified bone bright red and non-calcified bone red. Celestine Blue stains mesenchyme or other connective tissue components turquoise/green. Phosphomolybdic Acid selectively prevents staining of cartilage by direct red.

Slides were placed in Citrisolv 2x5 minutes to dissolve wax from around tissues. Slides were then rehydrated through an EtOH-distilled water series, 100%, 90%, 70%, 50%, for one minute each then, dH_20 for two minutes. Samples were stained in a series of Celestine Blue (five minutes), Haematoxylin (five minutes), Alcian Blue (five minutes), Phosphomolybdic Acid (one minute) and Direct Red (five minutes). Samples were quickly rinsed in 100% EtOH and washed four times in Citrisolv. Cover slips were mounted on slides using DPX (Sigma: 44581). Slides were placed flat on metal trays and left in the fume hood to dry overnight. A Nikon Eclipse 50i compound microscope was used to visualize sections. A Nikon camera and the NIS Elements Software package were used to photograph sections. Figure 7 shows a cross section of the sclera stained with HBQ stain. All sections at HH34-38 were stained with HBQ. Details for this HBQ staining procedure are provided in Appendix E.

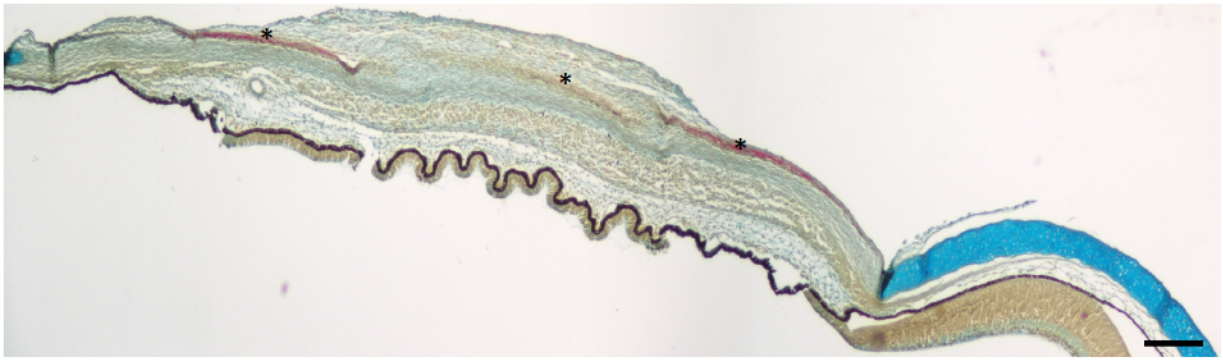

Figure 7. *Tissue section of the sclera at HH37 stained with Hall and Brunt's Quadruple stain. The ciliary process is the wavy black line seen at the bottom of the section. The scleral cartilage is stained bright blue by Alcian blue and indicated by an arrow. Nuclei are stained black by Mayer's Haematoxylin. Non-calcified bone is stained red in the developing condensations by Direct Red as indicated by asterisks. The mesenchyme and other connective tissue components are stained turquoise/green by Celestine Blue. Arrow, scleral cartilage. Asterisks, scleral condensations. Scale bar- 100µm.*

3.7. Measuring Condensation Depth and Area

To ensure that measurements were consistent throughout data collection, the condensation boundaries were defined. The outer most point of the condensation where an aggregation of cells and dark staining is seen with little to no visible spaces between the cells defines the 'end' of a condensation. If there were regions where epithelium was missing from the section, the line feature in the NIS elements software was used to connect the breaks in the epithelium, to create a presumed epithelium for missing regions. In order to quantify and compare the condensation depth within the temporal group at two different stages, pictures of cross sections through the scleral ossicle primordia at stages HH36 and HH37 were taken. Using NIS Elements, the condensations were also outlined (red dashed line, Figure 8). The parallel line

feature was used, first outlining the length of the condensation (black, dashed line, Figure 8), and then, the second line was drawn in parallel to the first line representing the level of the epithelium (black, continuous line, Figure 8). A double-sided arrow, joining the respective midpoints of both lines represents the distance from the epithelium to the condensation, and thus represents the condensation depth. Two to three condensations (depending on the visual clarity of each condensation) were measured from one section of a given eye. The average depth of the condensations within a given eye represents the condensation depth for that embryo (one section from one eye was measured from each embryo). In order to determine changes in depth over time, multiple embryos (n= 7-11 for HH36 and HH37) were measured in this way. Condensation area was measured on the same sections (at HH36 and HH37) by outlining the shape of the condensation using the computer mouse and the NIS elements area function (Figure 8, outlined in red). Again, averages were taken for condensation area within a given eye, representing the condensation area for that embryo (one eye was measured from each embryo). To investigate the tilt of the scleral ossicle ring, which is defined by the position of the ring with respect to the surface (epithelium), condensation depth was measured in different regions of the same eye at the same stage (HH38), and condensations were measured from three different embryos (n=3). For both measures of condensation depth and area, the number of embryos measured were n=7 for HH36; n=11 for HH37; and n=3 for HH38. The raw data for measures of condensation depth and area are listed in Appendix F.

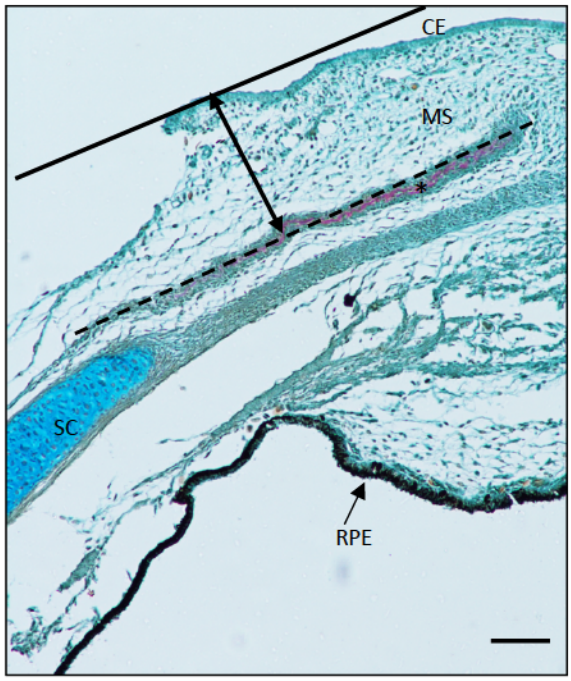

Figure 8. *Method of measuring the depth and area condensations. The area of the condensation is calculated using the area function on NIS Elements after outlining the condensation. The red dashed line was the contour used to generate the area measurement. Condensation depth is measured using parallel line feature on NIS Elements. The first line (black, dashed line) outlines length of condensation and a second line of similar length (black, continuous line) was placed in parallel to the first (dashed) line at the epithelium as shown. The length of the double-sided arrow represents the condensation depth. CE- Conjunctival epithelium; MS- mesenchyme; RPE- pigment epithelium; SC- scleral cartilage. Asterisk- scleral condensation outlined in red. Scale bar- 50µm.*

3.8. Immunohistochemistry

The immunohistochemistry protocol used in this thesis was adapted from Hammer and Franz-Odendaal (2017). Optimization of the protocol was conducted using a primary antibody for tenascin-C (M1-B4 Developmental Studies Hybridoma Bank) at a 1:2 concentration on chick scleral cartilage, known to be positive for tenascin-C (Hammer and Franz-Odendaal 2017). Rabbit anti-mouse IgG-HRP conjugated antibody (Sigma Aldrich A9044) was used at 1:200 concentration. See Table 17 (a & b) in Appendix L for further information on the antibodies used throughout this thesis. A rabbit serum block solution (Appendix G.4) and a milk block solution (Appendix G.5), were used to reduce background staining. A similar protocol (conditions as described below for tenascin-C) was used to test anti-syndecan-3 (1:200; 1:100, ABCAM63932) and four versions of anti-MMP1 (1:2, 14A302; 1:2, 3A6B4; 1:2, 3B8D12; 1:2, 5H7B1-Developmental Studies Hybridoma Bank). However, further optimization for these antibodies was not successful due to time constraints and therefore will not be included in this study.

Each immunohistochemistry experiment contained four slides of tissue sections from the same sample block: two positive controls with both primary and secondary antibody and two negative controls. One negative control was treated with only the primary antibody and no secondary antibody. The other negative control was treated with only the secondary antibody and no primary antibody. A distinct difference in intensity of expression between the positive and negative controls indicated whether or not the experiment was successful. Little to no background detection on negative control slides would mean that detection seen on positive control slides were attributed to the expression of the protein.

To initiate the protocol, slides were placed in Citrisolv to dissolve wax (two times for five minutes each). Sections were hydrated through an EtOH-distilled water series and brought to

distilled water. Super PAP Pen (Biotium: 22006) was used to create a hydrophobic barrier around the sections to keep solutions on the tissue. This barrier was reinforced throughout the protocol if needed. Tissue sections were incubated in 3% hydrogen peroxide in a humidity chamber for 20 minutes at room temperature to block endogenous peroxidase activity. The slides were washed in 1X PBS. Sections then underwent antigen retrieval for eight minutes at 90°C using 0.1 % triton X- 100 in 0.1% sodium citrate buffer (pH 6) (Appendix G.2). Sections were incubated with serum blocking solution for one hour in a humidity chamber at 37°C. Sections were washed briefly in 1X PBS, then incubated in a milk block solution for one hour in a humidity chamber at room temperature. Both blocking steps prevent non-specific binding of antibodies to proteins. Sections were washed briefly in 1X PBS, then the primary antibody, M1-B4 (at 1:2 dilution) was applied to the designated slides. The no-primary negative control was treated with serum block solution. Slides were then incubated in a humidity chamber overnight at 4°C.

Slides were washed in 1X PBS for 3x5 minutes the following morning. The appropriate slides were then treated with secondary antibody (rabbit anti-mouse IgG-HRP conjugated- Sigma Aldrich A9044) at a concentration of 1:200. The no-secondary negative control was treated with serum block solution. Sections were then incubated at room temperature for two hours in a humidity chamber. Sections were washed in 1X PBS, three times for five minutes each. During the washes, 3,3'- diaminobenzidene (DAB) peroxidase (Sigma D0426) was dissolved in deionized water. After the washes, DAB was applied to the sections for 8-12 minutes in a humidity chamber under the fume hood. In the reaction, DAB is oxidized by hydrogen peroxide (via hydrogen peroxidase) and precipitates as a brown to dark brown color at the site of protein detection or expression. Sections were washed in distilled water following DAB detection.

Coverslips were mounted onto slides with Fluoroshield (Sigma F6182) and left overnight at room temperature. Clear nail varnish was used to seal the edges of the coverslip the following morning. A Nikon Eclipse 50i compound microscope was used to observe results. A Nikon camera and the NIS Elements Software package were used to photograph results. HH37 chick sclera tissues were used to troubleshoot the protocol. For troubleshooting, n=3 embryos were used. For data analysis the, the number of embryos used were as follows: n=3 for HH34; n=3 for HH35; n=4 for HH36, n=4 for HH37. Details of this protocol are provided in Appendix G. Supplemental Information summarizing the experimental runs for each stage are provided in Appendix G.9.

3.9. Hydrocortisone Injection Experiments

Chicken embryos were staged to HH34 after incubating in an automatic rotating incubator as described above in 2.1. This experiment involved a hydrocortisone injection group, and two controls – a no injection control and a control injected with the solvent used to dissolve hydrocortisone. While tilted at a 60° angle, a hole was introduced to each eggshell on the end at the site of the air sac. Control injection HH34 embryos were administered 100µl of Howard Ringer's Solution and EtOH (Appendix H.1). Treatment group HH34 embryos were administered 100µl of 2mM Hydrocortisone in Howard Ringer's Solution and EtOH (Appendix H.2). Embryos were returned to a non-rotating egg incubator. A second injection of identical volume and concentration to the above was administered 28 hours after the first injection (now at HH35), as well as a second control injection. Embryos were returned to the incubator after the second injection. Three days after the second injection, at HH38, embryos were sacrificed and fixed in 4% PFA (Appendix A.2) and stored in 1X PBS (Appendix A.3). For troubleshooting

purposes, n=4 embryos for each group (control no injection, control injection and hydrocortisone treatment) were used. Figure 9 summarizes the developmental time frame of when hydrocortisone injections were administered. For data analysis, n=5 embryos for each group (control no injection, control injection and hydrocortisone treatment) analyzed. Details for this procedure are provided in Appendix H.

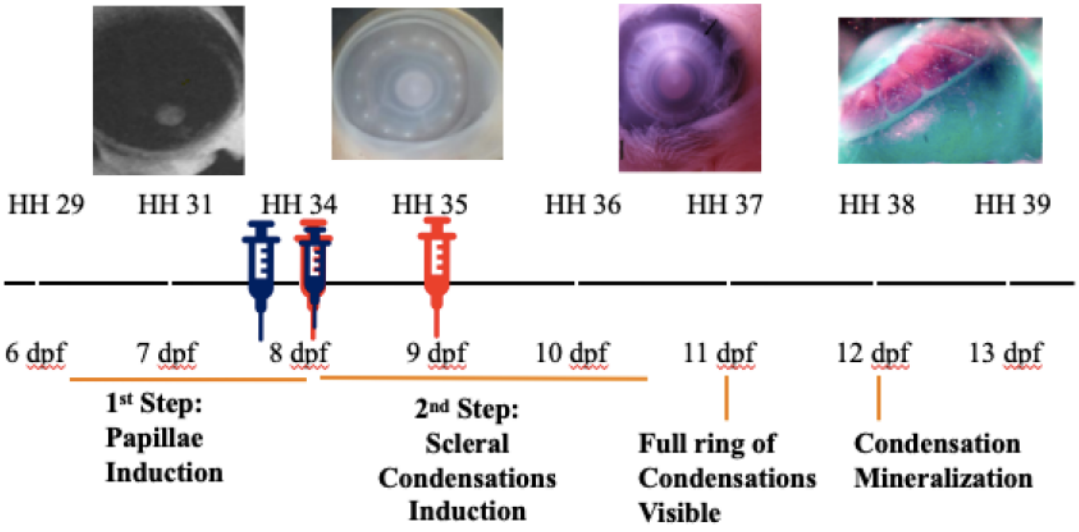

Figure 9. *Developmental time points for inhibitor injections in the context of scleral ossicle formation. A double hydrocortisone injection (red syringes) was administered at HH34 and then 28 hours later at HH35. CP-471474 was injected at HH34 (second blue syringe) when the full ring of papillae is visible. CP-471474 was also injected at HH33 (into different embryos, first blue syringe) which is just before the full ring of papillae forms. Red syringe, hydrocortisone. Blue syringe, CP-471474. Timeline modified from the Franz-Odendaal Lab.*

3.10. CP-471474 Injections Experiments

The global MMP inhibitor, CP-471474, (TRC #C781305) was received in powder form and reconstituted in dimethyl sulfoxide (DMSO) (Calbiochem #6010) to create a concentration of 5mg/ml of stock solution (Appendix H.3). This stock solution was further diluted to create the working concentrations (1:100, Appendix H.4 and 1:50, Appendix H.6) used in this thesis. The concentration of 1:100 was used as a starting point to find the lowest working concentration of CP-471474 in our model system, taking into account the high cost of the inhibitor. Chicken embryos were staged to desired stages as previously described. Various injection time points (early at HH33 or standard time point at HH34) and concentrations of this inhibitor (1:50 and 1:100) were tested since CP-471474 had not been previously used in the Franz-Odendaal lab and therefore, needed to be optimized. A standard injection timepoint refers to HH34, the stage after complete papillae formation (phase one of scleral ossicle development), and the early start of scleral condensation induction (phase two of scleral ossicle development). Early time point refers to injections administered at HH33, just before the full ring of papillae is formed and when there is no evidence of scleral condensations (Andrews and Franz-Odendaal 2018). Figure 9 summarizes the developmental time frame of when CP-471474 injections were administered.

As for concentrations of CP-471474, a 1:100 concentration was used to troubleshoot the potency of CP-471474. For troubleshooting purposes at a concentration of 1:100, n=5 for double injection treatment group; n=5 for single injection early treatment group; n=5 for single injection standard time treatment group; n=5 for control injection early group; n=5 for control injection standard group; n=3 for control no injection group. Table 1 shows the troubleshooting trials. For data analysis, n=3 for single injection early group 1:100; n= 3 for single injection early group 1:50; n=3 single injection standard group 1:50; n=2 single control injection early 1:100; n=2

single control injection standard 1:100; n=2 single control injection standard 1:50; n=2 single control injection early 1:50; n=2 control no injection. Table 2 shows the experimental trials. Single and double CP-471474 injections were delivered at various concentrations in the manner previously described for hydrocortisone injections.

Table 1. Summary Of CP-471474 Troubleshooting Experiments. CNI, control no injection; CI, control injection; CP, CP-471474; N/A, not applicable.

Group	Concentration	Number of Embryos
CNI	N/A	3
CI HH34	1:100	5
Double CP Injection (HH34 & HH35)	1:100	5
Single CP Injection HH34	1:100	5
Single CP Injection HH33	1:100	5

Table 2. Summary Of CP-471474 Data Analysis Experiments. CNI, control no injection; CI, control injection; CP, CP-471474; N/A, not applicable.

Group	Concentration	Number of Embryos
CNI	N/A	2
CI HH34	1:100	2
CI HH33	1:100	2
CI HH34	1:50	2
CI HH33	1:50	2
Single CP Injection (HH34-standard)	1:100	3
Single CP Injection (HH33-early)	1:100	3
Single CP Injection (HH34- standard)	1:50	3

Control injection embryos were administered 100µl of Howard Ringer's Solution and DMSO (Appendix H.5). Treatment group embryos were administered 100µl of various concentrations (1:100 and 1:50) of CP-471474 Inhibitor (Appendix H.4) in Howard Ringer's Solution and DMSO (Appendix H.5 and Appendix H.7, respectively). Embryos were returned to incubator and raised to desired stage HH37 or HH38, then sacrificed and fixed in 4% PFA and stored in 1X PBS. For the double injection treatment group, a second injection (of the same concentration as the first) was administered six hours after the first injection- likewise for the control double injection group. Embryos were returned to incubator after second injection. Three days after second injection, HH38 embryos were sacrificed and fixed in 4% PFA and stored in 1X PBS. Details for this protocol are provided in Appendix H.

3.11. Alkaline Phosphatase Staining

Fixed embryo heads from injection experiments (3.9 and 3.10 above) were bisected and eyelids were removed. Bisected heads were washed in distilled water and then incubated in tris-maleate buffer (Appendix I.3) pH 8.3 for one hour at room temperature. Samples were then incubated in alkaline phosphatase substrate solution (Appendix I.2) for one hour in a glass vial in the dark. Following, samples were washed in saturated sodium borate water (Appendix I.5) to stop the alkaline phosphatase reaction. Samples were left in bleach solution (Appendix I.6) overnight, then processed through a graded glycerol/KOH solution to 4:1 concentration of 100% glycerol: 1% KOH (Appendix I.7, I.8 and I.9, respectively) the next morning. Samples were visualized using a stereomicroscope and imaged using Nikon NIS Elements imaging software. A morphological scale was developed (Table 3) to characterize the extent of the effects observed

on the scleral condensations of both inhibitors after staining with alkaline phosphatase. Details for this protocol are provided in Appendix I.

***Table 3**. Morphological classification of scleral condensations following treatment with matrix inhibitors.*

Phenotype	**Description**
Normal	No defects
Mild	Change in morphology of condensation; No condensation loss
Moderate	Change in morphology of condensations; Loss of 2 condensations maximum
Severe	Loss of 3-14 condensations

3.12. Staging, Dissections and Tissue Extractions for Western Blot

Chicken embryos were staged to HH37. Corneas and scleral condensations were dissected separately from the eyes of 20 embryos as shown in Figure 10. Tissues were placed in 2ml centrifuge tubes containing radioimmunoprecipitation assay (RIPA) buffer on ice (see Appendix J.1 for recipe). RIPA buffer contains Roche cOmplete cocktail tablets (Roche: 11873580001) to prevent protein degradation. Four biological replicates were created for each tissue type. Each biological replicate contained 10 pieces of tissue (i.e., one biological replicate for cornea tissue contained 10 corneas, and one biological replicate for scleral condensations contained 10 complete scleral condensation rings). Each individual biological replicate contained tissues from five different embryos. Tissues for each biological replicate were homogenized as a single sample and placed on a shaker at 4°C for two hours. Tubes were centrifuged for 20 minutes at 12,000 rpm at 4°C. Supernatants were transferred to fresh tubes and pellets were

discarded. Supernatants were stored at -80°C. The procedure for protein extraction is outlined in Appendix J.1.

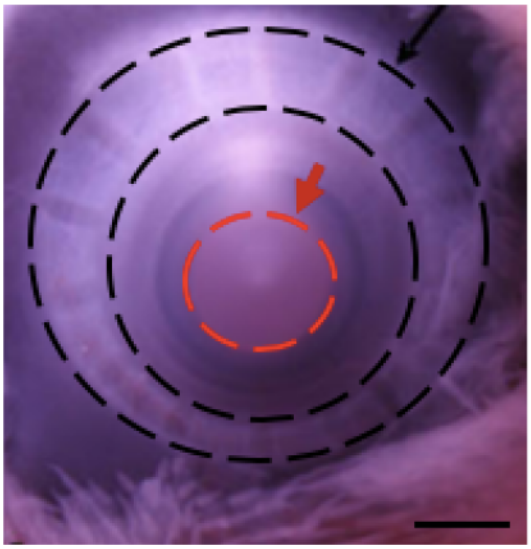

Figure 10. *Wholemount image of the anterior of the chicken eye at HH37 showing how dissections were made for tissue collection for Western Blot analyses. The black arrow points to the ring of scleral condensations outlined by the black dashed lines. The ring of scleral condensations was dissected out as a complete ring. The red arrow points to the cornea, outlined by the red dashed line. Both structures were dissected out using fine forceps and scissors. Scale bar- 1mm. Photo from The Franz-Odendaal Lab.*

3.13. Western Blot

Western Blot analysis was first carried out using standard procedures and are outlined in Appendix J.7-J.9. Proteins concentrations were quantified using the Pierce BCA Assay (Thermo Scientific # 23225, Appendix J.2). Protein lysates were separated by SDS-PAGE in equal amounts. SDS-PAGE (Appendix J.7) was tested out under reducing conditions (with beta-

mercaptoethanol- Calbiochem #6010). Then, proteins were transferred to nitrocellulose membranes via gel electrophoresis overnight at 50 mAmps (Appendix J.8). To establish a working control, the membrane was incubated with tubulin at a 1:1000 concentration (AB6046) for one hour at room temperature. The membrane was rinsed in cold PBST (Appendix J.6) then incubated with secondary antibody (Peroxidase AffiniPure Goat Anti-Mouse IgG (H+L)-Jackson Labs 115-035-003) at a 1:12000 concentration for one hour at room temperature. The membrane was rinsed again and stained with DAB for 10-15 minutes to detect protein signal (Appendix J.10). Membranes were rinsed in distilled water, then imaged for analyses.

Following the establishment of a working protocol using tubulin as the positive control, a similar approach was used to troubleshoot various concentrations for MMP1 (ABCAM 137332) and MMP2 (ABCAM 97779), the antibodies of interest. Through an extensive process of troubleshooting, it was shown that non-reducing (no beta-mercaptoethanol) conditions were optimal for these MMPs. The optimal working concentrations for MMP1 and MMP2 were established to be 1:1377 and 1:510 respectively. The details of the establishment of a working Western Blot protocol for MMP1 and MMP2 is reported in the results section as this was a significant portion of the work done to complete this thesis and is a significant contribution to this field of research as neither antibody had been verified to work against chicken tissues. Additional supplemental information on this western blot procedure is available in Appendix J.11-J.12. See Table 17 (a & b) in Appendix L for further information on the antibodies used throughout this thesis.

3.14. Statistical Analysis

Welch's t- test (two-tailed), was used to calculate statistical significance for measures of condensation depth and condensation area between developmental stages, and condensation depth between nasal and temporal/dorsal groups at HH38. Equal variances were not assumed for these analyses. A one-way ANOVA was performed to account for variance for measures of condensation depth and condensation area between developmental stages. Statistical analyses were performed on Minitab and all outputs are found in Appendix K.

4.0. RESULTS

4.1. Skeletogenic Condensation Morphology Changes Over Developmental Time

Understanding the histology of the intricate stages of scleral condensation growth over developmental time is a foundational step that provides important insight into the process of condensation formation in intramembranous ossification. In order to undertake such investigations, cross sections through the developing chick sclera were stained with HBQ stain to visualize the condensations and surrounding tissues. As the conjunctival papillae are degenerating at HH36, scleral condensations are developing beneath them (Figures 11A and 11D). (Franz-Odendaal 2008). Scleral mesenchymal cells continue to migrate to the future site of the bone at HH36. As the condensation grows to reach its critical size, differentiation occurs and osteoid is deposited (Figures 11B and 11E) until the entire condensation is mineralized (Figures 11C and.11F). These histological images confirm previous data in the literature describing the progressive phases of skeletogenic condensation development (Hamburger and Hamilton 1951; Franz-Odendaal 2008; Jabalee and Franz-Odendaal 2013). From HH36 to HH38, condensations grow more and the ring of condensations becomes more tightly packed. At HH38, cross sections through the sclera show an overlapping morphology as seen in Figure 11F. It is interesting to visualize how the structure of the condensations and the surrounding tissues change as the condensations grow and develop.

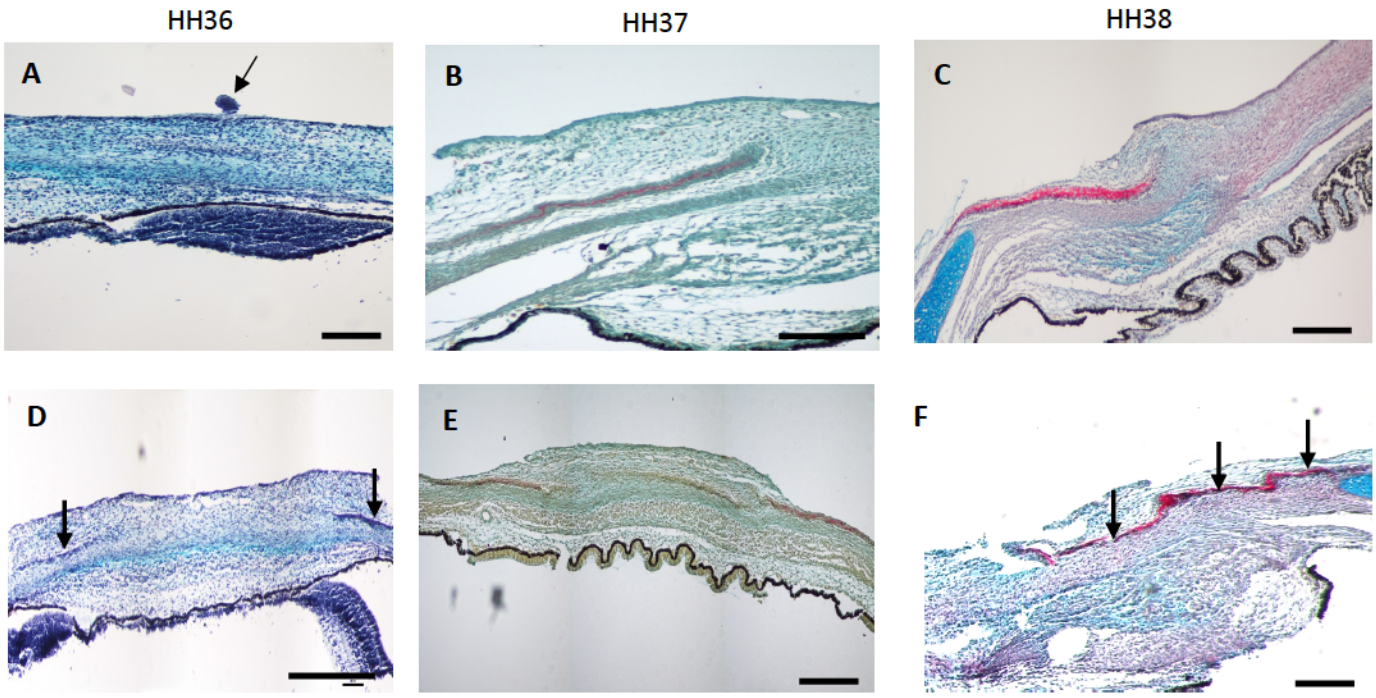

Figure 11. *Cross sections of the sclera show the growth and development of scleral condensations over developmental time. Sections are oriented with the conjunctival epithelium at the top and the retinal pigment epithelium or ciliary process (depending on the dissection). All slides are stained with Hall's and Brunt's Quadruple stain. Note the conjunctival papilla in A. A-C, Single condensations at developmental stages HH36-38. D-F, Multiple adjacent condensations at various developmental stages. A & D, HH36; B & E, HH37; C & F, HH38. Arrow (A) indicates conjunctival papillae. Arrows (D) indicate small developing condensations. Arrows (F) indicate overlapping mineralized ossicles. Scale bar A, C, D-F, 100μm. Scale bar B & D, 50μm.*

4.2. Skeletogenic Condensation Area Increases Over Developmental Time

Figure 11 highlights the remarkable morphological changes of the scleral condensation from when the condensations are clearly visible (with HBQ stain) to when the condensations grow and become mineralized bones marking the completion of scleral ossicle induction, and the start of differentiation into bone. Therefore as expected, the area of the condensations (i.e., their size) increases over developmental time (Figure 12). The data shows that from HH36 to HH37 (a period of 24 hours), the condensation area (of the temporal group of condensations) grows from $3524 \pm 387\ \mu m^2$ (n=7) to $7731 \pm 958\ \mu m^2$ (n=11) with statistical significance (two-tailed t-test: $p<0.05$, df=12; one-way ANOVA; $p<0.05$, df=1). Error values indicate standard error mean. That is, the condensations approximately double in size (via migration of mesenchymal cells into the condensations) between these two stages, a period that is only 24 hours. Raw data for this graph is provided in Appendix K.5.

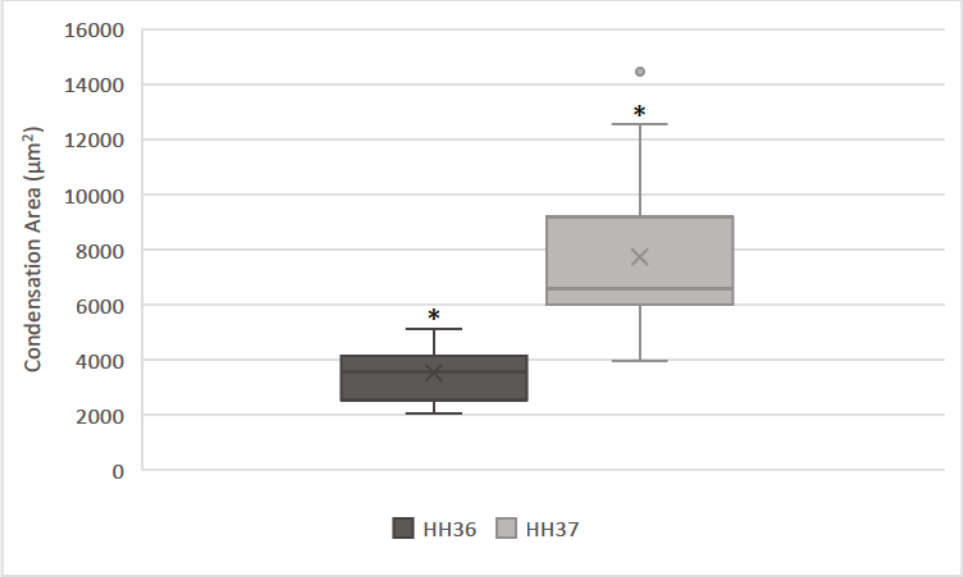

Figure 12. *The area of scleral condensations at HH36 and HH37. Condensation area is greater at HH37 than at HH36. X inside of boxes indicates mean. There is one outlier in the HH37 data set. Asterisks indicate statistical significance.*

4.3. Skeletogenic Condensation Depth Changes Over Developmental Time.

Through investigating the structure and histology of developing scleral condensations, one can understand the initial stages of scleral ossicle development. A 6µm thick cross section of the sclera, stained with HBQ, highlights the structural organization of tissues at HH37 (Figure 13), when a full ring of developing scleral condensations are first observed with the naked eye (see Figure 10, Materials and Methods). From Figure 13, it is apparent that some condensations are situated deeper in the scleral mesenchyme than others. This observation prompted the exploration of scleral condensation depth at different developmental stages.

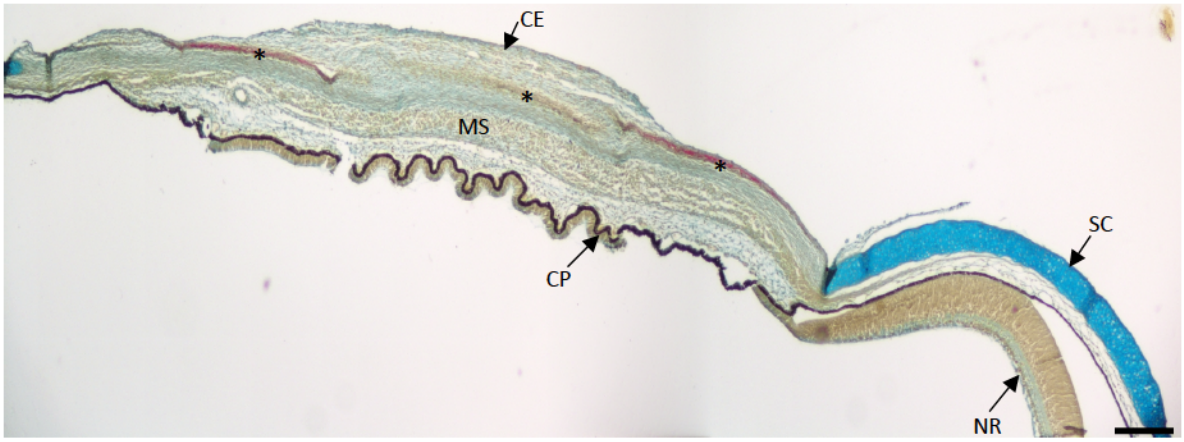

Figure 13. *Three developing scleral condensations are seen at varying depths, at HH37. Hall and Brunt's Quadruple stained tissue section of the sclera. Asterisks indicate developing condensations of the temporal group. Note that the view of the central condensation compared to the other two condensations and is at an intermediate depth. The red stain indicates bone osteoid, which indicate the sites of the osteogenic scleral condensation. CE, Conjunctival epithelium; CP, ciliary process MS, mesenchyme; SC, scleral cartilage, NR, neural retina. Scale bar, 100µm.*

The condensation depth of the temporal group of condensations at developmental stages HH36 and HH37 was measured as the distance of the condensation from the epithelium. Figure 14 represents the condensation depth between stages HH36, HH37 and HH38. When comparing the depth of the condensations between HH36 and HH37, the condensation depth was substantially greater at HH37. As previously mentioned, the area of the condensations increased over developmental time (Figure 12), illustrating a continuous growth and expansion as further development occurs. The data shows that from HH36 to HH37 (a period of 24 hours), the condensation depth increased from 97.7± 4.1 µm (n=7 embryos) to 117.2± 5.4 µm (n=11 embryos), with statistical significance (two-tailed t-test: $p<0.05$, df=15; one-way ANOVA,

$p<0.05$, df=1), then decreased to 97.5 ± 4.36 µm. That is, depth increased by approximately 20% between HH 36 and HH37, and then decreased by 17% from HH37 to HH38 (unable to carry out statistical test on HH38 data because of the small sample size, n=3). Raw data for Figure 14 is given in Appendix K.5.

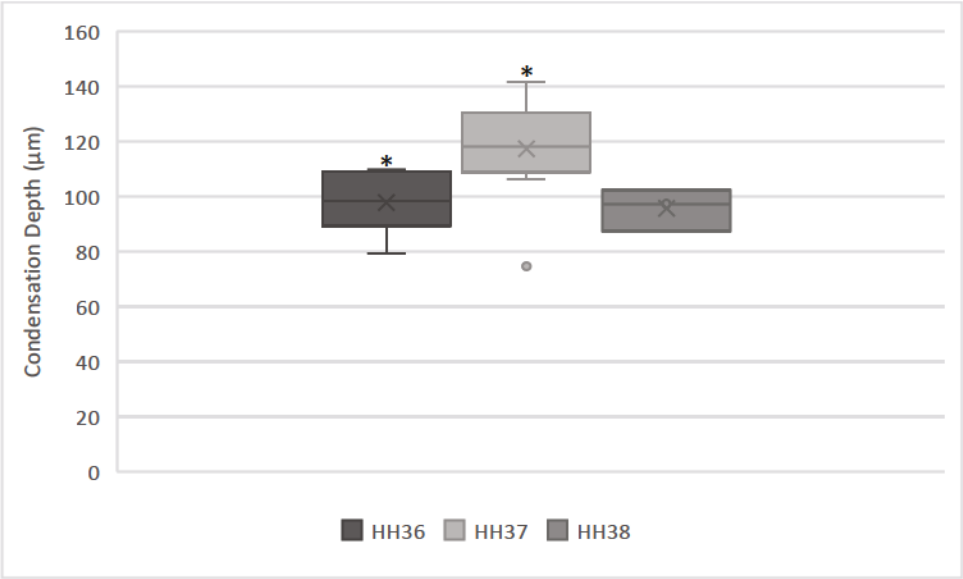

Figure 14. *The scleral condensation depth at HH36, HH37 and HH38. Scleral condensations appear to be deeper at HH37 in comparison to those at HH36 in the first condensation group, the temporal group. However, scleral condensations appear to more superficial at HH38 in comparison to those at HH38. X inside of boxes indicates mean. Asterisks indicate statistical significance. There is one outlier in the HH37 data set. Statistical analysis was not carried out on HH38 data due to small sample sizes.*

4.4. Skeletogenic Condensation Depth Varies Within A Given Stage of Development

A variation of scleral condensation depth was observed both over time (Figure 12) and at a specific stage (HH38, Figure 15). This was an interesting observation that led to the exploration of the orientation of the ring of scleral ossicles within a given eye. To further investigate this observation, the depth of larger mineralized condensations (temporal and dorsal groups) was measured and compared to the depth of the smaller opposite mineralized condensations (nasal group) within a given eye, at HH38.

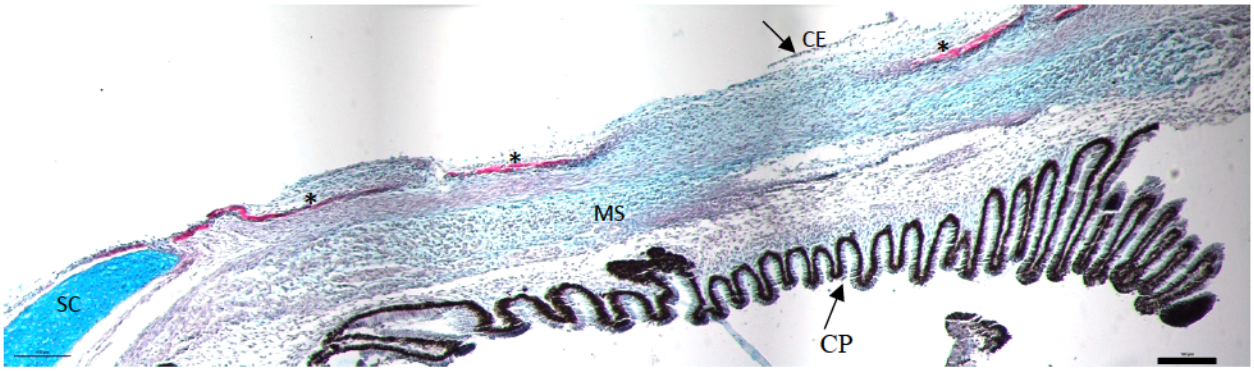

Figure 15. *Mineralized scleral condensations are seen at varying depths even at HH38. Halls and Brunt's Quadruple stain of the sclera. Note that the conjunctival epithelium is broken in some areas. Gray shadows resulted from the stitching of the image at two places. Asterisks indicate mineralized condensations. CE, Conjunctival epithelium; CP, ciliary process; MS, mesenchyme; SC, scleral cartilage. Scale bar, 100 µm.*

Within a given eye, the depth condensations in the temporal and dorsal groups at HH38 is greater than that of the condensations in the opposite nasal group at HH38 (Figure 16). The condensation depth in the nasal group was 81.73 ± 3.57 µm (n=3 embryos), while the depth of the temporal and dorsal groups was 95.70 ± 4.36 µm (n=3 embryos) at HH38. These are statistically

significant (two-tailed t-test: $p<0.05$, $df=3.85$). That is, the condensation depth changed by approximately 15% from one side of the eye to the other side. Variations of condensation depth within a given eye indicate that the scleral ossicle ring is orientated at a tilt and is not at a uniform distance from the epithelium in all positions around the eye.

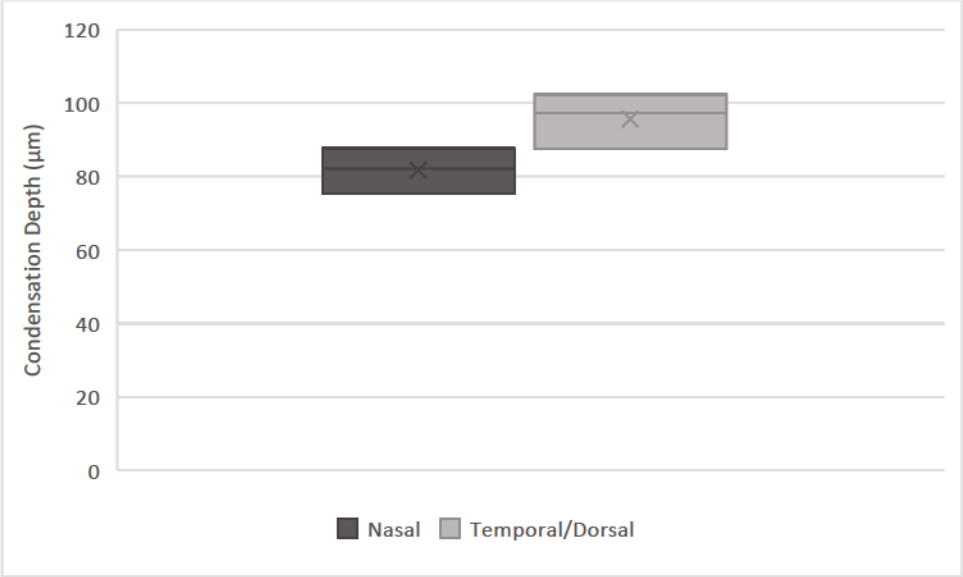

Figure 16. *The depth of the temporal and dorsal condensations is greater than the depth of opposite nasal condensations at HH38 within a given eye. X inside of the boxes indicates the mean.*

4.5. Tenascin-C, MMP1, And MMP2 are Potential Regulators of Skeletogenic Condensation Formation

An extensive literature search was conducted to determine which ECM proteins are expressed during skeletogenic condensation growth. The selection criteria and search words were formulated based on current knowledge that the condensations that give rise to scleral ossicles increase in size/grow due to the migration of cells into the mesenchyme, and not cell proliferation (e.g. Franz-Odendaal, 2008; Jabalee et. al. 2013). It is therefore important to

investigate what proteins are expressed at condensation boundaries to aid in the migration of cells into the condensations, within the chicken model. It is also important to be aware of what occurs in other model vertebrates, and other condensation types, to provide supporting evidence for the chosen candidate proteins. Hence, the initial searches were not specific to the chicken. The following criteria was used to narrow down a list of potential proteins to explore:

Expressed at condensation boundaries

Associated with osteogenic condensations

Data available showing expression or presence in the chicken model

Data suggesting a functional role of protein in skeletal condensation boundary regulation in chicken

Proteins that have a functional relationship with other proteins that meet all aforementioned requirements (i.e., ligand and receptor; or enzyme and substrate).

A number of different searches were conducted using Google Scholar as the main search engine to explore the literature. Each successive search was done based on the results of the previous search. A search for "proteins expressed at condensation boundaries" yielded 34,800 search hits. Most of the literature in this search focused on chondrogenic condensations. After reviewing the literature and becoming acquainted with different types of condensations, a subsequent search was conducted to find information regarding "skeletogenic condensation boundaries", which yielded 1,570 search hits and also included more information on chondrogenic condensations. Therefore, it can be concluded that the first search included hits for "proteins" and "expressed" rather than the region of interest. A literature search for "osteogenic condensation boundaries" was then conducted that yielded a larger number of hits, 4,750.

Focusing specifically on “regulation osteogenic condensation boundaries”, a subsequent search generated 4,100 search hits. This search presented a plethora of information on endochondral ossification. However, the chicken scleral ossicle forms via intramembranous ossification. Clearly these searches indicate the range of language used in the literature by various authors. Another search on “skeletogenic condensation boundaries in chicken” generated 1,200 search hits. After fine-tuning, another search was conducted on “skeletogenic condensation boundary chicken intramembranous” which produced 825 search hits. Tenascin was a reoccurring hit in most of the aforementioned searches as has been researched in the Franz-Odendaal lab (Hammer and Franz-Odendaal 2017). A search for “tenascin in scleral ossicles” generated 61 search hits which also included other proteins that potentially functioned in skeletogenic condensation boundary regulation. The number of hits generated per search are graphically displayed in Figure 17. Only the relevant information is summarized in Table 4 after eliminating redundancy or repeat hits.

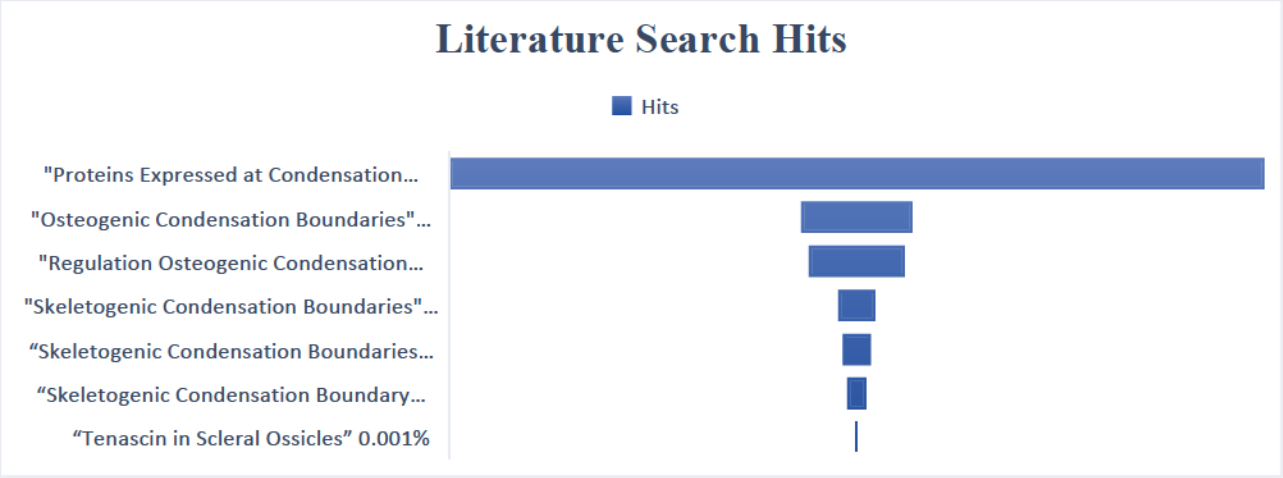

Figure 17*. Search hits summarized in this funnel chart were generated via Google Scholar search engine by using the selection criteria as a guide. Only 0.001% of the total hits were applicable to the overall research question and the model system.*

Table 4. *Initial list of candidate proteins drafted after assessing the applicability of each one to the research question and the model system being used.*

Protein of Interest	**Justification**
BMPs	Epithelial-mesenchymal interactions; cell recruitment; cell growth and survival.
Ephrin(ligand)-Eph(receptor)	Cell sorting, cell movement, condensation boundary formation
Epimorphin	Cell sorting and aggregation
Hoxa11	Patterning and development of bones
Hoxa13	Cell-to-cell adhesion
NCAM	Cell-to-cell adhesion
Notch	Negative regulation of prechondrogenic condensation
Syndecan 3	Epithelial-mesenchymal interactions; Regulation of condensation boundary and size
N-cadherins	Cell-to-cell adhesion
Fibronectin	Activates/regulates NCAM
Tenascin	Epithelial-mesenchymal interactions; Cell-to-cell adhesion; Boundary regulation
MMP 1-3; 19	Utilizes fibronectin and tenascin as substrates
MMP 7 -17; 24-26	Utilizes fibronectin as a substrate

From the hits summarized in Table 4, an assessment was done on the information available. This assessment involved briefly reviewing the studies that were identified. Following

this, a process of elimination was conducted and many candidates were eliminated. Candidates were eliminated if they were not ECM molecules or condensation boundary molecules, if there was insufficient data available for chicken, or if there was insufficient data to support their role in condensation boundary regulation.

BMPS were removed from the list because they are involved in the inductive signaling of epithelial-mesenchymal interactions during the initiation phase of condensation formation and enhance the survival of condensations during the growth phase and are not specifically associated with condensation boundaries (Gañan et. al. 1996; Pignatti et. al. 2014) The role of BMPs are more vital before and after a condensation has formed. Ephrin(ligand) and Eph(receptor) were eliminated because there was not sufficient information on a direct role in regulation of condensation boundaries. Research on abnormalities in Ephrin-Eph signaling resulted in abnormal cell segregation in developing calvariae (intramembranous bones) in mice, which then resulted in fusion across sutures (Rice 2008). Epimorphin was also eliminated because there was insufficient data available showing a direct role in condensation boundary regulation. Epimorphin extracellularly promotes cell sorting and aggregation (Rice 2008) and thus, may have a downstream effect on condensation formation. Hox (Hoxa11 and Hoxa13) genes were omitted because Hox genes are master controlling genes with a broad functional scope. Hoxa13 however, promotes adhesion during the growth phase of condensation formation (Stadler et. al, 2001) but not boundary regulation. NCAM was eliminated because it plays a role in adhesion, stabilization and maintenance of condensations in the initiation phase of condensation formation (Hall et. al. 2000). Notch was eliminated because it is primarily implicated in chondrogenesis (Karlsson et. al. 2009; Mead et. al. 2012). N-cadherin was eliminated because it plays a role in adhesion during the initiation phase of condensation

formation (Hall et. al. 2000). Fibronectin was a reoccurring hit in various searches. Interestingly, literature suggests that fibronectin and tenascin were once thought to be same molecule (Erickson and Inglesias 1984; Chiquet-Ehrismann et al. 1986;) which may explain why fibronectin was seen frequently in the search results. A distinction was made revealing that although both fibronectin and tenascin are ECM glycoproteins, fibronectin is a dimer while tenascin is hexamer, two distinct molecular species with distinct functions (Chiquet and Fambrough 1984; Chiquet-Ehrismann 1990). Fibronectin was eliminated because it is currently known to regulate NCAM during the initiation and growth phases of condensation formation but did not play a role in boundary regulation (Hall et. al. 2000).

The list was therefore narrowed down to tenascin-C, its cell surface receptor, Syndecan-3, and associated matrix metalloproteinases (MMPs), all of which are ECM molecules. Because MMPs degrade extracellular matrix and are either dispersed within the ECM or are membrane bound (Mott and Werb 2004), they were identified for a potential role in matrix remodeling to promote skeletogenic condensation growth by influencing condensation boundaries. Furthermore, the ECM molecules identified in the literature search that are expressed at condensation boundaries, are also substrates for certain MMPs (such as MMP 1-3, and 19; Table 5). MMPs that were not linked to tenascin-C and Syndecan-3 within the searches were also omitted. This assessment generated the list of potential candidates outlined in Table 5, now with particular focus on ECM molecules.

The list outlined in Table 5 was narrowed down further by assessing the feasibility of researching each molecule in terms of time and costs associated with a Master of Science degree. Tenascin-C emerged as the key player to investigate, along with its receptor, syndecan-3. Spatiotemporal expression of tenascin-C and syndecan-3 has been observed around both

chondrogenic and osteogenic condensations in chicken and murine limb buds (Mackie et. al. 1987; Chimal-Monroy et. al. 1999) Syndecan-3 is both an ECM protein and a cell surface receptor for tenascin-C (Thesleff et. al. 1990). Furthermore, a previous student in the Franz-Odendaal laboratory, identified a tenascin-C distribution pattern, particularly at the lateral ends of skeletogenic condensations at HH37 (only) in the scleral ossicle system (Hammer and Franz-Odendaal 2017). Thus, this ECM protein and its receptor (syndecan-3) are ideal candidates to further explore condensation development with respect to boundary regulation.

***Table 5**. Refined list of candidate ECM molecules with focus on Tenascin-C and Syndecan-3. Four MMPs utilize tenascin-C and syndecan-3 as substrates.*

Protein of Interest	**Justification**
Syndecan-3	ECM and cell surface receptor; Epithelial-mesenchymal interactions; Condensation boundary regulation.
Tenascin-C	Matrix glycoprotein; Epithelial-mesenchymal interactions; Cell-to-cell adhesion; Condensation boundary regulation.
MMP 1, 2, 19	Utilizes tenascin-C as a substrate
MMP 3	Utilizes tenascin-C and syndecan-3 as substrates

The localization of tenascin-C and syndecan-3 to condensation boundaries, their relationship with several matrix metalloproteinases (MMPs), and their timing and presence in osteogenic condensations, further strengthen their potential role in scleral condensation growth and development (Dunlop and Hall 1995; Chimal-Monroy and Díaz de León 1999; reviewed in Drake and Franz-Odendaal 2018, reviewed in Giffin et. al. 2019). The finalized list of ECM

molecules explored is given in Table 6. *The following parts of this thesis will thus focus on the ECM molecules listed in Table 6, namely Tenascin-C, Syndecan-3, MMP1, and MMP2.*

Table 6. *Finalized list of potential candidate ECM molecules that regulate condensation formation, after assessing feasibility of time and costs.*

Protein of Interest	**Justification**
Syndecan-3	ECM and cell surface receptor; Epithelial-mesenchymal interactions; Condensation boundary regulation.
Tenascin-C	Matrix glycoprotein; Epithelial-mesenchymal interactions; Cell-to-cell adhesion; Condensation boundary regulation; Present in scleral mesenchyme.
MMP 1 & 2	Utilizes tenascin-C as a substrate

4.6. Tenascin-C Expression in The Osteogenic Condensation Is Dynamic from HH34-HH37.

To understand the spatial and temporal expression profiles of the ECM molecules of interest, immunohistochemical analyses were attempted for each molecule. However, such analysis was only successful for tenascin-C.

In order to understand the complete spatial and temporal distribution of tenascin-C in skeletogenic condensation growth, tenascin-C expression was evaluated at various stages: while a full ring of papillae were present (HH34 and HH35), during papillae degeneration (HH36), and after complete papillae degeneration (and HH37). The aforementioned developmental timepoints are important as small condensations can be identified with wholemount alkaline phosphatase

staining as early as HH34 (Andrews and Franz-Odendaal 2018). Furthermore, a complete ring of condensations is seen with the naked eye first at HH37. The results for each stage are described below in sections 4.6.1-4.6.2.

4.6.1. Tenascin Expression at The Beginning of Condensation Formation

The expression pattern of tenascin-C was investigated during the very early phases of condensation formation, namely HH34 and HH35, when the conjunctival papillae that induce scleral condensations are still visible. Immunohistochemical analysis for tenascin-C indicates very little expression at the early stages, HH34 and HH35 (*n=3 embryos per stage* Figure 18). There are faint bands of staining within the mesenchyme (arrows in Figure 18B and E), at sites that have not been previously described within the literature. It is unknown whether these are presumptive condensation sites or not, as this stain appears deeper within the mesenchyme than the site of the future condensations. Note that during the tissue sectioning process, it is very easy to miss the conjunctival papillae, thus they are only present on a few sections. Controls show no staining (Figure 18C, D, G, and H).

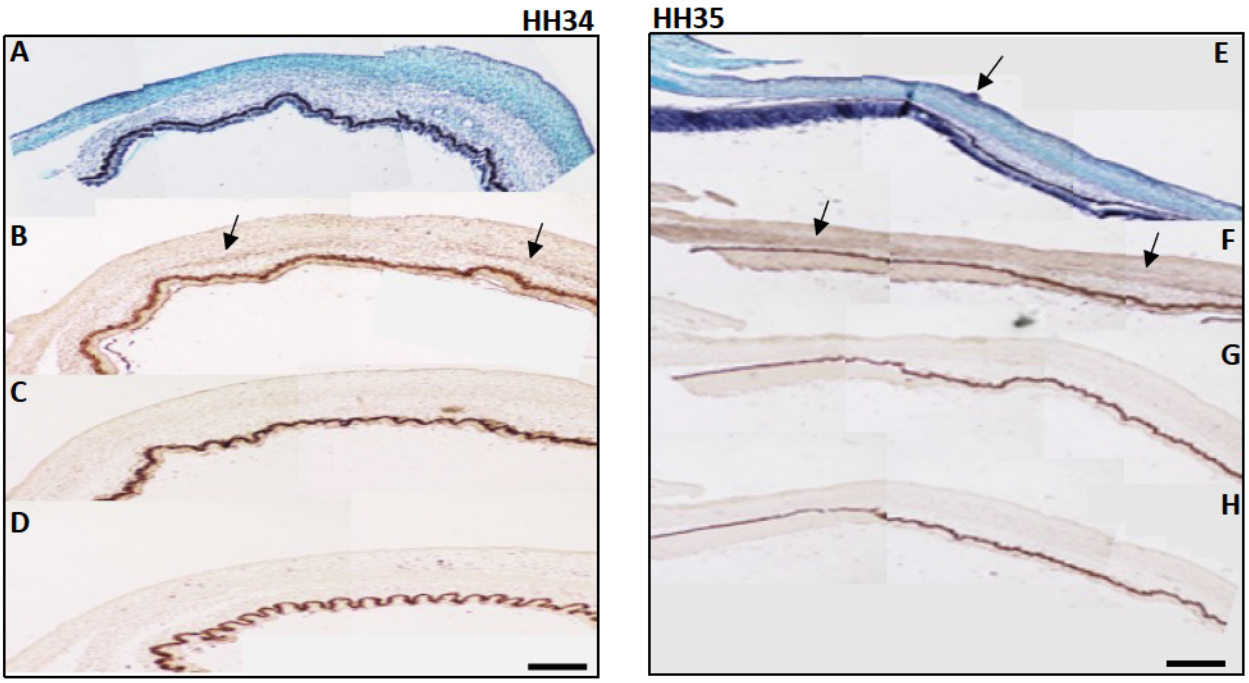

Figure 18. *Section immunohistochemistry of tenascin-C shows limited to no tenascin-C expression at stages HH34 (A-D) and HH35 (E-H) on cross sections through the sclera within the temporal group. A, HH34 HBQ Stained Histology; B, HH34 immunohistochemistry experimental slide with tenascin-C, arrows indicate slight bands of tenascin-C expression; C, HH34 Control with no primary antibody; D, HH34 Control with no secondary antibody; E, HH35 HBQ Stained histology, arrow indicates a papilla; F, HH35 immunohistochemistry experimental slide with tenascin-C, arrows indicate slight bands of tenascin-C expression; G, HH35 Control with no primary antibody; H, HH35 Control with no secondary antibody. Scale bars, 100µm.*

4.6.2. Tenascin-C Expression During and After Papillae Degeneration

The expression pattern of tenascin-C was investigated during early papillae degeneration (HH36), and at advanced stages of papillae degeneration (HH37). At HH36, conjunctival papillae are beginning to degenerate concomitantly as condensations continue to develop. The histology shows the position of the condensation at HH36 (Figure 19A). Immunohistochemical analysis at HH36 shows tenascin-C surrounding the scleral cartilage (Figure 19B), throughout the developing scleral condensation (Figure 19D), and at the lateral ends of the developing scleral condensations (Figure 19B and C) (n=3 embryos). The deeper band of tenascin-C that was observed in earlier stages, continues to be present at HH36. Immunohistochemistry controls are shown in Figure 19 E and F. Conversely at HH37, immunohistochemical analysis shows a reduced expression domain of tenascin-C (Figure 20B, highlighted in 20E&F), limited to the lateral ends of the scleral condensations (Figure 20B, highlighted in Figure 20F) and once again, surrounding the scleral cartilage (Figure 20E) (n=3 embryos). The histology shows the position of the condensation at HH37 (Figure 20A). No staining was detected in the controls (Figure 20C & D).

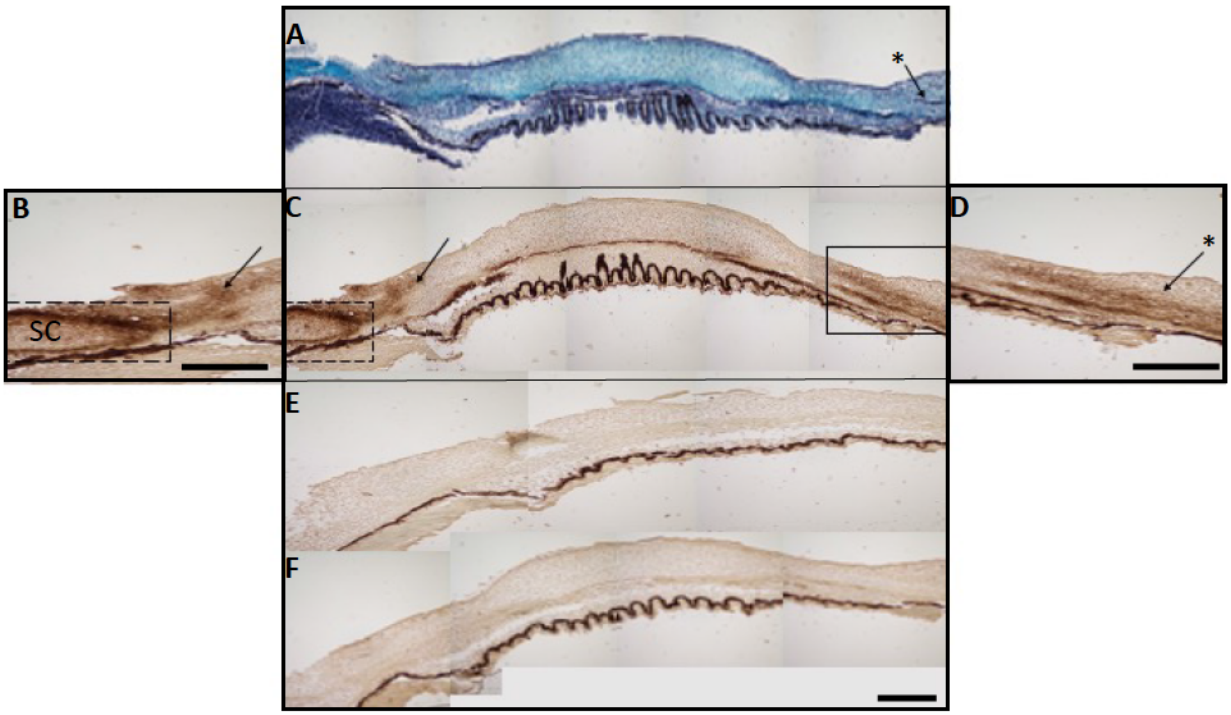

Figure 19. *Distribution of tenascin-C around the scleral cartilage (dashed box, B and C), throughout the condensation (continuous box, C; asterisk, in D), and at the lateral ends of the condensations (arrows B and C) at stage HH36. Note the deeper band of expression below the condensations (in D). A, HBQ Stained histology, arrow and asterisk indicate condensation; B, magnified view of left portion of the cross section, arrow points to tenascin-C expression at the lateral end of the condensation; C, immunohistochemistry experimental; D, magnified view of right portion of the cross section, arrow and asterisk indicate condensation; E, Control with no primary antibody; F, Control with no secondary antibody. Arrows indicate regions of tenascin-C expression. Asterisk- scleral condensations. SC- scleral cartilage. Scale bar, 100µm.*

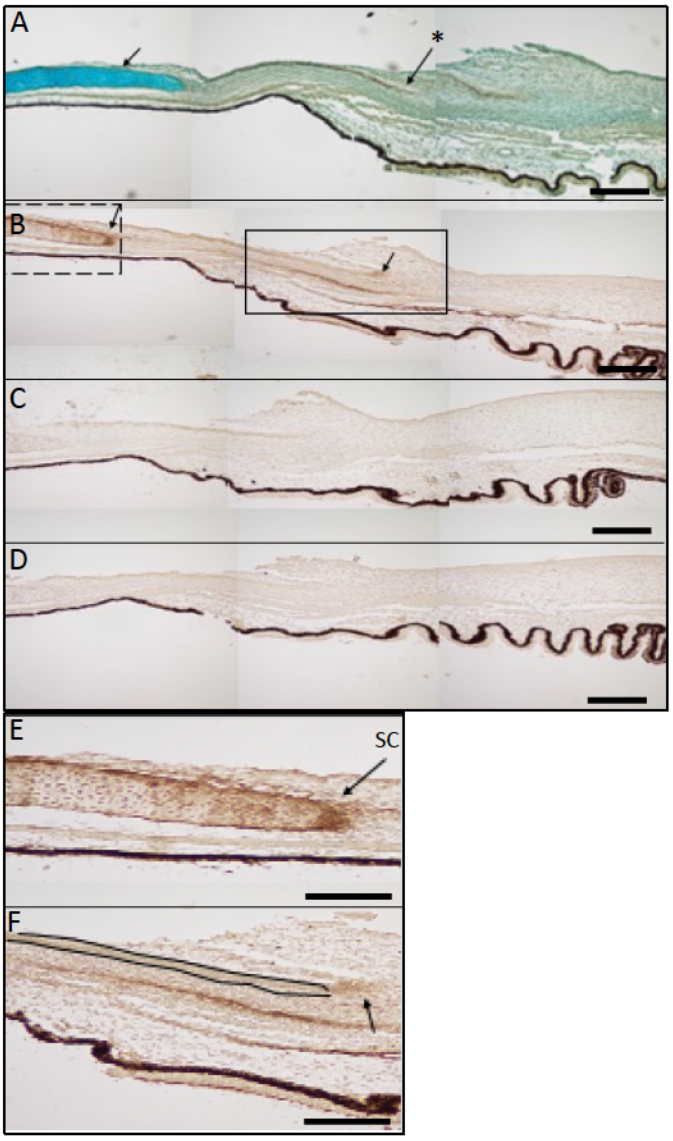

Figure 20. *Distribution of tenascin-C surrounding and at the ends of the scleral cartilage and at the lateral ends of the condensation at HH37. A, HBQ stained histology; B, immunohistochemistry experimental slide; C, Control no primary antibody; D, Control with no secondary antibody. Arrows indicate regions of tenascin-C expression. Asterisk- scleral condensation. SC- scleral cartilage. MS- mesenchyme. Scale bar, 100µm.*

4.7. Manipulation of The Osteogenic Condensation Via Matrix Regulators

In order to obtain insight into the role of MMPs and ECM in skeletogenic condensation growth, scleral condensation development was manipulated using known matrix inhibitors. Manipulation of condensation size, shape and number was attempted using two matrix inhibitors – hydrocortisone and a global MMP inhibitor, CP-471474. A scale was used to characterize the morphological effects of the inhibitors on condensation number and morphology (Table 3) ranging from normal (no defects) to severe (loss of 3 or more condensations).

4.7.1. The Global MMP Inhibitor CP-471474 Had A Limited to No Effect on Ossicle Development

The effects of the global MMP inhibitor CP-471474 were tested at various developmental timepoints (HH33 and HH34) and inhibitor concentrations (1:50, 1:100). In the control no injection group and in the control injection group, 100% of the embryos had very mild effects or no effects on the scleral ossicle condensations (n=2 for each control, Figure 21A, B, D, E, G, H) regardless of injection time point or CI solution concentration. Alkaline phosphatase (AP) staining is intense and visible throughout all 14 mineralized condensations in all controls (e.g. Figures 21A, D, G).

In samples treated with the inhibitor CP-471474, again 100% of the embryos had mild effects (n=3 embryos for each treatment group). Some changes in AP activity (based on AP staining) were observed in the different treatment groups, with various effects. Samples treated with 1:100 dilution of CP-471474 at HH33 have a reduction in AP stain intensity particularly in the nasal group (n=3 embryos, Figure 21C). Samples treated with 1:50 dilution of CP-471474 at HH33 have the greatest reduction of AP activity among the treatment groups, as seen by the decrease in the intensity of the AP stain (n=3 embryos, Figure 21I). Regions of no staining in the

middle of each mineralized condensation created the illusion of an unstained ring within the ring of mineralized condensations (Figure 21I, arrow). Samples treated 1:50 dilution of CP-471474 at HH34 resulted in a very slight reduction in AP activity (n=3 embryos, Figure 21F). None of the CP-471474 injected embryos had a loss of scleral ossicles. Overall, the manipulation of osteogenic condensation was only mildly successful using this global MMP inhibitor. Nonetheless, CP-471474 appears to be more effective in disrupting scleral condensation development at earlier developmental timepoints as CP-471474 was more effective at HH33 than HH34. This inhibitor has not been previously used in chicken and additional troubleshooting is required to achieve more effective MMP inhibition, that might trigger more severe phenotypes (i.e. loss of scleral ossicle condensations).

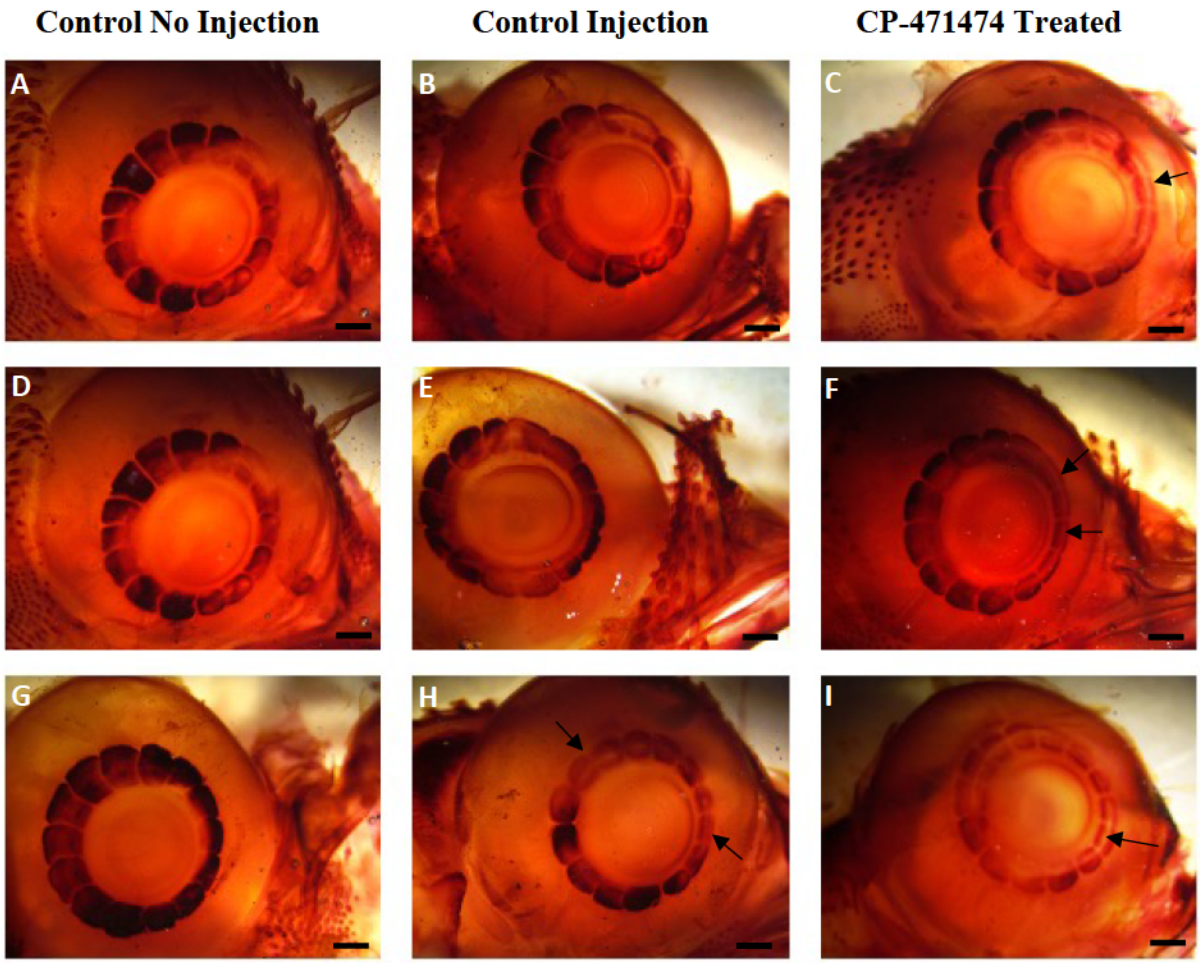

Figure 21. *CP-471474 Inhibitor injections show a limited to no effect on condensation development in the developing chicken eye. Samples are stained with alkaline phosphatase (AP) at HH38. A, CNI sample. 14 normal AP positive condensations are present. Some of the nasal/dorsal condensations were partially covered by a membrane during the staining process. B, Sample treated with 1:100 dilution of CI solution at HH34. 14 normal condensations are observed, with a slight reduction in the AP stain intensity. No membrane covered the condensations.*

C, Sample treated with 1:100 dilution of CP at HH33. All condensations are present. A reduction in the AP stain intensity is seen in mostly in nasal group (arrow). D, CNI sample. 14 normal AP-positive condensations are seen within the eye of a developing chick. Some of these condensations were partially covered by a membrane during the staining process. E, Sample

treated with 1:50 dilution of CI solution at HH34. 14 normal condensations are observed, with a slight reduction in the AP stain intensity. No membrane covered the condensations. F, Sample treated with 1:50 dilution of CP at HH34. There is an unstained region in the middle of each of the 8-9 condensations in the nasal and dorsal regions (arrows). AP activity is reduced. G, CNI sample. 14 normal AP-positive condensations are present. H, Sample treated with 1:50 dilution of CI solution at HH33. There is a reduction in the AP stain intensity in the dorsal and nasal groups (arrows). No membrane covered the condensations. I, Sample treated with 1:50 dilution of CP at HH33. Greatest reduction in AP stain intensity is seen at this timepoint and inhibitor concentration. There is an unstained region within the scleral ossicle ring (arrow). CNI, control no injection; CI, control injection; CP- CP-471474. n=3 embryos for each sample group. Scale bar = 1000µm.

4.7.2. Hydrocortisone Severely Affects the Development of Scleral Condensations

Hydrocortisone was used as matrix inhibitor to manipulate the ECM composition in order to elucidate the potential role of the ECM in scleral condensation development. In the control no injection group, alkaline phosphatase (AP) staining is intense and visible throughout all 14 mineralized condensations in 100% of the embryos (n=3 embryos, Figure 22A). No effect was observed in the control injection group (n= 5 embryos, Figure 22B). A double injection of 2mM hydrocortisone was administered into the developing chicken embryos (n=5 embryos). The first injection was administered at HH34 and the second injection at HH35. This injection combination resulted in complete loss of AP activity, with no scleral condensations present in 80% of embryos (4/5 samples), a severe phenotype (Figure 22D). Interestingly however, upon closer observation of the eyes with a complete loss of condensations, a ring of papillae (or papillae-like structures) were visible under the microscope in these samples (Figure 23). In 20% of the hydrocortisone treated embryos, (1/5 samples) six substantially underdeveloped condensations were observed (Figure 22C). The papillae-like structures are not observed in Figure 22C.

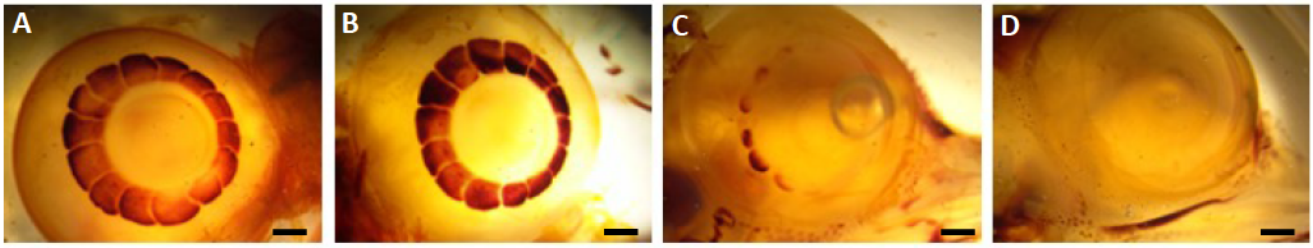

Figure 22. *Samples injected with hydrocortisone showing a severe effect on scleral condensation development. Samples are stained with AP at HH38. A, CNI sample. 14 normal AP-positive condensations are present. B- Sample treated with a CI solution injected twice, at HH34 and HH35. 14 normal AP-positive condensations are present. C and D- Samples treated with a 2mM hydrocortisone injected twice, at HH34 and again at HH35. Six underdeveloped condensations* are present *opposite the beak in 20% of samples (1/5 embryos) (C), while complete loss of AP activity was observed in 80% of the samples (4/5 embryos) (D). CNI, control no injection; CI, control injection. Scale bars, 1000μm.*

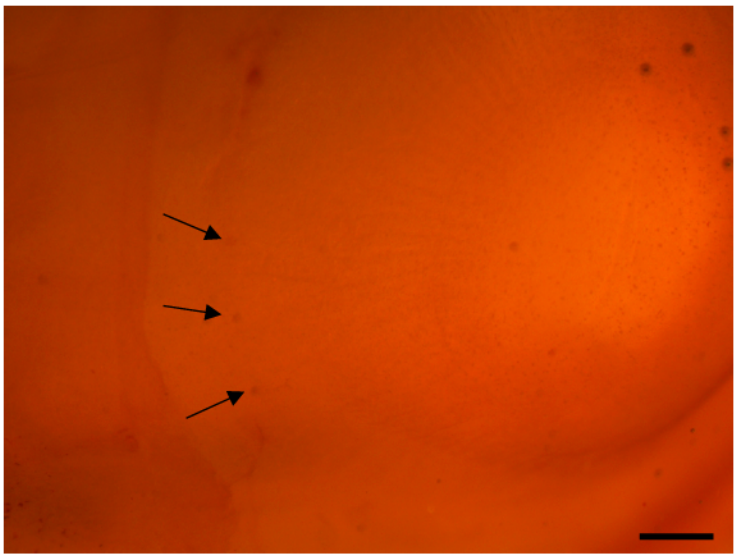

Figure 23. *Hydrocortisone treated embryo at HH37. Papillae (or papillae-like structures) were seen in samples with a complete loss of the condensations. Papillae are difficult to see in alkaline phosphatase stained samples, however three are indicated by the arrows. Scale bar, 500μm.*

4.8. Manipulation of The Osteogenic Condensation Affects MMP Expression

In order to determine whether the absence of scleral condensations after hydrocortisone injection was a result of a change in MMP expression, the presence of the MMPs was evaluated. Expression of MMP1 and MMP2 in proteins from the treatment group should be different from MMP1 and MMP2 expression in the control group if hydrocortisone influences a change in the expression of MMPs. It was hypothesized that expression of MMP1 and MMP2 will decrease in the hydrocortisone treated groups compared to the controls.

Before these studies could be conducted, the mouse anti-MMP1 and mouse anti-MMP2 polyclonal antibodies (ABCAM) needed to be tested and optimized for Western Blot analysis (See Appendix J for optimization details).

4.8.1. Optimization of The Western Blotting Protocol for a Control Antibody

Protein extractions were carried out after dissecting out the corneas and scleral ossicles from 20 embryos (Appendix J.1). Corneal tissue was used as a positive control after it was found in the literature that Western blot analysis detected MMP2 in the chicken cornea (Huh et. al. 2007). The integrity of the extracted proteins were tested (Appendix K.1 for details). To calculate the protein concentrations of the four biological replicates for each tissue type (see Methods), a standard curve was created (Appendix K.2). A Western Blot was conducted to confirm that tubulin was present in all samples (Figure 24). Tubulin (54 kDa) was used as the positive control for the subsequent Western blots because tubulin is abundantly expressed in all tissues.

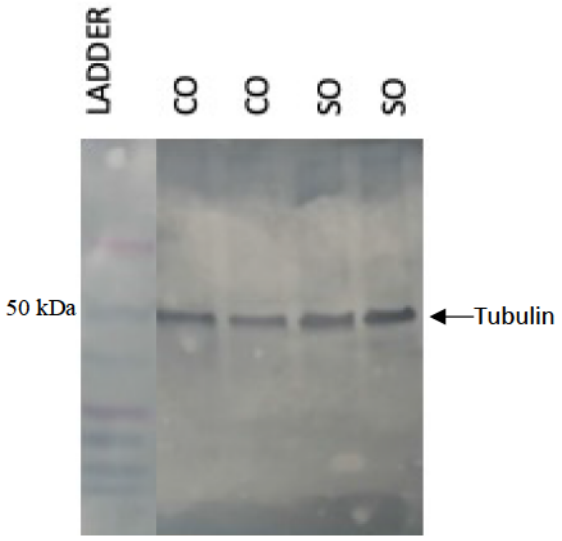

Figure 24. *Proteins extracted from scleral condensations and corneas from HH37 embryos were tested with a Western blot protocol for tubulin. A 250 kDa ladder is shown with the 50kDa band indicated. The molecular weight of tubulin is 54kDa. CO- cornea; SO- mineralized scleral condensations.*

4.8.2. Non-Reducing Conditions Are Optimal for Western Blot of MMP1 And MMP2

Various concentrations of MMP1 and MMP2 were tested using chick cornea, the MMP2 positive tissue (Huh et al. 2007), and scleral ossicle tissue. Troubleshooting the Western blot protocol also involved carrying out the experiment under reducing and non-reducing conditions. Reducing conditions involves the use of beta-mercaptoethanol (2-BME) to reduce disulfide bridges in the proteins in order for them to adopt random coil conformation and to separate more easily by size using SDS-PAGE (Litman et. al. 2002). However, certain antibodies cannot detect proteins in their reduced forms. In that case, non-reducing conditions are required. The anti-MMP1 and MMP2 antibodies were tested against scleral ossicle proteins under reducing conditions at various concentrations. However, only the control, tubulin, was detected (Figure 25). This indicated that the protocol itself is correct, and perhaps that reducing conditions impair the efficient detection of MMP proteins. Thus, non-reducing conditions were explored for the detection of MMP.

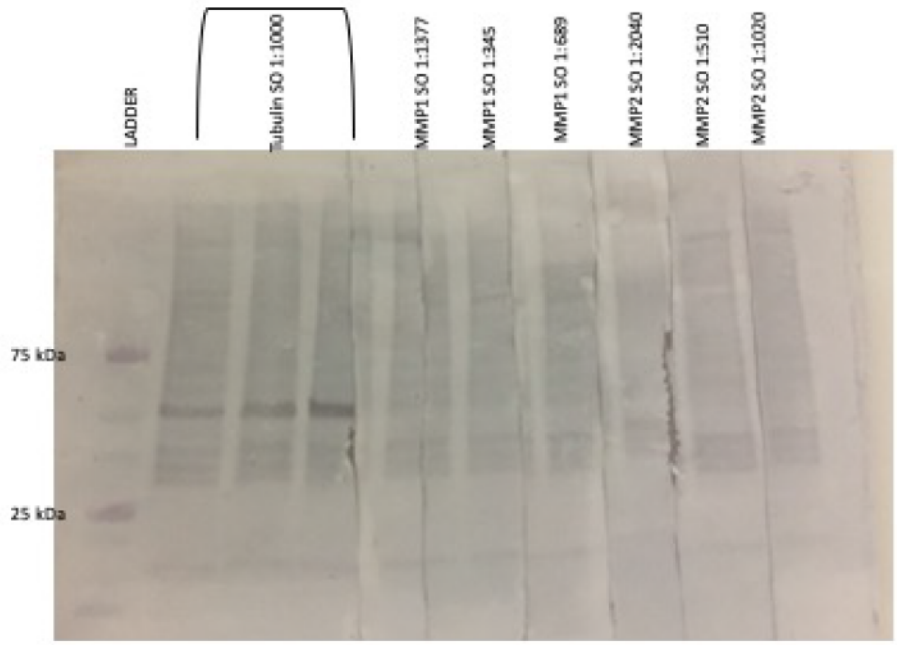

Figure 25. *MMP1 and MMP2 antibodies were tested on scleral ossicle protein samples under reducing conditions at various concentrations. Tubulin (54kDa) was detected in the scleral ossicle protein sample indicating that the blot protocol works. However, MMP1 and MMP2 were not detected in adjacent lanes despite a range of antibody concentrations that were tested. SO, scleral condensations.*

Therefore, a similar approach with varying concentrations of MMP antibodies under non-reducing conditions was attempted, and a signal was detected for both MMPs at concentrations ranging from 1:510-1:1377 (Figure 26). Here, MMP1 and MMP2 are detected at approximately 34 kDa and 44 kDa, respectively. ABCAM (abcam.ca) lists the expected size for murine MMP1 and MMP2 as 54kDa and 72kDa, respectively. However their website also shows protein bands that have lower weights (namely 46kDa for MMP1, and 68kDa for MMP2). Additionally Hu et. al. (2007) detected an active MMP2 form of a molecular weight of 66 kDa, and a pro MMP2 form of a molecular weight of 97 kDa in the chicken cornea. These latter MMP antibodies were

from a different supplier to those used in this thesis. A repeat Western Blot using non-reducing conditions, showed the MMP1 and MMP2 detected, closer to the 54 kDa size, similar to tubulin, however this blot did not run well and is therefore not pictured. Clearly, the data in this study along with data from the literature, indicate that further investigation of MMP antibody sizes is required.

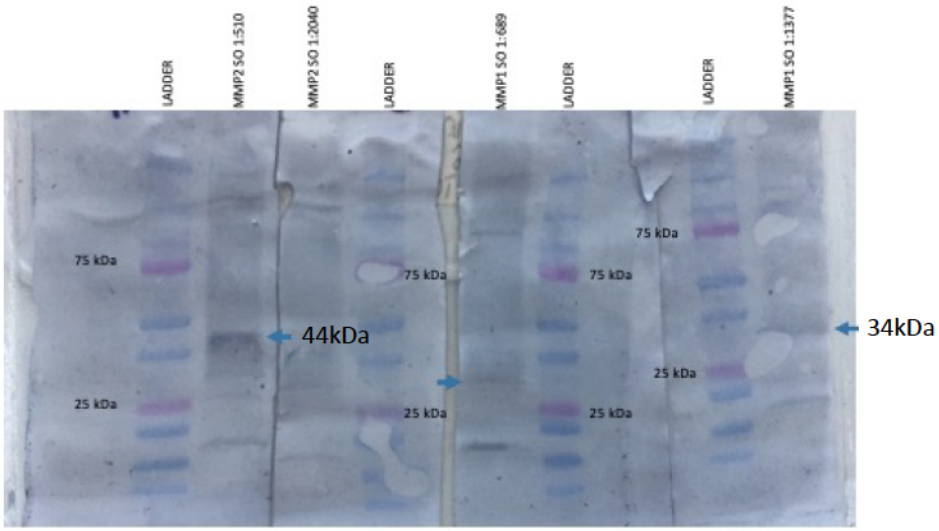

Figure 26. *MMP1 and MMP2 were tested on scleral ossicle proteins under non-reducing conditions at various concentrations. Both MMP1 and MMP2 were detected (blue arrows), indicating that non-reducing conditions are optimal for these antibodies.*

In summation, these Western blot results indicate that:

i) MMP1 and MMP2 are potentially present in the scleral mesenchyme and cornea at HH37, but further investigation is necessary to verify if true bands were detected.

ii) Non-reducing conditions are optimal for the detection of these MMPs.

iii) The lowest concentration of antibody needed is 1:1377 for putative MMP1 and 1:510 for putative MMP2 in scleral mesenchyme.

5.0. DISCUSSION

5.1.Variation in Condensation Depth

This study describes the first investigation on the mesenchymal depth of the chicken scleral ossicle primordia. Condensation depth variation within a given cross section through the sclera of the developing chicken embryo prompted the investigation of condensation depth over developmental time. The data shows that the distance of the scleral condensation from the conjunctival epithelia increases over developmental time. A one-way ANOVA and Welch's t-test determined that the 20% increase in depth from HH36 to HH37 was statistically significant. On the contrary, condensation depth unexpectedly decreases by 17% from HH37 to HH38. It can be speculated that this result was due to the small sample size used for HH38. A sample size of at least seven embryos for each stage would be more ideal for comparison between the stages. Alternatively, although not measured, the sclera at HH38 seems visibly larger in size to that of HH37 (when comparing cross sections at various stages). Measuring the size of the sclera would help to clarify whether or not the increase in size if the sclera is correlated with the measured decrease in condensation depth. No previous data in the literature describes this observation in any other organism with scleral ossicles. However, it can be speculated that the condensations might initially be positioned more superficially and might move deeper within the mesenchyme because neural crest derived mesenchymal cells are highly migratory (Weiss and Garber 1952; reviewed in Hall 1975; Hall and Ekanayake 1991; Cordero et al. 2011; Snider and Mishina 2014). Alternatively, condensation depth may vary due to tissue tension and growth dynamics. That is, condensations may be displaced deeper by cells above them proliferating and pushing them deeper within the mesenchyme. Interestingly, scleral ossicle condensation growth has been

shown to increase in size by active migration (Jabalee and Franz-Odendaal. 2013) suggesting that migration is a key element to establishing the final condensation size and possibly also its position.

To support this hypothesis, cell labeling would be an ideal and more accurate methodology to show active migration. However, cell labeling would be very challenging at such late stages of embryo development when embryos are no longer transparent. An alternative experimental approach would be similar to that of Jabalee and Franz-Odendaal (2013) where histological analyses were used to measure the angle of alignment of cells following the Sepich et al. (2005) method. Wyngaarden et al. (2010) demonstrated that migrating cells align their long axes parallel to the direction of their movement (Jabalee and Franz-Odendaal 2013). If condensations are themselves moving deeper within the mesenchyme, they should have a different orientation relative to the conjunctival epithelium than that of surrounding stagnant cells. This should be examined at early stages of condensation growth, HH 34-35. This method was however designed to measure individual cells as opposed to tissue structures, and would therefore likely need to be modified.

5.2. The Tilt of The Scleral Ossicle Ring

The present study examines, for the first time, the orientation of the scleral ossicle ring. Prior to this investigation, the general assumption was that the ring of scleral ossicles was positioned at a planar surface orientation (i.e. equidistant from the epithelium at all positions in the eye). Antithetically, my measurement data clearly shows that the scleral ossicle ring is orientated at a tilt, as condensations are not at a uniform distance from the epithelium in all positions around the eye. A Welch's t-test determined that the 15% change in condensation depth

between the temporal/dorsal and nasal groups was statistically significant. The condensation depth data in this study gives a better understanding of the arrangement of the scleral ossicle ring within the avian eye. It would be interesting to explore the orientation of the scleral ossicle ring in other species in order to elucidate more details about its functional relevance across different vertebrates. Scleral ossicles are currently speculated to function in structural support and visual accommodation (Lima et. al. 2009; Franz-Odendaal and Krings 2020; reviewed in Franz-Odendaal 2020). The tilt of the scleral ossicle ring, relative to the epithelium, could be a simple consequence of the slight tilt at which the eye sits within its socket in the chicken skull. A way to explore the relevance of the orientation of the scleral ossicle ring would be to investigate whether or not birds with more forward-facing eyes like the barn owl (investigated in Franz-Odendaal and Krings 2020) show the same tilt of the scleral ossicle ring.

5.3. Tenascin-C Expression in Late Condensation Development

Elucidating the role of the ECM in scleral condensation development can reveal a plethora of information about osteogenic condensations and intramembranous ossification. Tenascin-C, syndecan-3, MMP1 and MMP2 were chosen as the ECM molecules to explore in this study. Immunohistochemical analyses was only successful for tenascin-C, but also attempted for syndecan-3 and MMP1. Further optimization of an immunohistochemistry protocols for syndecan-3, MMP1, and MMP2 was not possible due to time constraints. Furthermore, more antibodies need to be developed for immunohistochemical applications with chicken specificity. Nonetheless, immunohistochemical analysis of tenascin-C demonstrated its dynamic spatial expression over developmental time.

Tenascin-C expression during the early phases of condensation development (HH34 and HH35), was very limited. Slight bands of staining were observed in the mesenchyme that were perhaps sites of early developing condensations that were not identified in the histology. To investigate this, a future study could determine whether those bands are marking the future condensation sites. Alternatively, those bands of tenascin-C may not be future condensations sites but rather serve some other role. Tenascin-C expression at these early stages of development within the scleral mesenchyme has not been previously described in the literature. The expression of tenascin-C at stages HH36 and HH37, when condensations are more developed, points towards its potential role in condensation development. Hammer and Franz-Odendaal (2017) demonstrated tenascin-C expression at the lateral ends of condensations at HH37, which was also confirmed in this study. Tenascin-C expression also surrounded the scleral cartilage at HH37 in this study. For the first time, this study demonstrates tenascin-C expression at HH36 surrounding the scleral cartilage, throughout the developing condensations, and at the lateral ends of the condensations Figure (19B, C & D).

It has been previously described in the literature that scleral condensations grow via migration of mesenchymal cells into the developing condensation (Jabalee and Franz-Odendaal 2013). Additionally, mesenchymal cells enter the condensation only at the lateral ends at HH37 (Jabalee and Franz-Odendaal 2013). It has not been previously shown via any direct methods whether cells are entering HH36 condensations at the lateral ends or at multiple points of entry. However, tenascin-C expression at the lateral ends of condensations at two active growth stages (HH36 and HH37) suggests that tenascin-C could be guiding migrating cells into condensations. It would be important to examine the expression patterns of the other ECM molecules of interest that have functional relationships with tenascin-C. For example, if tenascin-C is guiding cells

into condensations at the boundaries, increased and co-localized expression of its cell surface receptor, syndecan-3 may be observed. This study reveals the need to explore migration of cells into scleral condensations over various developmental timepoints and again highlights the importance of exploring the chosen ECM molecules of interest.

5.4. Condensation Morphology Following Matrix Manipulation

Extracellular matrix manipulation further reveals a potential role for matrix remodeling in scleral condensation development. Again, it was hypothesized that matrix metalloproteinases (MMPs) could be involved in enabling migratory mesenchymal cells to join growing skeletogenic condensations. MMPs may potentially enable the migration of mesenchymal cells into condensations particularly at their lateral ends, by degrading the ECM. Matrix manipulators, hydrocortisone and the global MMP inhibitor, CP-471474, were therefore used to manipulate condensation morphology and amount.

Hammer and Franz-Odendaal (2017) achieved conjunctival papillae knockout during the first inductive phase of scleral ossicle development, and indirect scleral condensation disruption, using a double injection of hydrocortisone. Hydrocortisone was utilized in their study for matrix manipulation based on previous data describing its effect on feather, conjunctival papillae and scleral condensation development (Stuart et al. 1972; Johnson 1973; Desbiens et al. 1992; and Turque et al. 1997). The effects of hydrocortisone are transient (due to its one to two-hour half-life) (Peterson and Wyngaarden 1955; Hindmarsh and Charmandari 2015) and therefore, a double injection was required to have a greater effect on papillae and scleral condensation development. Hammer and Franz-Odendaal (2017) modified Johnson's (1973) protocol and determined that a relatively high dose administered twice was necessary to significantly affect

papillae and consequently, scleral ossicle number and morphology. Hammer and Franz-Odendaal (2017) administered the hydrocortisone at HH29 and HH30 as they were targeting papillae formation – the first phase of ossicle formation. Hammer and Franz-Odendaal (2017) achieved complete papillae knockout in their study. However, consistent complete knockout of conjunctival papillae was recently achieved by the Franz-Odendaal lab using a similar approach as Hammer and Franz-Odendaal (2017), but with a 2mM concentration of hydrocortisone for the injections (Pers. comm, P. Drake, Franz-Odendaal Lab). A similar approach was used in this thesis study, but injections were administered after phase one of scleral ossicle induction. Complete condensation inhibition was achieved in 80% of the treated embryos (4/5 samples) in this study. Interestingly, papillae- like structures were observed in samples with complete condensation loss. Hence, it is not clear if complete inhibition of scleral condensations was achieved in these samples, or if there was a developmental delay in these embryos as papillae should be completely degenerated by HH38. Importantly, each embryo was not staged prior to injection but the batch of eggs was staged by sub-sampling one or two eggs. To clarify this finding, embryos can be raised to later developmental time points after injection to observe whether or not scleral condensation development recovers, or embryos could be staged prior to injection. Staging embryos however would require windowing each egg which makes tilting the egg after injection (to prevent solution loss from the injection hole) impossible.

Hammer and Franz-Odendaal (2017) showed that scleral condensation development did not recover when two hydrocortisone injections were administered over two developmental stages (HH29 and HH30). That is, embryos did not have sufficient time to recover and compensate for the disruption of papillae. The current thesis study involved administering the first injection at HH34, when a full ring of papillae was already present (Hamburger and

Hamilton 1951) and scleral condensations start to be induced. A second injection at HH35 ensured that the effect of hydrocortisone did not wear off because of the transient nature of hydrocortisone. Notwithstanding, the hydrocortisone injections were administered at much earlier timepoints in Hammer and Franz-Odendaal (2017) compared to what was done in this study (HH 29 and HH30, vs HH34 and HH35, respectively), and so it is perhaps possible that scleral condensation development could recover if the inductive signal to induce them persists after the effects of hydrocortisone wear off. While the developmental window of induction has been explored for the papillae (Jourdeuil and Franz-Odendaal 2017), it has not been explored for the condensations, which is the second phase of ossicle formation. Interestingly in 20% of the hydrocortisone treated samples (1/5 embryos) where full inhibition was not achieved, underdeveloped scleral condensations were observed in the temporal group. Although this study targeted the second inductive phase of scleral ossicle development, this observation is consistent with previous studies in the literature showing that the temporal group was least affected by hydrocortisone treatment (Johnson 1973; Hammer and Franz-Odendaal 2017).

Genetic factors may contribute to how a developing chick embryo responds to stress (Cheng et al. 2002; Cheng and Muir 2004). It is possible that the high levels of hydrocortisone administered in this study stressed the developing embryos. The individual variations in endogenous cortisol levels between samples could contribute to the overall effect of hydrocortisone treatment. In future, the endogenous cortisol of the embryos could be measured prior to and following hydrocortisone injections. This will help to determine whether or not there is a correlation between endogenous cortisol levels and the degree of hydrocortisone disruption of the scleral ossicle condensations.

Furthermore, the scleral ossicle ring has a compensatory system whereby larger ossicles will form to compensate for gaps within the scleral ossicle ring (Franz-Odendaal 2008; Duench and Franz- Odendaal 2012) such that neighboring condensations will expand to complete the ring. This interesting phenomenon was demonstrated in the scaleless (sc/sc) chick mutant that develops a few unusually large/elongated ossicles (Stuart et al. 1972; reviewed in Hall and Miyake 1992). However, 20% (1/5 embryos) of the hydrocortisone treated samples in this thesis study (with incomplete condensation knockout) do not appear to demonstrate this compensatory mechanism, following hydrocortisone treatment since scleral condensations were abnormally small, if present. It is plausible that compensation was disrupted due to the later injection timepoints (HH34& HH35 vs. HH29 &HH30), as well as the dose (2mM) of hydrocortisone administered. Perhaps, embryos need to be raised to a later stage to reassess whether or not the compensatory mechanism is exhibited.

Hammer and Franz-Odendaal (2017) observed that the effects of hydrocortisone on conjunctival papillae were less severe than the effects observed on scleral condensations, despite the 1:1 ratio at which they develop. To parse out why this occurred, they examined scleral vasculature following treatment with hydrocortisone and found that vasculature was substantially reduced in treated samples. Thus, they proposed that not only is the inductive signaling of conjunctival papillae important for scleral condensation development, but so is the maintenance of scleral vasculature. A future direction for this study could be to assess scleral vasculature following hydrocortisone injections during the second inductive phase, and determine if this disruption is similar to what Hammer and Franz-Odendaal (2017) observed. Because vasculature is being disrupted, this could also be why condensations formed abnormally small in some (1/5) samples in this study.

In summary, the results of the hydrocortisone injection experiments could be explained by the use of a high concentration and double injection of hydrocortisone that disturbs the compensatory mechanism of the scleral ossicle development. Complete loss of the scleral ossicle ring was observed in 80% of the hydrocortisone treated samples. In order to determine if scleral condensation development recovers, embryos could be raised to later developmental timepoints or staged prior to injection administration. Genetic and physiological factors could contribute to why complete scleral condensation loss was not equally observed in all of the treated samples. Measuring endogenous cortisol levels before and after hydrocortisone treatment could determine whether cortisol levels affect hydrocortisone treatment severity. Scleral vasculature needs to be investigated to determine how vasculature disruption correlates with scleral condensation disruption during the second inductive phase of scleral ossicle development. Further research that utilizes the aforementioned methods should be conducted to fully understand the results described this study (5.4).

CP-471474 inhibitor was used as the first chemical for the manipulation studies. Very mild effects on condensation development were achieved with the use of this inhibitor. My data suggests that CP-471474 is more potent in disrupting scleral condensation development at earlier developmental timepoints as CP-471474 was more effective at HH33 than HH34. Injections administered at HH33 showed the greatest decrease in AP activity. However, sample size for this experiment was quite small. Additionally, the data also shows that increasing the concentration of CP-471474 from 1:100 to 1:50, results in decreases in AP activity in the chick scleral ossicle primordia- although the effect is still mild, according to the morphological characterization scale. While troubleshooting CP-471474, a double injection was tested at various concentrations. The double injections did not have a greater effect on scleral ossicle development than any of the

treatment groups (Figure 21). The half-life of CP-471474 is unknown and so it is unclear as to how half-life affects CP-471474 function. A thorough dose response study for CP-471474 on the chick scleral mesenchyme is required to parse out the ideal concentration and ideal developmental time point to administer CP-471474 in order to achieve scleral condensation inhibition and consequently, scleral ossicle inhibition. Also, the IC_{50} values for CP-471474's inhibitory effect on MMP activity in chicken are unknown. If these values were known, it would be easier to parse out which concentration of CP-471474 would be most effective. However, the values available for murine MMPs are: MMP1: 90 ng/mL and MMP2: 0.4 ng/mL. In this study, concentration of 1:100 (0.1mg/mL = 100000ng/mL), and 1:50 (0.2 mg/mL = 200000ng/mL) were used, far exceeding the murine IC_{50} values listed and would therefore be expected to exhibit some effect on MMP activity. It could be that there are additional unidentified MMPs in chicken with functional redundancy that compensate for the inhibition of the known chicken MMPs, or that this inhibitor is not ideal for chicken tissues. Nonetheless, identifying how MMPs function under certain physiological conditions is crucial to understanding the unexpected results that are observed with the use of MMP inhibitors, as most MMP-deficient vertebrates generally develop normally (Lint and Libert 2007).

Treatment with the global MMP-inhibitor, CP-471474, revealed that the nasal group of condensations was the most often affected. This is interesting because the nasal group is the second group to form, and it would be expected that the last forming group (ventral) would be affected the most, according to the sequence at which the various groups develop (see section 1.5, Introduction). The differences in the effects of the hydrocortisone and CP-471474 inhibitors alludes to a possible difference in disruption/inhibition mechanisms (e.g. potency) and/or diffusion rates and should be explored further.

5.5. Verification of Presence of MMPs Following Matrix Manipulation

This study reports, for the first time, troubleshooting data for the potential presence of MMP1 and MMP2 in the embryonic chicken scleral mesenchyme. The establishment of a Western Blot protocol for the aforementioned MMPs is well underway, such that in the future one would be able to verify a potential change in distribution of MMP1 and MMP2 following matrix inhibition (e.g. with Hydrocortisone or CP-471474 or other chemicals) and consequently determine whether MMPs are important for scleral condensation development and growth. While the preliminary data looks promising, western blot for the MMPs still requires further verification. The MMP antibodies used in this study were not previously tested in the chicken, *Gallus gallus*. The investigation of both MMP1 and MMP2 was important because they both utilize tenascin-C as a substrate (Bonnans et. al. 2014; reviewed in Drake and Franz-Odendaal 2018). Tenascin-C having been identified to be present during scleral condensation growth, points to a potential role for the MMPs in scleral ossicle development. It was hypothesized in this study that degradation of the ECM by MMPs may potentially enable the migration of mesenchymal cells into condensations particularly at their lateral ends, and may be necessary for condensation growth to reach critical size.

Previous studies have shown an increase in MMP13 expression following treatment with hydrocortisone in humans and zebrafish (Hillegass et. al. 2007 and 2008; Weidenfeller et. al. 2005). Additionally, tenascin-C expression was reduced to some degree within the scleral tissues following treatment with hydrocortisone in some samples compared to their controls (Hammer and Franz-Odendaal 2017). This suggests that a reduction in tenascin-C expression is associated with a disruption in scleral condensation development. Using the information from these studies (Hammer and Franz-Odendaal 2017; Hillegass et. al. 2007 and 2008; Weidenfeller et. al. 2005),

it can be hypothesized that increasing the expression of MMPs in their active form will lead to a decrease in presence of their substrate, tenascin-C. However, other studies have shown that glucocorticoid treatment can conversely lead to a decrease in expression of MMPs within chicken tissues (Turque et al. 1997). Therefore, it is important to verify whether there are any changes in MMP expression in the scleral mesenchyme following manipulation by matrix inhibitors. Unfortunately due to time constraints, this experiment could not be completed as part of this thesis.

Additionally, an interesting future direction would be to investigate the expression of the TIMPs associated with the MMPs researched in this study. TIMPs are inhibitors of MMPs and they help to regulate matrix remodeling (Sternlicht and Werb 2001; Hu et. al. 2007). Hu et. al. (2007) demonstrated that MMP/TIMP expression plays a role in regulating matrix swelling, cell migration, and corneal maturation during ocular development in the chick. Therefore, both MMPs and TIMPs are necessary for matrix remodeling and homeostatic response to physiological changes during embryonic development. As such, exploring the tissue inhibitors of the MMPs of interest in this study would provide greater insight into the role of MMPs in skeletogenic condensation growth.

5.6. Study Limitations

There were several limitations in this study. The foremost limitation was the abrupt closure of research labs due to the COVID-19 pandemic in mid-March 2020. Because research labs were closed, Objective 4 (2.2.4) was not completed. Nonetheless, prior to lab closures, inhibitor injection experiments were sufficiently completed and a Western Blot protocol was

established for MMP1 and MMP2 in chick scleral mesenchyme. Following the reopening of research labs and the defense of this thesis, completion of Objective 4 will resume.

Additionally, small sample sizes (namely n=3 embryos) were used in this study, for Objective 1B (tilt analysis) while larger samples sizes were used for Objective 1A, Objective 3 and Objective 4A (minimum n=7). Increasing the sample size for the tilt analysis would provide a better representation of the chicken scleral ossicle system.

Limitations could also have arisen from embryo staging. The Hamburger and Hamilton embryonic chick staging table (1951) itself has limitations and relies on the observer to identify morphological changes by eye to determine the age of the embryo. The staging table provides discrete anatomical descriptions of stages but development is a continuum so any one embryo could be at various time points between two discrete stages. The staging table also only allows for staging within 12 to 24 hours. Furthermore, small differences in incubation temperatures could also affect the developmental age of the embryos (Hall 1981).

A further limitation is that the embryos used in this study were produced by different hens and were obtained over a 1.5-year time frame. Thus there is genetic variation among the embryos analyzed. The overall genetic fitness of the embryos could thus differ, and could determine how the embryos respond to stimuli (Cheng et al. 2002; Cheng and Muir 2004), such as the matrix inhibitors. The maternal stress hormone levels of the hens before oviparity can affect egg-yolk cortisol levels in birds and can also be at play in affecting embryonic development (Hayward and Wingfield 2004). Furthermore, larger embryos are likely to have larger eyes and thus more papillae and scleral condensations (Coulombre et. al 1962), which should be taken into account when measuring condensation depth and area. Also, the size of the embryos could affect the diffusion rate of the matrix inhibitors. Although injections were

administered into the air sac of the developing embryos, it is possible that there were slight differences in the positioning and angulation of the injection sites and consequently, the ability of the inhibitors to reach the embryo.

The positions of the condensations on the slides could also present a limitation when taking measurements for condensation area. It is possible that some measurements may have been taken from the center of the condensations while others may not have been. The condensation itself is only about 600µm wide and 85µm thick. Serial sectioning, without the loss of a single section, is extremely tricky. More time would enable a more detailed assessment of condensation area measurements.

Lastly, the MMP antibodies used in this study were not previously verified to be present in scleral mesenchyme. However, Hu et. al. (2007) detected an active MMP2 form of a molecular weight of 66 kDa, and a pro MMP2 form of a molecular weight of 97 kDa in embryonic chicken cornea, using MMP antibodies from a different supplier to those used in this thesis. The variations in MMP size in this study and data within the literature indicate the need for further investigation of MMP antibodies against chicken tissue. These implications along with the extensive troubleshooting for immunohistochemical analysis of syndecan-3 and MMP1, highlight the scarcity of working antibodies and data that are readily available for chicken tissues.

6.0. CONCLUSIONS

In summary, a number of novel findings were made in this study. The results from this study showed that scleral condensation depth increases over developmental time, from stage HH36 to HH37 by approximately 20%. Variations of condensation depth within a given eye suggests that the ring of scleral ossicles in the domestic chicken is oriented at a tilt within the eye. Further studies are needed to determine if the orientation of the scleral ossicle ring is related to its function. Tenascin-C, syndecan-3, MMP1 and MMP2 were identified as important ECM molecules to explore in scleral ossicle development. The spatial and temporal expression of tenascin-C was examined, confirming tenascin-C as a potential regulator of scleral condensation boundary integrity and consequently condensation growth. Alternative experimental methods need to be explored to study the involvement of the cell surface receptor of tenascin-C, syndecan-3. Hydrocortisone was established as a potential matrix manipulator during scleral condensation development. Specifically a 2mM double injection of hydrocortisone administered over two developmental stages (HH34 and HH35) achieved complete inhibition of scleral condensations in 80% of the treated samples. The global MMP inhibitor CP-471474 had an overall mild effect on scleral ossicle development. A single injection of a 1:50 dilution administered at HH33 showed the greatest effect on scleral condensation development, although the effect was mild. A thorough dose response study is needed to determine if scleral condensation inhibition can be achieved with this inhibitor. Putative MMP1 and MMP2 have been identified in chick scleral ossicle primordia for the first time. The next step is to verify their presence in scleral mesenchyme, and confirm a role for these MMPs in scleral condensation development by verifying whether a change in their expression follows matrix manipulation by

inhibitors. These findings have provided important additional insight into the intricate processes of skeletogenic condensation formation, an essential step in intramembranous ossification.

REFERENCES

Andrews D. D., & Franz-Odendaal T. A. 2018. Organotypic Culture Method to Study the Development of Embryonic Chicken Tissues. J. Vis. Exp. (138), e57619, doi:10.3791/57619.

Atkins, J. B., & Franz-Odendaal, T. A. 2016. The sclerotic ring of squamates: an evo-devo-eco perspective. Journal of Anatomy, DOI: 10.1111/joa.12498.

Aykul, S., & Martinez-Hackert, E. 2016. Determination of half-maximal inhibitory concentration using biosensor-based protein interaction analysis. Analytical Biochemistry, 508, 97-103.

Batsos C. 2010. An environmental scan of cleft lip and palate clinics and dental benefit programs in Canada. Office of the Chief Dental Officer, Health Canada. Canadian Association of Public Health Dentistry. http://www.caphd.ca/sites/default/files/1008-CleftLipAndPalateScan.pdf

Canavese B, Vignolini C, Fazzini U, Bellardi S. 1987. Pardcolarica morfologiche dell'anello osseo sclerae della quaglia domestica. Ann Fac Med Vet Di Torino 32: 3–10.

Cheng, H.W., Singleton, P., and Muir, W.M. 2002. Social stress in laying hens: Differential dopamine and corticosterone responses after intermingling different genetic strains of chickens. Poultry Science, 81(9), 1265-1272.

Cheng, H. W., & Muir, W. M. 2004. Chronic social stress differentially regulates neuroendocrine responses in laying hens: II. Genetic basis of adrenal responses under three different social conditions. Psychoneuroendocrinology, 29(7), 961-971.

Chimal-Monroy, J. & Díaz de León, L. 1999. Expression of N-cadherin, N-CAM, fibronectin and tenascin is stimulated by TGF-β1, β2, β3 and β5 during the formation of precartilage condensations. Int. J. Dev. Biol. 43, 59–67.

Chiquet-Ehrismann R. 1990. What distinguishes tenascin from fibronectin? FASEB. 4. doi.org/10.1096/fasebj.4.9.1693347.

Chiquet M. & Fambrough D.M. 1984. Chick myotendinous antigen. I. A monoclonal antibody as a marker for tendon and muscle morphogenesis. j Cell Biol. 98, 1926-1936.

Chiquet M. & Fambrough D.M. 1984. Chick myotendinous antigen. II. A novel extracellular glycoprotein complex consisting of large disulfide-linked subunits. j Cell Biol. 98, 1937-1946.

Chuong, C.M., Yeh, C.Y., Jiang, T.X., & Widelitz, R. 2013. Module based complexity formation: Periodic patterning in feathers and hairs. Wiley Interdisciplinary Reviews: Developmental Biology, 2(1): 97-112.

Cobourne, M.T. & Sharpe, P.T. 2010. Making up the numbers: The molecular control of mammalian dental formula. Seminars in Cell and Developmental Biology, 21: 314-324.

Cordero, D. R., Brugmann, S., Chu, Y., Bajpai, R., Jame, M., & Helms, J. A. 2011. Cranial neural crest cells on the move: Their roles in craniofacial development. American Journal of Medical Genetics Part A, 155(2), 270-279.

Coutinho, A., Kazatchkine, M. D., & Avrameas, S. 1995. Natural autoantibodies. Current Opinion in Immunology, 7(6), 812-818. doi:10.1016/0952-7915(95)80053-0

Cruz-Munoz, W., & Khokha, R. 2008. The Role of Tissue Inhibitors of Metalloproteinases in Tumorigenesis and Metastasis. Critical Reviews in Clinical Laboratory Sciences, 45(3), 291-338.

Démarchez, M., Mauger, A., Herbage, D., & Sengel, P. 1984. Effect of hydrocortisone on skin development in the chick embryo: Ultrastructural, immunohistological, and biochemical analysis. Developmental Biology, 106(1), 15-25.

Desbiens, X., Turque, N., & Vandenbunder, B. 1992. Hydrocortisone perturbs the cell proliferation pattern during feather morphogenesis: Evidence for disturbance of cephalocaudal orientation. The International Journal of Developmental Biology, 36(3), 373-380.

Docherty, B. 2007. Skeletal system: part four--the appendicular skeleton. Nurs Times.103(8):26-7.

Drake, P.M. & Franz-Odendaal, T.A. 2018. A Potential Role for MMPs during the Formation of Non-Neurogenic Placodes. J Dev Biol. 6, 3:20.

Drake, P.M., Jourdeuil, K. & Franz-Odendaal, T.A. 2020. An overlooked placode: Recharacterizing the papillae in the embryonic eye of Reptilia. Developmental Dynamics. 249: 164– 172. https://doi.org/10.1002/dvdy.128

Duench, K. & Franz-Odendaal, T.A. 2012. BMP and Hedgehog signaling during the development of scleral ossicles. Developmental Biology 365: 251-258.

Dunlop, L.T. & Hall, B.K. 1995. Relationships between cellular condensation, preosteoblast formation and epithelial-mesenchymal interactions in initiation of osteogenesis. Int. J. Dev. Biol. 39, 357–371.

Erickson, H. & Inglesias, J. 1984. A six-armed oligomer isolated from cell surface fibronectin preparations. Nature 311, 267–269.

El Shabaka, H.A. 1986. Effect of hydrocortisone on the skin of the developing chick embryo. Qatar University Science Bulletin, 1986(6), 181-197.

Franz-Odendaal, TA. 2008. Towards understanding the development of scleral ossicles in the chicken, *Gallus gallus*. Developmental Dynamics 237:3240-3251.

Franz-Odendaal, TA. 2011. Induction and patterning of intramembranous bone. Frontiers in Bioscience 16, 2734-2746.

Franz-Odendaal, T.A. 2020. Skeletons of the Eye: An Evolutionary and Developmental Perspective. Anat Rec, 303: 100-109. doi:10.1002/ar.24043

Franz-Odendaal, T.A. & Hall, B.K. 2006. Skeletal elements within teleost eyes and a discussion of their homology. J. Morphol., 267: 1326-1337. doi:10.1002/jmor.10479

Franz-Odendaal, T.A. & Krings, M. 2019. A heterochronic shift in skeletal development in the barn owl (Tyto furcata): A description of the ocular skeleton and tubular eye shape formation. Developmental Dynamics. 248: 671– 678. doiorg.ezproxy.library.dal.ca/10.1002/dvdy.65

Franz-Odendaal, T.A., Ryan, K. and Hall, B.K. 2007. Developmental and morphological variation in the teleost craniofacial skeleton reveals an unusual mode of ossification. J. Exp. Zool., 308B: 709-721. doi:10.1002/jez.b.21185

Franz-Odendaal, T. A., & Vickaryous, M. K. 2006. Skeletal elements in the vertebrate eye and adnexa: Morphological and developmental perspectives. Developmental Dynamics, 235(5), 1244-1255.

Fu, L., Das, B., Mathew, S. & Shi, Y.B. 2009. Genome-wide identification of Xenopus matrix metalloproteinases: Conservation and unique duplications in amphibians. BMC Genom, 10, 81.

Fyfe, D.M., Ferguson, M.W., Chiquet-Ehrismann, R. 1988. Immunocytochemical localization of tenascin during the development of scleral papillae and scleral ossicles in the embryonic chick. J Anat 159, 117.

Gañan, Y., Macias, D., Duterque-Coquillaud, M., Ros, M.A. & Hurle, J.M. 1996. Role of TGFβs and BMPs as signals controlling the position of the digits and the areas of interdigital cell death in the developing chick limb autopod. Development. 122, 2349–2357.

Giffin, J.L.. Gaitor, D. & Franz-Odendaal, T.A. 2019. The Forgotten Skeletogenic Condensations: A Comparison of Early Skeletal Development Amongst Vertebrates. J. Dev. Biol, 7, 4.

Hall, B.K. 1975. Evolutionary consequences of skeletal differentiation. American Zoologist, 15(2), 329-350.

Hall, B.K. 1988. The Embryonic Development of Bone. American Scientist, 76(2), 174-181.

Hall, B.K., & Ekanayake, S. 1991. Effects of growth factors on the differentiation of neural crest cells and neural crest cell-derivatives. The International Journal of Developmental Biology, 35(4), 367-387.

Hall, B.K., & Miyake, T. 1992. The membranous skeleton: The role of cell condensations in vertebrate skeletogenesis. Anatomy and Embryology, 186(2), 107-124.

Hall, B.K., & Miyake, T. 2000. All for one and one for all: Condensations and the initiation of skeletal development. *Bioessays*, *22*(2), 138-147.

Hamburger, V., & Hamilton, H.L. 1992. A series of normal stages in the development of the chick embryo. Developmental Dynamics, 195(4), 231-272.

Hammer, C.L. & Franz-Odendaal T.A. 2018. Towards understanding the dose and timing effect of hydrocortisone treatment on the scleral ossicle system within the chicken eye. J. Anat. 232, 270–282.

Hayward, L. S., & Wingfield, J.C. 2004. Maternal corticosterone is transferred to avian yolk and may alter offspring growth and adult phenotype. General and Comparative Endocrinology, 135(3), 365-371.

Herrera, I., Cisneros, J., Maldonado, M., Ramírez, R., Ortiz-Quintero, B., Anso, E., Chandel, N. S., Selman, M., & Pardo, A. 2013. Matrix metalloproteinase (MMP)-1 induces lung alveolar epithelial cell migration and proliferation, protects from apoptosis, and represses mitochondrial oxygen consumption. The Journal of biological chemistry, 288(36), 25964–25975. https://doi.org/10.1074/jbc.M113.459784

Hessel, S. V., Eichinger, A. V., Isken, A. V., Amengual, J. V., Hunzelmann, S. V., Hoeller, U. V., . . . Wyss, A. V. 2007. CMO1 Deficiency Abolishes Vitamin A Production from β-Carotene and Alters Lipid Metabolism in Mice. Journal of Biological Chemistry, 282(46), 33553-33561. doi:10.1074/jbc.m706763200

Hillegass, J. M., Villano, C. M., Cooper, K. R., & White, L. A. 2007. Matrix metalloproteinase-13 is required for zebra fish (Danio rerio) development and is a target for glucocorticoids. Toxicological Sciences, 100(1), 168-179.

Hillegass, J. M., Villano, C. M., Cooper, K. R., & White, L. A. 2008. Glucocorticoids alter craniofacial development and increase expression and activity of matrix metalloproteinases in developing zebrafish (Danio rerio). Toxicological Sciences,102(2), 413-424.

Hindmarsh, P. C., & Charmandari, E. 2015. Variation in absorption and half-life of hydrocortisone influence plasma cortisol concentrations. Clinical endocrinology, 82(4), 557-561.

Hu, J., Van den Steen, P., Sang, Q. 2007. Matrix metalloproteinase inhibitors as therapy for inflammatory and vascular diseases. Nat Rev Drug Discov 6, 480–498. https://doi.org/10.1038/nrd2308.

Huang, S., Zhu, X., Liu, Y., Tao, Y., Feng, G., He, L., Guo, X., & Ma, G. 2012. WIs is expressed in the epidermis and regulates embryonic hair follicle induction in mice. PLoS ONE, 7(9): e45904.

Jabalee J., Hillier S. &Franz-Odendaal T.A. 2013. An investigation of cellular dynamics during the development of intramembranous bones: the scleral ossicles. Journal of Anatomy 223(4):311-20.

Jackman, W.R., Yoo, J.J., & Stock, D.W. 2010. Hedgehog signaling is required at multiple stages of zebrafish tooth development. BMC Developmental Biology, 10: 119.

Jackson, B.C., Nebert, D.W. & Vasiliou, V. 2010. Update of human and mouse matrix metalloproteinase families. Hum. Genom, 4, 194–201.

Johnson, L.G. 1973. Development of chick embryo conjunctival papillae and scleral ossicles after hydrocortisone treatment. Developmental Biology, 30(1), 223-227.

Johnson, D. & Wilkie, A. 2011.Craniosynostosis. Eur J Hum Genet 19, 369–376.

Jourdeuil, K.A. 2015. Deciphering the induction and patterning of the conjunctival papillae in the chicken, *Gallus gallus*. Ph.D. Thesis. Dalhousie University.

Jourdeuil, K. & Franz-Odendaal, T.A. 2017. A wide temporal window for conjunctival papillae development ensures the formation of a complete sclerotic ring. Dev. Dyn., 246: 381-391. doi:10.1002/dvdy.24489

Karlsson C. & Lindahl A. 2009. International Review of Cell and Molecular Biology. Volume 275. 65-88.

Karsenty, G., & Wagner, E. F. 2002. Reaching a Genetic and Molecular Understanding of Skeletal Development. Developmental Cell, 2(4), 389-406. doi:10.1016/s1534-5807(02)00157-0

Lajeunie, E., Le Merrer, M., Bonaïti-Pellie, C., Marchac, D. & Renier, D. 1995. Genetic study of nonsyndromic coronal craniosynostosis. Am J Med Genet, 55: 500–504.

Leśniak-Walentyn, A., & Hrabia, A. 2016. Involvement of matrix metalloproteinases (MMP-2, -7, -9) and their tissue inhibitors (TIMP-2, -3) in the chicken oviduct regression and recrudescence. Cell and Tissue Research, 366(2), 443-454.

Lima, F., Vieira, L., Santos, A., De Simone, S., Hirano, L., Silva, J. & Romão M. 2009. Anatomy of the scleral ossicles in Brazilian birds. Braz J Morph Sci 26:165–169.

Lint, P. V., & Libert, C. 2007. Chemokine and cytokine processing by matrix metalloproteinases and its effect on leukocyte migration and inflammation. Journal of Leukocyte Biology, 82(6), 1375-1381. doi:10.1189/jlb.0607338

Long, M., Zhan, M., Xu, S., Yang, R., Chen, W., Zhang, S., Shi, Y., He, Q., Mohan, M., Liu, Q., & Wang, J. 2017. miR-92b-3p acts as a tumor suppressor by targeting Gabra3 in pancreatic cancer. Molecular cancer, 16(1), 167. https://doi.org/10.1186/s12943-017-0723-7

Mackie, E.J., Thesleff I. & Chiquet-Ehrismann R. 1987. Tenascin is associated with chondrogenic and osteogenic differentiation in vivo and promotes chondrogenesis in vitro. J. Cell. Biol. 105, 2569–2579.

Markus, A.F. 2012. Cleft and Craniofacial anomalies. J Oral Biol Craniofac Res. May-Aug; 2(2): 75–76.

McCawley, L. J., Matrisian, L. M. 2001. Matrix metalloproteinases: they're not just for matrix anymore! Curr. Opin. Cell Biol. 13, 534 –540.

Mead T.J. & Yutzey K.E. 2012. Notch Signaling in Embryology and Cancer. 114-130.

Meyer, T., Gustafsson, J., & Carlstedt-Duke, J. 1997. Glucocorticoid-Dependent Transcriptional Repression of the Osteocalcin Gene by Competitive Binding at the TATA Box. DNA and Cell Biology, 16(8), 919-927. doi:10.1089/dna.1997.16.919.

Mott, J.D. & Werb, Z. 2004. Regulation of matrix biology by matrix metalloproteinases. Curr. Opin. Cell Biol. 16, 558–564.

Nagase, H. & Visse, R. & Murphy, G. 2006. Structure and function of matrix metalloproteinases and TIMPs. Cardiovasc. Res. 69, 562–573.

Olson, M.L., Meighan, P.C., Brown, T.E., Asay, A.L., Benoist, C.C., Harding, J.W. & Wright, J.W. 2008. Hippocampal MMP-3 elevation is associated with passive avoidance conditioning. Regul Pept 146:19–25.

Patterson, R.A., Cavanaugh, A.M., Cantemir, V. Brauer, P.R. & Reedy, M.V. 2013. MT2-MMP expression during early avian morphogenesis. Anat Rec (Hoboken) 296, 64-70.

Peterson, J.T. 2006. The importance of estimating the therapeutic index in the development of matrix metalloproteinase inhibitors, Cardiovascular Research, Volume 69, Issue 3, Pages 677–687.

Peterson, R.E., & Wyngaarden, J. B. 1955. The physiological disposition and metabolic fate of hydrocortisone in man. Annals of the New York Academy of Sciences, 61(2), 297-305.

Pignatti, E., Zeller, R. & Zuniga, A. 2014. To BMP or not to BMP during vertebrate limb bud development. Semin. Cell Dev. Biol. 32, 119–127.

Pinto, C.B. & Hall, B.K. 1991. Toward an understanding of the epithelial requirement for osteogenesis in scleral mesenchyme of the embryonic chick. J. Exp. Zool., 259: 92-108.

Pujuguet, P., Hammann, A., Moutet, M., Samuel, J. L., Martin, F., & Martin, M. 1996. Expression of fibronectin ED-A+ and ED-B+ isoforms by human and experimental colorectal cancer. Contribution of cancer cells and tumor-associated myofibroblasts. The American journal of pathology, 148(2), 579–592.

Rice, D.P. 2008. Craniofacial Sutures. Development, Disease and Treatment. Front Oral Biol. Basel, Karger, vol 12, pp 22–40.

Rohde, L. E., Ducharme, A., Arroyo, L. H., Aikawa, M., Sukhova, G. H., Lopez-Anaya, A., . . . Lee, R. T. 1999. Matrix Metalloproteinase Inhibition Attenuates Early Left Ventricular Enlargement After Experimental Myocardial Infarction in Mice. *Circulation, 99*(23), 3063-3070. doi:10.1161/01.cir.99.23.3063

Saint-Jeannet, J.P., & Moody, S.A. 2014. Establishing the pre-placodal region and breaking it into placodes with distinct identities. Developmental Biology, 389: 13- 27.

Schäcke, H., Döcke, W.D., & Asadullah, K. 2002. Mechanisms involved in the side effects of glucocorticoids. Pharmacology and Therapeutics, 96(1), 23-43.

Sepich D.S., Calmelet, C., Kiskowski, M. & Solnica-Krezel, L. 2005. Initiation of convergence and extension movements of lateral mesoderm during zebrafish gastrulation. Dev Dyn 234, 279–292.

Shames, R.B., Bade, B.C., Sawyer, R.H. 1994. Role of epidermal–dermal tissue interactions in regulating tenascin expression during development of the chick scutate scale. J Exp Zool 269, 349–366.

Shames R.B., Jennings, A.G., Sawyer R.H. 1991. The initial expression and patterned appearance of tenascin in scutate scales is absent from the dermis of the scaleless (sc/sc) chicken. Dev Biol 147, 174–186.

Smith, M.F., McIntush. E.W., Ricke W.A., Kojima, F.N., & Smith, G.W. 1999. Regulation of ovarian extracellular matrix remodeling by metalloproteinases and their tissue inhibitors: effects on follicular development, ovulation and luteal function. J Reprod Fertil Suppl. 54:367-381.

Snider, T.N., & Mishina, Y. 2014. Cranial neural crest cell contribution to craniofacial formation, pathology, and future directions in tissue engineering. Birth Defects Research Part C: Embryo Today: Reviews, 102(3), 324-332.

Stadler, H.S., Higgins, K.M. & Capecchi, M.R. 2001. Loss of Eph-receptor expression correlates with loss of cell adhesion and chondrogenic capacity in Hoxa13 mutant limbs. Development 128: 4177-4188.

Sternlicht, M.D., & Werb, Z. 2001. How Matrix Metalloproteinases Regulate Cell Behavior. Annual Review of Cell and Developmental Biology, 17(1), 463-516.

Stuart, E.S., Garber, B., & Moscona, A.A. 1972. An analysis of feather germ formation in the embryo and in vitro, in normal development and in skin treated with hydrocortisone. Journal of Experimental Zoology, 179(1), 97-118.

Thesleff I., Mackie E., Vaino S. & Chiquet-Ehrismann R. 1987. Changes in the distribution of tenascin during tooth development. Development. 101: 289-296.

Thesleff I., Kantomaa T., Mackie E., Vaino S. & Chiquet-Ehrismann R. 1988. Immunohistochemical localization of the matrix glycoprotein tenascin in the skull of the growing rat. Arch Oral Biol. 33:383-390.

Thesleff I., Mackie E.,Vaino S., Salmivirta M. & Jalkanen M. 1990. Syndecan and tenascin: induction during early tooth morphogenesis and possible interactions. Cell Differ Dev 32:383-390.

Turque, N., Buttice, G., Beuscart, A., Stehelin, D., Crepieux, P., & Desbiens, X. 1997. Hydrocortisone modulates the expression of c-ets-1 and 72 kDa type IV collagenase in chicken dermis during early feather morphogenesis. International Journal of Developmental Biology, 41, 103-109.

Vegiopoulos, A., & Herzig, S. 2007. Glucocorticoids, metabolism and metabolic diseases. Molecular and Cellular Endocrinology, 275(1), 43-61.

Weidenfeller, C., Schrot, S., Zozulya, A., & Galla, H. J. 2005. Murine brain capillary endothelial cells exhibit improved barrier properties under the influence of hydrocortisone. Brain Research, 1053(1), 162-174.

Weiss, P., & Garber, B. 1952. Shape and Movement of Mesenchyme Cells as Functions of the Physical Structure of the Medium: Contributions to a Quantitative Morphology. Proceedings of the National Academy of Sciences of the United States of America, 38(3), 264–280.

Wells, K.L., Hadad ,Y., Ben-Avraham, D., Hillel, J., Cahaner, A., & Headon, D.J. 2012. Genome-wide SNP scan of pooled DNA reveals nonsense mutation in FGF20 in the scaleless line of featherless chickens. BMC Genom 13, 1.

Widelitz, R.B. 2008. Wnt signaling in skin organogenesis. Organogenesis, 4(2): 123- 133.

Wyatt, R.A., Keow, J.Y., Harris, N.D., Hache, C.A., Li, D.H., & Crawford B.D. 2009. The zebrafish embryo: a powerful model system for investigating matrix remodeling. Zebrafish 6, 347-54.

Wyngaarden, L.A., Vogeli, K.M., Ciruna, B.G., Wells, M., Hadjantonakis, A. & Hopyan, S. 2010. Oriented cell motility and division underlie early limb bud morphogenesis. Development 137, 2551–2558.

Yang, H., Makaroff. K., Paz, N., Aitha, M., Crowder, M.W., Tierney, D.L. 2015. Metal Ion Dependence of the Matrix Metalloproteinase-1 Mechanism. Biochemistry. 54(23):3631-3639. doi:10.1021/acs.biochem.5b00379

Yang, M., Zhang, B., Zhang, L. & Gibson, G. 2008. Contrasting expression of membrane metalloproteinases, MT1-MMP and MT3-MMP, suggests distinct functions in skeletal development. Cell Tissue Res 333, 81-90.

Appendix A. General Recipes

Appendix A.1. Chick Saline Recipe

Chick Saline (1L)

In 900 mL distilled water:

7.2 g sodium chloride (Sigma S9888)

0.37 g potassium chloride (MP Biomedicals 191427)

0.23 g calcium chloride dihydrate (EMD Millipore CX0130)

Top up to 1 L with distilled water

Appendix A.2. 4% Paraformaldehyde (PFA) (pH 7.4, 500 mL)

Heat 400 mL 1x PBS in glass beaker to 60˚C on hot plate under the fume hood.

Set hot plate dial between two and three.

Use thermometer to monitor temperature.

Avoid heating solution above 60˚C; *max temperature for the pH meter.*

Avoid heating solution above 70˚C; *PFA will break down above this temperature*.

Measure 20g PFA (Sigma P6148; stored in fridge).

Wear a mask.

Use two large weigh boats.

Add PFA to beaker and add stir bar.

Stir until solution is completely homogeneous.

Cover loosely with foil.

Add NaOH pellets (Sigma S5881) one at a time until solution goes clear.

PFA only dissolves at pH 7.4–7.6.

Turn off heat and adjust pH to 7.4.

Top up to 500 mL with 1x PBS.

Pour beaker contents into graduated cylinder and top up from there.

Divide PFA into 50 mL aliquots and store in -20˚C freezer.

Appendix A.3. 1X Phosphate Buffered Saline (PBS) (1L)

In a 1L beaker, add:

8.0 g sodium chloride (NaCl, EMD Millipore SX0420)

0.2 g potassium chloride (KCl, MP Biomedicals LLC 191427)

1.15 g sodium phosphate dibasic (Na_2HPO4, EMD SX0720-1)

0.2 g potassium phosphate monobasic (KH_2PO4, Sigma-Aldrich,P5655)

Add 800 mL of distilled water to the beaker (graduated cylinder)

On the hot plate, add a stir bar and stir until dissolved.

Adjust pH to 7.4.

Top up to 1L with distilled water.

Appendix B. Wax Embedding Protocol

Wash samples in 2x in PBS for 15 minutes each time.

Place slides in the following reagents for the following time series:

Dehydrate

25% EtOH- 1 hour

50% EtOH- 1 hour

70% EtOH- 1 hour

90% EtOH- 1 hour

100% EtOH- 1 hour

Wash briefly in 100% EtOH.

Citrisolv- 1 hour (Leave cap unscrewed for EtOH to evaporate)

Citrisolv- 1 hour

Wax- 2 hours in vacuum oven

Change wax

Wax overnight in vacuum oven

Following Day

Turn forceps oven on

Change wax

Wax- 2 hours in vacuum oven

Label plastic blocks

Change wax

Orient samples using forceps

Allow wax to cool

Put metal tray on ice pack to harden wax

Secure plastic block holder onto metal tray.

Gently fill plastic block with wax.

Allow wax to cool while holding plastic block in place.

Let block sit and cool at room temperature.

Store blocks at -20°C.

Appendix C. APTES- Slide Coating Protocol

Fill histology koplin jar with 300 ml of 100% EtOH.

Fill another histology koplin jar with 300 ml of H_20.

Place slides in metal tray holders. Make sure that all slides are facing the same direction.

Dip holders in 100% EtOH and let drip for a few seconds.

Dip holders in water and let drip for a few seconds.

Place trays in oven overnight at 38°C to dry.

Following Day

Remove trays from oven and allow slides to cool.

Prepare 300 ml solution of 2% amino-propyl-thioethoxy silicone in acetone in histology glass.

6ml of amino-propyl-thioethoxy silicone (Sigma: A3648) + 294 ml of acetone (Fisher Scientific: A18-4).

Fill two histology koplin jars with 300 ml of 100% acetone each.

Dip holders in solution of 2% amino-propyl-thioethoxy silicone and let drip for a few seconds.

Dip holder in 100% acetone and let drip for a few seconds.

Dip holder in 100% acetone and let drip for a few seconds.

Dip holders in water and let drip for a few seconds.

Place trays in oven overnight at 38°C to dry.

Store slides.

Appendix D. Tissue Sectioning Protocol

Place glass box on warmer and add distilled water.

Trim sample block.

Secure block onto microtome.

Unlock microtome handle.

Line up block with microtome knife as close as possible.

Sample sections should be 6µm.

Lock dial once the knife starts to cut through the block.

Remove sections with forceps or a brush.

Place sections on cardboard grid.

Wet brush and add a few drops of water to slide.

Pick up sections using wet brush and place on top of water on slide.

Place slides on warmer to dry.

Clean up all wax. Reposition knife stage and lock it. Lock handle.

Place slides on metal tray, then place tray in oven. Leave overnight at 37°C to dry.

Appendix E. Hall's and Brunt's Quadruple Stain Protocol

Place slides in the following reagents for the following time series:

Hydration

Citrisolv- 5 minutes

Citrisolv- 5 minutes

100% EtOH- 1 minute

100% EtOH- 1 minute

90% EtOH- 1 minute

70% EtOH- 1 minute

50% EtOH- 1 minute

H_2O- 2 minutes

Staining

Celestine Blue (BK Hall Lab)- 5 minutes. Rinse in H_2O.

H_2O- 1 minute

Hematoxylin (Sigma Aldrich MKCD8359)- 5 minutes. Rinse in H_2O.

H_2O- 1 minute

Alcian Blue (BK Hall Lab)- 5 minutes. Rinse 2x in H_2O.

H_2O- 2 minutes

Phosphomolybdic Acid (Sigma Aldrich SLCB5310)- 1 minute. Rinse in H_2O.

H_2O- 1 minute

Direct Red (BK Hall Lab)- 5 minutes. Rinse in H_2O.

H_2O- 2 minutes

Processing

100% EtOH- 5 seconds

100% EtOH- 10 seconds

100% EtOH- 15 seconds

Clearing

Citrisolv- 1 minute

Citrisolv- 1 minute

Citrisolv- 1 minute

Citrisolv- 1 minute

Mounting

Add Dibutylphthalate Polystyrene Xylen (DPX, Sigma 44581) to coverslip. Lover coverslip onto slide at a 45° angle. Use forceps to position coverslip, to even out DPX, and to remove any bubbles. Leave slides overnight in fume hood to dry.

Appendix F. Raw Data for Measures of Condensation Area and Depth

Table. *7. Raw Data for Histological Analyses of Developing Condensations. Data represents the average measurements per embryo calculated by averaging two-three condensations per embryo.*

HH 36 Area Average	HH 37 Area Average	HH36 Average Depth	HH37 Average Depth
2052.18	12559.93	95.70	134.98
2540.44	14454.21	102.27	141.48
3560.72	7801.51	109.00	130.34
3925.48	5994.27	98.38	108.71
5123.46	6157.05	109.66	124.66
4152.61	3968.45	89.40	118.18
3311.13	5297.84	79.28	111.87
	6000.16		123.96
	7025.44		106.27
	6589.63		74.66
	9190.58		114.00
N= 7 embryos	N=11 embryos	N=7 embryos	N=11 embryos

Table 8. *Raw Data for Histological Analyses of condensation depth of nasal group vs. temporal/dorsal groups at HH38.*

Nasal Condensation Depth (µm)	Temporal/Dorsal Condensation Depth (µm)
75.34	102.34
87.68	87.48
82.18	97.28

Appendix G. Immunohistochemistry Protocol

Adapted from Hammer and Franz-Odendaal (2017)

Start with sections on APTES coated slides. See Appendix C. Recipes for solutions used in this protocol are provided in Appendix G.1-G.8.

HH34-HH37 Tenascin-C (M1-B4 Developmental Studies Hybridoma bank)

Day 1:

Set incubator to 37°C.

1. Rehydrate sections

- 2 x 5 minutes in Citrisolv

- 2 x 2 minutes in 100 % EtOH

- 2 minutes in 90 % EtOH

- 2 minutes in 70 % EtOH

- 2 minutes in 50 % EtOH

- 2 minutes in distilled water

Dry back of slides and around the sections. Circle sections with hydrophobic PAP pen. 50µL of solution per slide is normally more than enough when using the PAP pen. Lay slides horizontally in a humidity chamber. Put a drop of water on each section if necessary, to prevent drying. After each step, solutions were removed by gently tilting the slide and allowing the solution to be soaked up by a Kim wipe (without touching the sections).

2. Use a pipette to apply 3% hydrogen peroxide in 1 x PBS on sections for 20 minutes in humidity chamber with moistened Kim wipes at room temperature.

- Start heating sodium citrate buffer/triton mix in eppi tube to 90°C in a beaker on a hotplate

Label beaker “water”. Heat water in beaker and place eppi tubes in hot water. Turn stove knob to 4. Do not overheat. Monitor temperature.

Get ice and serum

3. Wash slides in 1xPBS (2 x 5 minutes) in a coplin jar; dry back of slides

Check beaker on stove.

4. Add 0.1% Triton-100x / 0.1 % sodium citrate buffer (8 minutes) with a glass Pipette

Put hot sign on stove.

- Make serum block solution

5. Add serum block solution to slides in humidity chamber for 1 hour in 37°C incubator

- Place small pieces of parafilm over the slide to minimize evaporation

- Make milk block solution

6. Rinse briefly in 1x PBS in coplin jar to remove parafilm (less than 1 minute)

7. Add milk block solution to slides in humidity chamber for 1 hour at room temperature

- Place small pieces of parafilm over the slide to minimize evaporation

- Make primary antibody solution on ice

8. Rinse briefly in 1x PBS in coplin jar to remove parafilm (less than 1 minute)

9. Incubate overnight with primary antibody, M1-B4 (Developmental Studies Hybridoma Bank, 1:2), at 4°C in humidity chamber

Treat secondary no primary controls with serum block instead

- Place small pieces of parafilm over the slide to minimize evaporation

Get serum block and 2° antibody ready because the next step moves fast. Get parafilm ready.

Day 2:

10. Rinse 3 x 2 minutes in 1x PBS the following morning (coplin jar). Dry backs of slides.

- Make secondary antibody on ice

11. Incubate for 2 hours in secondary antibody, Rabbit anti-mouse IgG-HRP conjugated antibody (Sigma Aldrich A9044, 1:200), in humidity chamber at room temperature

- Treat primary no secondary controls with serum block instead

- Place small pieces of parafilm over slides to minimize evaporation

Start dissolving DAB.

12. Rinse 1x PBS (3 x 5 minutes) in coplin jar; dry back of slides

13. 8-12 minutes DAB (wrap tube in foil and use in fume hood)

- Place in cupboard for safety for the 8 minutes

- After 8 minutes, remove excess DAB using a pipette. Dry the back of slide

and put a drop of 1x PBS on the slide to view under microscope. If no staining, remove PBS and add DAB again. Wait another 2 minutes. Repeat.

14. Rinse 3 x 5 minutes distilled water after pipetting off excess DAB (coplin jar)

15. Dab off excess water on the slide, and then place a drop of Fluoroshield (Sigma F6182) on the section. Add a glass coverslip. Repeat for each slide.

16. Leave slides to dry overnight in humidity chamber in cupboard

Day 3:

17. Seal the slides with clear nail polish

18. Observe under compound microscope

19. Store in slide box in 4°C

IHC RECIPES

Appendix G.1.3% hydrogen peroxide in 1x PBS (50 mL)

30 % stock in fume hood covered in foil (and wear gloves)

- 1ml 30% hydrogen peroxide (BDH: 3742) (Invert 2-3 times before opening and diluting)

- 10 mL 1x PBS

- Store wrapped in foil at 4°C with lid not on too tight

Appendix G.2. 0.1% sodium citrate buffer (100 mL)

In 80 mL distilled water:

- Add 0.1 g sodium citrate (Sigma: S1804). Stir until dissolved.

- Adjust to pH 6 and top up to 100 mL with distilled water

Appendix G.3. 0.1% triton-100x / 0.1 % sodium citrate buffer (10 mL)

Place a small beaker on a stir plate loosely covered in foil.

- 9.990 mL 0.1% sodium citrate buffer

- Add 10 µL triton-100x (BDH RQ8433)

- Heat until temperature 90°C

Appendix G.4. Serum block solution (2 mL)

- 1.78 mL 1xPBS (on ice)

- 200 µL rabbit serum (Sigma Aldrich R9133)

- 0.02 g bovine serum albumin (Sigma A9647)

Appendix G.5. Milk block solution (2 mL)

- 1.976 mL 1x PBS (on ice)

- 0.02 g bovine serum albumin (Sigma A9647)

- 0.004 g Carnation instant skim milk powder

Appendix G.6. Primary antibody (150 µL)

Primary antibodies were received as supernatants from the Developmental Studies Hybridoma Bank. As per supplier instructions, primary antibodies were aliquoted and diluted in a 1:1 ratio with glycerol. Antibodies were stored at -20°C.

For a working 1:2 concentration (on ice) **Tenascin-C**

- 85 µL antibody aliquot (this is 25 µL antibody with 25 µL glycerol)

- 170 µL serum block solution (See "Serum Block Solution" recipe above)

Use approximately 85 µL/slide (3 slides total)

Appendix G.7. Secondary antibody (Rabbit anti-mouse IgG-HRP conjugated antibody, Sigma Aldrich: A9044) (200 µL)

For a working 1:200 concentration (on ice)

- 1 uL secondary antibody **(flick and spin down)**

- 199 uL serum block solution (see Serum Block recipe above)

Appendix G.8. Color detection buffer (3,3'-diaminobenzidene peroxidase substrate solution) (~ 5 mL)

- Dissolve one gold and one silver tablet of SigmaFast DAB with metal enhancer (Sigma: D0426) in 5 mL dH2O in a fume hood. Mix well.

Cover with foil

Appendix G.9. Immunohistochemical Analyses of Tenascin-C over developmental time.

During immunohistochemistry, a primary antibody binds to the target protein. A secondary antibody binds to the primary antibody, and then to DAB allowing for protein expression to be visualized. This is how one distinguishes between the experimental runs and the controls. Each experimental run is documented below.

Table 9. Immunohistochemical Analyses of Tenascin-C over developmental time.

An "INCONCLUSIVE" run denotes the inability to distinguish between the experimental slides and the controls. A "SUCCESSFUL" run denotes the ability to clearly distinguish the experimental slides from the controls- strong detection (antibody detected) on an experimental slides and no detection (or background) on control slides. "BACKGROUND" indicates that there is staining on a control slide. Cont. No 1º, control with no primary antibody. Cont. No 2º, control with no secondary antibody.

IMMUNOHISTOCHEMISTRY TENASCIN M1-B4 ON CHICK EYE TISSUES

STAGE	DATE OF STAGING	EMBRYO	EYE	EXPERIMENT DATE	SLIDE NUMBER	SLIDE TYPE	NO. OF SECTIONS	RESULTS	COMMENTS
HH37	3/31/16	unknown	unknown	3/11/18	17	EXPERIMENTAL	N/A	STRONG DETECTION	
HH37	3/31/16	unknown	unknown	3/11/18	18	EXPERIMENTAL	N/A	STRONG DETECTION	
HH37	3/31/16	unknown	unknown	3/11/18	26	CONT. NO 1º	N/A	BACKGROUND	
HH37	3/31/16	unknown	unknown	3/11/18	20	CONT. NO 2º	N/A	BACKGROUND	INCONCLUSIVE
HH37	2/9/19	1- SECT. B	unknown	4/6/19	13	EXPERIMENTAL	6	NO DETECTION	
HH37	2/9/19	1- SECT. B	unknown	4/6/19	19	EXPERIMENTAL	6	STRONG DETECTION	
HH37	2/9/19	1- SECT. B	unknown	4/6/19	17	CONT. NO 1º	6	BACKGROUND	
HH37	2/9/19	1- SECT. B	unknown	4/6/19	15	CONT. NO 2º	6	BACKGROUND	INCONCLUSIVE
HH37	4/18/19	1 B	unknown	4/25/19	18	EXPERIMENTAL	6	STRONG DETECTION	
HH37	4/18/19	1 B	unknown	4/25/19	26	EXPERIMENTAL	4	STRONG DETECTION	
HH37	4/18/19	1 B	unknown	4/25/19	28	CONT. NO 1º	4	NO DETECTION	
HH37	4/18/19	1 B	unknown	4/25/19	21	CONT. NO 2º	7	NO DETECTION	SUCCESSFUL
HH37	5/7/19	4	unknown	5/27/19	16	EXPERIMENTAL	9	STRONG DETECTION	
HH37	5/7/19	4	unknown	5/27/19	22	EXPERIMENTAL	10	STRONG DETECTION	
HH37	5/7/19	4	unknown	5/27/19	20	CONT. NO 1º	5	NO DETECTION	
HH37	5/7/19	4	unknown	5/27/19	18	CONT. NO 2º	8	NO DETECTION	SUCCESSFUL
HH37	5/11/19	2	unknown	6/25/19	18	EXPERIMENTAL	8	STRONG DETECTION	
HH37	5/11/19	2	unknown	6/25/19	22	EXPERIMENTAL	9	STRONG DETECTION	
HH37	5/11/19	2	unknown	6/25/19	24	CONT. NO 1º	8	NO DETECTION	
HH37	5/11/19	2	unknown	6/25/19	20	CONT. NO 2º	9	NO DETECTION	SUCCESSFUL
HH37	5/7/09	4	unknown	6/25/19	24	EXPERIMENTAL	5	STRONG DETECTION	
HH37	5/7/09	4	unknown	6/25/19	28	EXPERIMENTAL	9	STRONG DETECTION	
HH37	5/7/09	4	unknown	6/25/19	30	CONT. NO 1º	6	NO DETECTION	
HH37	5/7/09	4	unknown	6/25/19	26	CONT. NO 2º	9	NO DETECTION	SUCCESSFUL
HH37	2/9/19	1- SECT. B	unknown	6/25/19	2	EXPERIMENTAL	3	STRONG DETECTION	
HH37	2/9/19	1- SECT. B	unknown	6/25/19	6	EXPERIMENTAL	5	STRONG DETECTION	
HH37	2/9/19	1- SECT. B	unknown	6/25/19	8	CONT. NO 1º	8	NO DETECTION	
HH37	2/9/19	1- SECT. B	unknown	6/25/19	4	CONT. NO 2º	3	NO DETECTION	SUCCESSFUL
HH36	6/6/19	#4	unknown	7/4/19	13	EXPERIMENTAL	9	STRONG DETECTION	
HH36	6/6/19	#4	unknown	7/4/19	17	EXPERIMENTAL	6	STRONG DETECTION	
HH36	6/6/19	#4	unknown	7/4/19	19	CONT. NO 1º	7	NO DETECTION	
HH36	6/6/19	#4	unknown	7/4/19	15	CONT. NO 2º	6	NO DETECTION	SUCCESSFUL
HH36	6/6/19	#1	unknown	7/4/19	10	EXPERIMENTAL	8	STRONG DETECTION	
HH36	6/6/19	#1	unknown	7/4/19	14	EXPERIMENTAL	7	STRONG DETECTION	
HH36	6/6/19	#1	unknown	7/4/19	16	CONT. NO 1º	7	NO DETECTION	
HH36	6/6/19	#1	unknown	7/4/19	12	CONT. NO 2º	8	NO DETECTION	SUCCESSFUL
HH36	6/6/19	#3	unknown	7/11/19	2	EXPERIMENTAL	4	STRONG DETECTION	
HH36	6/6/19	#3	unknown	7/11/19	6	EXPERIMENTAL	6	STRONG DETECTION	
HH36	6/6/19	#3	unknown	7/11/19	8	CONT. NO 1º	4	NO DETECTION	
HH36	6/6/19	#3	unknown	7/11/19	4	CONT. NO 2º	6	NO DETECTION	SUCCESSFUL
HH36	6/6/19	#2	unknown	7/22/19	3	EXPERIMENTAL	6	STRONG DETECTION	
HH36	6/6/19	#2	unknown	7/22/19	7	EXPERIMENTAL	10	STRONG DETECTION	
HH36	6/6/19	#2	unknown	7/22/19	9	CONT. NO 1º	8	NO DETECTION	
HH36	6/6/19	#2	unknown	7/22/19	5	CONT. NO 2º	8	NO DETECTION	SUCCESSFUL
HH35	7/20/19	1	RIGHT	8/20/19	10	EXPERIMENTAL	7	STRONG DETECTION	
HH35	7/20/19	1	RIGHT	8/20/19	15	EXPERIMENTAL	6	STRONG DETECTION	
HH35	7/20/19	1	RIGHT	8/20/19	12	CONT. NO 1º	5	NO DETECTION	
HH35	7/20/19	1	RIGHT	8/20/19	17	CONT. NO 2º	8	NO DETECTION	SUCCESSFUL
HH35	7/20/19	2	RIGHT	8/20/19	10	EXPERIMENTAL	9	STRONG DETECTION	
HH35	7/20/19	2	RIGHT	8/20/19	14	EXPERIMENTAL	8	STRONG DETECTION	
HH35	7/20/19	2	RIGHT	8/20/19	12	CONT. NO 1º	7	NO DETECTION	
HH35	7/20/19	2	RIGHT	8/20/19	16	CONT. NO 2º	4	NO DETECTION	SUCCESSFUL
HH35	7/20/19	4	RIGHT	8/20/19	8	EXPERIMENTAL	8	STRONG DETECTION	
HH35	7/20/19	4	RIGHT	8/20/19	12	EXPERIMENTAL	8	STRONG DETECTION	
HH35	7/20/19	4	RIGHT	8/20/19	10	CONT. NO 1º	9	NO DETECTION	
HH35	7/20/19	4	RIGHT	8/20/19	14	CONT. NO 2º	7	NO DETECTION	SUCCESSFUL
HH34	4/1/19	3	RIGHT	8/9/19	5	EXPERIMENTAL	11	STRONG DETECTION	
HH34	4/1/19	3	RIGHT	8/9/19	9	EXPERIMENTAL	10	STRONG DETECTION	
HH34	4/1/19	3	RIGHT	8/9/19	11	CONT. NO 1º	10	NO DETECTION	
HH34	4/1/19	3	RIGHT	8/9/19	7	CONT. NO 2º	8	NO DETECTION	SUCCESSFUL
HH34	7/19/19	4	RIGHT	8/20/19	8	EXPERIMENTAL	7	STRONG DETECTION	
HH34	7/19/19	4	RIGHT	8/20/19	12	EXPERIMENTAL	6	STRONG DETECTION	
HH34	7/19/19	4	RIGHT	8/20/19	10	CONT. NO 1º	6	NO DETECTION	
HH34	7/19/19	4	RIGHT	8/20/19	14	CONT. NO 2º	5	NO DETECTION	SUCCESSFUL
HH34	7/19/19	3	RIGHT	8/20/19	6	EXPERIMENTAL	7	STRONG DETECTION	
HH34	7/19/19	3	RIGHT	8/20/19	10	EXPERIMENTAL	7	STRONG DETECTION	
HH34	7/19/19	3	RIGHT	8/20/19	8	CONT. NO 1º	7	NO DETECTION	
HH34	7/19/19	3	RIGHT	8/20/19	12	CONT. NO 2º	6	NO DETECTION	SUCCESSFUL

Appendix H. Matrix Inhibitor Injection Experiments

Preparations

1. Begin experiment by incubating eggs. Allow for ¾-1-day warm up time when tracking the development of the eggs and predicting the injection times. Incubator should be maintained at 37° C and ~40-50% humidity.
2. Identify which eggs are fertilized 4-5 days before injections. Weighing eggs could also be used to identify which ones are unfertilized.
3. Stage 2-3 eggs one day prior to injecting to estimate whether the batch is developing on track or not and make adjustments accordingly. Eggs should be at HH34+-35 on injection day 1.
4. Transfer eggs from vertical incubator into horizontal incubator 2-3 days before injections.

Hydrocortisone

Hydrocortisone treatment concentration should be 2.0mM.

CP-471474

CP-471474 treatment involves using two treatment concentrations- 1:100 and 1:50.

Delivering First Injections

1. In a separate egg carton (small pieces that have been cut from a full carton), tilt a single egg on its end (roughly 60° angle) so that the end with the air sac is facing upwards.

2. Use a 19-guage needle to make injection site bigger if needed. Begin firmly applying pressure to the shell until it makes a small crack. Then, gently twist the needle as you continue to press

down. Be careful not to penetrate very far past the hole, as this could damage the membranes and be lethal for the embryo.

3. Using a P200 pipette, deliver 100uL of the appropriate injection solution (control or treatment) through the hole in the eggshell. Make sure solution does not drip out. If solution drips out, suck it up with a pipette, reintroduce solution to the egg, and make note of it.

4. Return the egg to its carton in a tilted position (roughly 45 degrees).

5. Repeat this procedure for all the eggs receiving an injection and then return eggs to the incubator.

6. If a second injection is required, repeat the injection steps above with the exception of step 3, as the injection holes will already be there.

7. After eggs have reached desired stage, sacrifice embryos and fix heads in 4% PFA overnight. Rinse in PBS the following morning. Then, store at 4°C in PBS.

8. Before Alkaline Phosphatase staining protocol, bisect heads and remove eyelids. Use one half of the head for Alkaline Phosphatase protocol and store the other half of the eye in 1X PBS at 4°C.

Hydrocortisone Injection Solutions

Appendix H.1. Howard Ringer's Solution with EtOH

0.15 mL 100% EtOH

4.85 mL Howard's Ringer Solution

Appendix H.2. To make 2mM Hydrocortisone in Howard Ringer's Solution with EtOH

0.15 mL 100% EtOH

4.85 mL Howard's Ringer Solution

0.0036g hydrocortisone (Sigma H4001)

CP-471474 Injection Solutions

Appendix H.3. CP-471474 Stock Solution

5mg CP-471474 (TRC #C781305) powder

1mL Dimethyl sulfoxide (DMSO) (Calbiochem #6010)

Appendix H.4. 1:100 CP-471474 in Howard Ringer's Solution

10µl stock solution of CP 471474 in DMSO (5mg/ml)

990µl Howard Ringer's Solution

Appendix H.5. 1:100 Control Injection Solution

10µl DMSO

990µl Howard Ringer's Solution

Appendix H.6- 1:50 CP-471474 in Howard Ringer's Solution

20µl stock solution of CP 471474 in DMSO (5mg/ml)

980µl Howard Ringer's Solution

Appendix H.7- 1:50 Control Injection Solution

20µl DMSO

980µl Howard Ringer's Solution

Appendix I. Alkaline Phosphatase Staining Protocol (Chicken)

1. 3 x 15 minutes washes in dH2O at room temperature

2. 1 hour in Tris-Maleate Buffer (pH 8.3) at room temperature

· Make the AP Substrate Solution here (this should be made in a glass vial in the dark)

3. 1 hour in AP substrate solution at room temperature (keep samples in the dark)

4. 3 x 15 minutes washes in Saturated Sodium Borate Water to stop the reaction

Make the Bleach solution now.

5. Bleach overnight in 3% bleach solution at room temperature

6. In the morning, process embryos to 80% glycerol in 1% KOH

1 hour in 25%/75% glycerol in 1% KOH

1 hour in 50%/50% glycerol in 1% KOH

1 hour in 80%/20% glycerol in 1% KOH

Alkaline Phosphatase Recipes

Appendix I.1. Chick Saline / Howard Ringer Solution (1L)

In 900 mL distilled water:

7.2 g sodium chloride (Sigma: S9888)

0.37 g potassium chloride (MP Biomedicals: 191427)

0.23 g calcium chloride dihydrate (EMD Millipore: CX0130)

Top up to 1 L with distilled water

Appendix I.2. ALP Substrate Solution

2 Jars (labelled: "A" & "B")

JAR A: - 1 mL N,N-dimethylformamide (Sigma-Aldrich 319937)

0.012 g Naphthol AS-TR (Sigma-Aldrich N6125)

JAR B: - 10 mL Tris-Maleate Buffer (pH = 8.3)

0.0082 g Fast Blue (Sigma-Aldrich D9805)

Transfer 1 mL from "JAR A" to "JAR B"

Appendix I.3. Tris-Maleate Buffer (pH = 8.3)

2.42 g Tris Base (Roche #122009)

2.2 g Maleic Acid (Sigma M0375)

Add 70ml dH_2O

pH to 8.3

Top up to 100ml with dH_2O

Appendix I.4. 1% KOH

1g KOH (Sigma 221473)

100ml dH_2O

Appendix I.5. Saturated Sodium Borate Water

5g Sodium Tetraborate Decahydrate (Sigma B9876)

100ml dH_2O

Appendix I.6. 3% Bleach Solution

2ml 3% hydrogen peroxide (Pharmasave, commercial drugstore)

18ml 1% KOH

Appendix I.7. 25% Glycerol in 1% KOH

12.5ml glycerol (BDH 1172)

37.5ml 1% KOH

Appendix I.8. 50% Glycerol in 1% KOH

25ml glycerol (BDH 1172)

25ml 1% KOH

Appendix I.9. 80% Glycerol in 1% KOH

40ml glycerol (BDH 1172)

10ml 1% KOH

Appendix J. Western Blot Protocol

Developed by Nick Zinck (Graduate student in Franz- Odendaal Lab)

Appendix J.1. Lysate Preparation

1. Add 300µl of ice cold RIPA buffer per 5mg of tissue to each 2ml microcentrifuge tube and place on ice.
2. Quickly dissect tissue of interest (scleral condensations and corneas) and place in a 2ml microcentrifuge containing RIPA buffer on ice.

   Recipe for 50mL RIPA buffer

   - 2.5mL 1M Tris-HCL- pH to 8.0
   - 0.438g of NaCl (EMD Millipore SX0420)
   - 1mL triton-X (BDH RQ8433)
   - 0.5ml of 10% SDS (BioRad #1610302)
   - Top up to 50mL dH_20
   - RIPA buffer should contain 1 EDTA-free Roche cOmplete cocktail tablet (Roche: 11873580001) per 50mL of RIPA buffer. RIPA buffer can be stored at -20ºC. Add tablet on day of use.
3. Homogenize at 40Hz for 5 minutes using one steal bead per tube.
4. Place tube on shaker with gentle agitation at 4°C for 2 hours.
5. Centrifuge tubes for 20 minutes at 12,000 rpm (at 4°C).
6. Transfer supernatant to fresh tube – discard pellet.
7. Store supernatant at -80°C.

Appendix J.2. Protein Quantification Using Pierce BCA Assay (Thermo Scientific # 23225)

1. Prepare two replicates of the dilution series of BSA standard using table below:

Tube	Volume of Diluent (µl)	Volume/Source of BSA (µl)	Final BSA Concentration (µg/µL)
A	0	150 of Stock	2000
B	62.5	187.5 of Stock	1500
C	162.5	162.5 of Stock	1000
D	87.5	87.5 of Tube B	750
E	162.5	162.5 of Tube C	500
F	162.5	162.5 of Tube E	250
G	162.5	162.5 of Tube F	125
H	200	50 of Tube G	25
I	200	0	0 (blank)

   - Table copied from Pierce BCA Protein Assay Kit Protocol

2. Prepare Working Reagent using 50:1 parts BCA Reagent A with BCA Reagent B. (i.e. 50ml Reagent A with 1ml Reagent B)
   - Use following formula to calculate volume of WR needed:
   - (# standards + # unknowns) × (# replicates) × (volume of WR per sample) = total volume WR required.
   - (9+ 8) × (2) × (1mL) = 34 tubes total used in this study
3. Transfer 50µl of each stock sample and protein sample to be quantified into fresh 1.5ml Eppendorf tubes.
   - Do this twice for the unknown sample to have a replicate.
4. Into each stock tube and sample tube add 1ml of working reagent.
5. Incubate the tubes at 37°C for 30 minutes and allow to cool to room temperature (about 10 minutes).
6. Read the 562nm absorbance of all samples using 2µl of sample in the BioDrop within 10 minutes (as quickly as possible).

7. Create a standard curve of known concentration vs absorbance using the BSA standards in Excel. Use the linear equation function to determine unknown concentrations.

Western Blot Recipes

Appendix J.3. 2X SDS Reducing Loading Buffer (Laemmli sample buffer) Make in fume hood.

· 0.125 M Tris (Roche #122009)

· 20% Glycerol (BDH 1172)

· 4% SDS (BioRad #1610302)

· 0.1% Bromophenol blue (Sigma GE17-1329-01)

· pH to 6.8

· 10% 2-Mercaptoetanol ß (Extremely smelly. Handle under fume hood.)

2X SDS Reducing Loading Buffer (Laemmli sample buffer) Make in fume hood.

· 0.125 M Tris (Roche #122009)

· 20% Glycerol (BDH 1172)

· 4% SDS (BioRad #1610302)

· 0.1% Bromophenol blue (Sigma GE17-1329-01)

· pH to 6.8

Appendix J.4. 10X Running Buffer (500 mL) – Store at room temp

In 400 mL of distilled water:

· 15.15 g Tris (Roche #122009)

· 72.1 g Glycine (Amresco #2622C211)

· 5.0 g SDS (BioRad #1610302)

· pH should be ~ 8.3. Do not adjust.

· Top up to 500 mL with distilled water

Appendix J.5. Transfer Buffer (1000 mL) Can be stored at r/t but needs to be 4°C upon use

In 600 mL of distilled water:

· 5.82 g Tris (Roche #122009)

· 2.93 g Glycine (Amresco #2622C211)

· 0.4 g SDS (BioRad #1610302)

· Add 200 mL methanol (final concentration of 20%) (BDH 1135-4LP)

· Top up to 1000 ml with distilled water

· pH should be ~9.2, but do not adjust

Appendix J.6. 1X PBS containing 0.1% Tween (500 mL) (1X PBST) Store at 4°C

In 400 mL distilled water

· 3.80 g NaCl (EMD Millipore, SX0420)

· 0.76 g NaH2PO4 * 2H2O (EMD SX0720-1)

· Adjust pH to 7.5

· Add 500 µL Tween-20 (Sigma #SLB28563)

Appendix J.7. SDS-PAGE Part 1: Determining Linear Dynamic Range

1. Prepare required buffers for electrophoresis (See each recipe in Appendix J.8)
    a. Running Buffer
    b. Loading Buffer

        For **reducing conditions**, loading buffer contains beta-mercaptoethanol. For **non-reducing conditions,** no beta-mercaptoethanol is added to the loading buffer.
    c. Transfer Buffer (store at 4°C)
2. Create a pooled protein sample with the same amount of protein from each sample.

- Allot a lane for a molecular weight marker (ladder).

3. Prepare samples by adding a 1:1 volume of loading buffer to protein lysate, and heat mixture at 90-100°C for 10 minutes.
4. Assemble electrophoresis chamber and power supply.
5. Remove pre-cast gel from package, remove tape on bottom, and gently remove comb.
6. Place gel in holder, with wells facing inwards.
7. Fill inner and outer chambers with 1X running buffer (inner chamber is filled above wells, while outer chamber is filled to designated line).
8. Load ladder (Bio-Rad #161-0374) in the first well then, load samples into remaining wells.
9. Plug in and run apparatus at 200V until dye front has travelled approximately ¾ of the gel.
    - Cover tank correctly (red on red, black on black)
    - Plug wires into power supply correctly (red on red, black on black)
10. Power off and unplug the apparatus. Remove the gel from the casing using the green metal tool.
11. Cut gel at top right corner to remember correct orientation.
12. Immediately place gel in cold transfer buffer to equilibrate.

Appendix J.8. Gel-Membrane Transfer

1. Have a small ice pack ready prior to beginning (frozen).
2. Have transfer buffer cooled to 4°C.
3. Equilibrate the gel in transfer buffer.
4. Cut filter paper, nitrocellulose membrane, and scotchbrite pads to the size of gel.

- Do not touch with membrane with bare hands as it will increase background during development. Use forceps when handling.

5. Equilibrate materials above in transfer buffer for 10 minutes.
6. Prepare gel sandwich using plastic cassette in transfer buffer bath.
    - **Bottom (black)**
    - Equilibrated scotchbrite pad
    - Equilibrated filter paper
    - Equilibrated gel
    - Equilibrated nitrocellulose membrane
    - Equilibrated filter paper
    - Equilibrated scotchbrite pad
    - **Top (clear)**
7. It is very important that no air pockets form between gel and membrane. Avoid this by rolling a falcon tube over the sandwich when constructing.
8. Carefully close cassette as to not disrupt sandwich,
9. Place cassette in rig with membrane facing positive electrode (red), and gel facing negative electrode (black).
10. Place ice pack in rig (frozen).
11. Fill rig with transfer buffer to specified level.
    - Use buffer that was used to equilibrate materials and build sandwich.
12. Place stir bar at bottom of rig, set rig on stir plate set to low. This ensures even distribution of temperature and ions.
13. Plug in rig to power supply and run at 30V overnight.

14. When finished, power off rig, and unplug from power supply.

15. Disassemble sandwich and gently remove membrane. Cut in top right corner to remember correct orientation.

Appendix J.9. Western Blot

1. Transfer membrane to container and cover with ponceau stain for 10 minutes. Use just enough ponceau stain to cover the membrane.
2. Make notches in membrane with a razor to outline where to cut the lanes (if necessary).
3. Rinse in dH_2O 3x5 minutes on shaker to remove ponceau stain.
4. Roll membrane and add to 20 mL tube.
5. Block membrane with 5% milk in PBST (milk block solution) for one hour.
    - 0.5g Carnation instant skim milk powder
    - 10mL 1X PBST
6. Incubate membrane with primary antibody in milk block solution for one hour at room temperature on shaker.

    Tubulin at a working 1:1000 concentration

    5µL Tubulin (AB6046)

    5mL milk block solution

    MMP1 concentrations tested:

    1:345; 1:680; 1:1377

    <u>MMP1 at a working 1:1377 concentration</u>

    3.63µL MMP1 (ABCAM137332)

    5mL milk block solution

MMP2 concentrations tested:

1:510; 1:1020; 1:2040

MMP2 at a working 1:510 concentration

7.35µL MMP2 (ABCAM 97779)

5mL milk block solution

7. Rinse membrane 3x5 minutes in cold PBST.
8. Incubate membrane for one hour with secondary antibody solution at room temperature on shaker.

   Goat Anti-Mouse IgG (H+L)-Jackson Labs 115-035-003) at a 1:10000 concentration

   1µL Goat Anti-Mouse IgG (H+L)-Jackson Labs 115-035-003)

   10mL milk block solution

9. Rinse membrane 3x5 minutes in cold PBST.
10. Start dissolving DAB tablets in 5mL dH_2O. Cover tube with foil.

Appendix J.10. Signal Development using, 3'- diaminobenzidene (DAB) peroxidase (Sigma D0426)

1. Dissolve DAB (allow tablets to come to room temperature) in 5mL dH_2O in a tube covered with foil.
2. Drain excess wash solution from membrane by holding vertically with forceps and touching the edge to a tissue.
3. Place membrane on a clean petri dish and cover with DAB solution.
4. Incubate at room temperature for 10-15 minutes until desired color intensity is reaches.

5. Stop the reaction by rinsing membrane three times with 20 ml of distilled water (30 seconds per rinse)
6. Cover membrane with distilled water and cover petri dish with foil. Store at 4ºC.

Appendix J.11. Western Blot Troubleshooting Supplemental Information

Only the last four lanes on the gel contain samples used in this study. Cornea tissues are in the first two wells, and scleral ossicles are in the in the last two. As indicated by the distinct bands, the integrity of the protein is good.

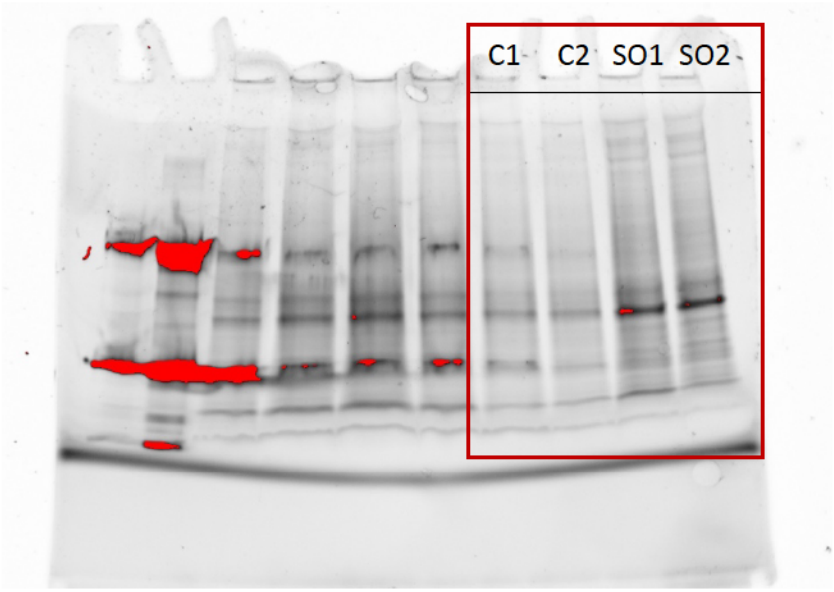

Figure 27. *SDS-PAGE- gel was imaged to check the integrity of the protein. Distinguishable bands indicate good protein integrity, while undistinguishable bands indicate the opposite. C, Cornea; SO, Scleral ossicle.*

Appendix J.12. Protein Quantification & Standard Curve/BCA Assay

Table 10. *Average absorbances for each protein standard.*

Standard Concentration (ug/mL)	**Average Absorbance** (562nm)
2000	0.114
1500	0.101
1000	0.075
750	0.051
500	0.039
250	0.021
125	0.012
25	0.003
0	0

These values were used to plot the standard curve, yielding an equation of
y-0.0055= 6E-05x
Therefore,
x= y-0.0055/6E-05

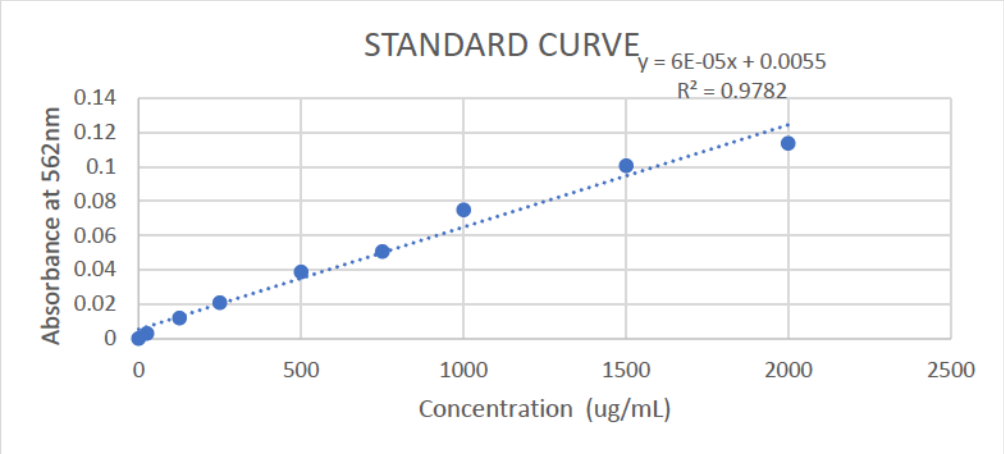

Figure 28. *Standard Curve used to calculate unknown sample protein concentrations using the slope of the curve.*

Table 11. *Unknown sample concentrations are calculated based on the slope of the standard curve.* C1-4, corneal tissue, SO1-4, scleral ossicle primordia tissue.

Unknown Concentrations (ug/mL)	Sample Absorbance (562nm)	Samples
1008.333	0.066	C1
925.000	0.061	C2
908.333	0.06	C3
875.000	0.058	C4
1558.333	0.099	SO1
1358.333	0.087	SO2
1275.000	0.082	SO3
1291.667	0.083	SO4

Appendix K. Statistical Analysis for Measurements of Condensation Area and Condensation Depth

Table 12. *Welch's t-test on data for condensation area for stages HH36 and HH37.*

	N	Mean	Standard Deviation	Standard Error Mean		Welch's t-test	
HH36 Area	7	3524	1024	387			
HH37 Area	11	7731	3178	958			
					***t*-value**	***df***	***p*-value**
					-4.07	12	0.001

Table 13. *Welch's t-test on data for condensation depth HH36 and HH37.*

	N	Mean	Standard Deviation	Standard Error Mean		Welch's t-test	
HH36 Depth	7	97.7	10.8	4.1			
HH37 Depth	11	117.2	17.9	5.4			
					***t*-value**	***df***	***p*-value**
					-2.88	15	0.006

Table 14. *One-way ANOVA on Condensation Area.*

	Groups			
	HH36	HH37	Total	
N	7	11	18	
∑X	24666.02	85039.07	109705.09	
Mean	3523.7171	7730.8245	6094.727	
$\sum X^2$	93210992.3554	758444539.7051	851655532.0605	
Standard Deviation	1024.2814	3178.4023	3281.2563	
Result Details				
Source	***SS***	***df***	***MS***	
Between-treatments	75715608.7593	1	75715608.7593	*F* = 11.28848
Within-treatments	107317324.8618	16	6707332.8039	
Total	183032933.6212	17		

The f-ratio value is 11.28848. The p-value is .003984. The result is significant at p < .05.

Table 15. *One-way ANOVA on Condensation Depth.*

	Groups			
	HH36	HH37	Total	
N	7	11	18	
∑X	683.69	1289.11	1972.8	
Mean	97.67	117.1918	109.6	
$\sum X^2$	67480.2613	154293.6055	221773.8668	
Standard Deviation	10.834	17.9456	18.0766	
Result Details				
Source	***SS***	***df***	***MS***	
Between-treatments	1630.267	1	1630.267	*F* = 6.64615
Within-treatments	3924.7198	16	245.295	
Total	5554.9868	17		

The f-ratio value is 6.64615. The p-value is .020223. The result is significant at p < .05.

Table 16. *Welch's t-test on data for condensation depth f of nasal group vs. temporal/dorsal groups at HH38.*

	Mean	**Standard Deviation**	**Standard Error Mean**		**Welch's t-test**	
Nasal Condensation Depth	81.73333	6.182	3.569245			
Temporal/Dorsal Condensation Depth	95.70000	7.5549	4.36185			
				***t*-value**	***df***	***p*-value**
				-2.4781	3.8493	0.0354

Appendix L. Supplemental Antibody Information.

Table 17a. Summary of relevant details for primary antibodies used in this study. All primary antibodies have been previously described in the literature in various systems.

Antibody	Supplier	Catalogue No.	Clonality	Product Form	Concentration (ug/mL)	Species of Origin	Tissue Reactivity	Antigen Molecular Weight (kDa)	Positive Control	References
Tenascin-C	Developmental Studies Hybridoma Bank	M1-B4	Monoclonal	Supernatant	19	Mouse	Chicken, Newt	150-240	Embryonic chick limb cartilage	See Chiquet and Fambrough (1984) for verification tests and controls used for antibody
Tubulin	ABCAM	AB6046	Polyclonal	Liquid	1	Rabbit	Mouse, Rat, Chicken, Human, Zebrafish, Chinese hamster	50-54	HeLa Cell lysate	Hessel et al. 2007
MMP1	ABCAM	AB137332	Polyclonal	Liquid	1.47	Rabbit	Mouse, Human	54	Raji and HUVEC whole cell lysates.	Herrera et al. 2013
MMP2	ABCAM	AB97779	Polyclonal	Liquid	0.46	Rabbit	Mouse, Human	74	293T, A431, H1299, HeLa, HepG2, MOLT4 or Raji cell lysate	Long et al. 2017

Table 17b. Summary of relevant details for secondary antibodies used in this study. All secondary antibodies have been previously described in the literature in various systems.

Antibody	Supplier	Catalogue No.	Clonality	Product Form	Concentration (ug/mL)	Species of Origin	Tissue Reactivity	Antigen Molecular Weight (kDa)	References
Peroxidase AffiniPure Goat Anti-Mouse IgG (H+L)	Jackson Labs	15-035-003	Polyclonal	Whole IgG	0.8	Goat	Mouse	160	Pujuguet et al. 1996
Rabbit anti-mouse IgG-HRP conjugated antibody	Sigma Aldrich	A9044	Polyclonal	Whole IgG	10	Rabbit	Mouse	150	Coutinho et al. 1995